2014

Analysis of Solid State Bonding in the Extrusion Process of Magnesium Alloys -Numerical Prediction and Experimental Verification

Nabeel Hussain Alharthi
Lehigh University

Analysis of Solid State Bonding in the Extrusion Process of Magnesium Alloys -Numerical Prediction and Experimental Verification

by
Nabeel H. Alharthi

Presented to the Graduate and Research Committee
of Lehigh University
in Candidacy for the Degree of
Doctor of Philosophy

in
Mechanical Engineering

Lehigh University
Bethlehem PA

September 2014

Approved and recommended for acceptance as a dissertation in partial fulfillment of the requirements for the degree of Doctor of Philosophy

_____
Date

_____
Prof. Wojciech Z. Misiolek,
Chairman and Dissertation Advisor

_____
Accepted Date

Committee Members:

_____
Prof. David C. Angstadt

_____
Prof. John P. Coulter

_____
Prof. Alprslan Oztekin

_____
Prof. Timotius Pasang

ACKNOWLEDGMENT

Foremost, I would like to thank ALLAH for helping me in my life and for giving me the ability to complete this work. Then, I would like to give my most respect and loving to my great parents who support me since I was a child. I dedicate this work to them. Also, I would thank my lovely wife and my children for their patient and continuous support. Many thanks to all who were supportive through my graduate studies.

Special thanks to my advisor Prof. Wojciech Z. Misiolek for his technical guidance and encouragement throughout my graduate studies at Lehigh University. Moreover, I would like to thank the faculty members who serving on my dissertation committee. Special thanks for my best friends Bandar Alzahrani and Hamad Alharbi for their support, technical discussions and sharing ideas.

I would like to thank all my colleagues in Institute for Metal Forming especially Joseph Sabol and Anthony Ventura at Lehigh University for useful discussion and technical comments. Also, I would like to thank Prof. Timotius Pasang the head of the Mechanical Engineering Department at AUT University, Auckland, New Zealand for inviting me at AUT and facilitating my training at Fletcher Aluminium-NZ. Also, many thanks to late Samuel Lawrence and William Mushock for their guidance in the lab.

Finally, I would like to thank King Saud University and the government of Kingdom of Saudi Arabia for supporting me throughout my graduate studies at Lehigh University, Pennsylvania, USA.

TABLE OF CONTENTS

List of Tables

List of Figures

Abstract

The automotive industry developments focused on increasing fuel efficiency are accomplished by weight reduction of vehicles, which consequently results in less negative environmental impact. Usage of low density materials such as Magnesium alloys is an approach to replace heavier structural components. One of the challenges in deformation processing of Magnesium is its low formability attributed to the hexagonal close packed (hcp) crystal structure. The extrusion process is one of the most promising forming processes for Magnesium because it applies a hydrostatic compression state of stress during deformation resulting in improved workability. Many researchers have attempted to fully understand solid state bonding during deformation in different structural materials such as Aluminum, Copper and other metals and alloys. There is a lack of sufficient understanding of the extrusion welding in these materials as well as very limited knowledge on this subject for hollow profiles made from Magnesium alloys. The weld integrity and the characteristic of the welding microstructure are generally unknown. In this dissertation three related research projects are investigated by using different tools such as microstructure characterization, mechanical testing, thermo-mechanical physical simulation and finite element numerical modeling. Project 1: Microstructure characterization supported by mechanical testing of the extrusion welding regions in Magnesium alloy

AM30 extrudate. The microstructure characterization was conducted using Light Optical Microscopy (LOM), in addition to LOM the electron backscattered diffraction (EBSD) technique was implemented to characterize in depth the deformed and welded microstructure.

Project 2: Finite element numerical simulation of AM30 extrudate to model different process parameters and their influence on localized state variables such as strain, strain rate, temperature and normal pressure within the weld zone.

Project 3: Physical simulation of the extrusion welding by using Gleeble 3500 thermo-mechanical simulator to create deformation welds in Magnesium alloy AM30 samples in compression test under various temperatures and strain rates conditions.

Based on the obtained results from the performed research projects and literature review, a new qualitative criterion of extrusion welding has been introduced as contribution to the field. The criterion and its analysis have provided better understanding of material response to processing parameters and assisted in selecting the processing windows for good practices in the extrusion process. In addition, the new approach contributed to better understanding and evaluating the quality of the solid state bonding of Mg alloy. Accordingly, the criteria help to avoiding formation of potential mechanical and metallurgical imperfections.

1. Introduction:

1.1 *Motivation*

The automotive industry developments in increasing the fuel efficiency are accomplished by weight reduction of vehicles, which consequently result in less negative environmental impact. Magnesium is considered one of the lightest metals for structural usage in automotive industry. It has low density of 1.7g/cm^3, only two third of Aluminum density. The global consumption of Magnesium alloys in automotive industry reached 214,000 tons in 2012 [1] (see Figure 1-1). It was reported in 2006 that the growth rate in the consumption of Magnesium was around 10-15 % per annum [2]. The average weight of Magnesium is around 10-12 lbs in the U.S. car's weight of an average 3,360 lbs, which is considered small in comparison to Steel/ Cast Iron of 2,150 lbs, Aluminum of 280 lbs and plastics of 260 lbs. There is a strategic goal [2] to increase the total average vehicle Magnesium content to 350 lbs by year 2020, which is equal to 340 lbs increase that will replace 630 lbs of ferrous and/or Aluminum parts. This substitution will reduce the car weight by around 290 lbs and will result in consequently less energy consumption and less environmental impacts. Magnesium is used also in motorcycles, aircrafts, electronic devices such as personal computers, cell phones and laptops etc.

1.2 *Magnesium and its alloys*

Magnesium has interesting advantages but also has some disadvantages as an engineering structural material in comparison to Steel and Aluminum. The advantages are high specific strength, suitable for die casting, good machinability in high speed and good weldability in certain atmospheric conditions [3]. In comparison to polymer materials, Magnesium has better mechanical properties, better thermal conductivity and it is recyclable. On the other hand, Magnesium has some disadvantages such as limited corrosion resistance in some application [3], low elastic modulus around 45GPa in comparison with other light metal Aluminum has 69GPa and Iron has 207 GPa.

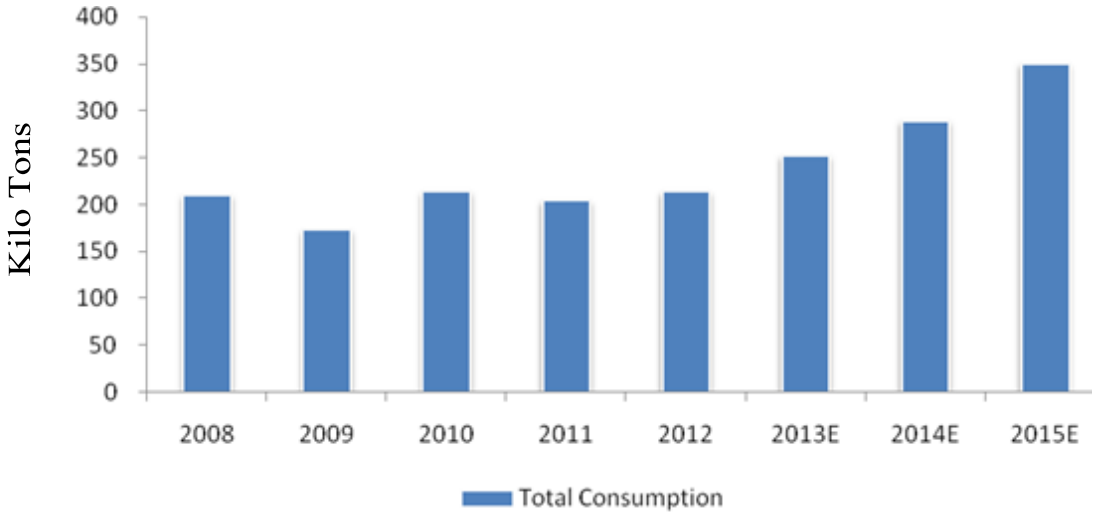

Figure 1-1. Global Automotive Magnesium Alloys Consumption, 2008-2015 (estimated) [1]

Magnesium is a crystalline material with hexagonal closed pack (HCP) crystal structure. It exhibits more brittle behavior compared to other crystal structures such as face centered cubic (FCC) and body centered cubic (BCC). This behavior is attributed to the deformation mechanisms in HCP metals [4]. In terms of workability, Magnesium deformation is limited under cold working conditions. To overcome this limitation it is recommended to deform Magnesium and its alloy at elevated temperature 200°C- 400°C. However, Magnesium has limited strength and creep resistance at these temperatures [3]. It is well known that deformation in metals occurs as a result of slip or twinning. In HCP, at room temperature, the number of independent activated slip systems is limited to two. According to von Mises yield criterion, five independent systems are needed for a homogeneous deformation [5]. The crystal tends to be deformed by twinning rather than slipping. The slip can occur along the basal planes (0001) where the slip directions are perpendicular to c-axis of the crystal. However, this will not allow for contraction or extension of the c-axis. To accommodate for the crystal shape change during deformation, Magnesium prefer to twin on $\{10\bar{1}2\}$ planes to extend the c-axis, or twin on the $\{10\bar{1}1\}$ planes followed by re-twinning on the $\{10\bar{1}2\}$ planes to contract the c-axis [5][6]. The formability of the Magnesium alloys can be increased by the hot working at elevated temperature above 200°C where the activation of additional slip systems

such as pyramidal one at $\{1\bar{1}01\}\langle 11\bar{2}0\rangle$ and/or prismatic one at $\{10\bar{1}0\}\langle 1\bar{2}10\rangle$ and $\{1\bar{2}12\}\langle 1\bar{2}13\rangle$ <c+a> occurs see Table 1-1 [7][8].

Table 1-1. Slip systems and twining system in HCP crystal structure [8]

Slip systems	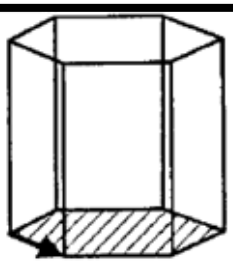 $\{0001\}\langle 1\bar{2}10\rangle$ Basal	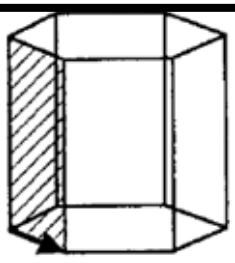 $\{10\bar{1}0\}\langle 1\bar{2}10\rangle$ Prismatic
	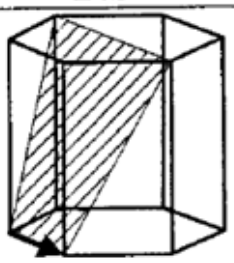 $\{1\bar{1}01\}\langle 11\bar{2}0\rangle$ Pyramidal	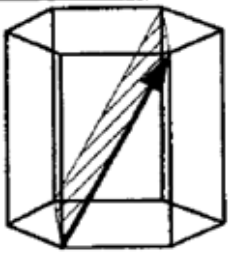 $\{1\bar{2}12\}\langle 1\bar{2}13\rangle$ <c+a>
Twinning systems	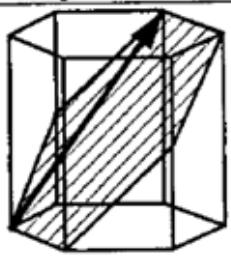 $\{10\bar{1}2\}\langle\bar{1}011\rangle$ Extension	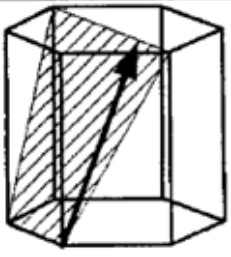 $\{1\bar{1}01\}\langle\bar{1}102\rangle$ Contraction

Like most pure metals Magnesium does not have a high strength. So it is alloyed with other elements in order to modify its mechanical properties. However, The limited solubility of alloying elements in Magnesium is curbing the improving of the mechanical properties and chemical behavior [3].

ASTM International has designated Magnesium alloys based on chemical composition and tempers [9] as follows: using AZ91E-T6 as an example, first part, indicates the two principal alloying elements consists of two code letters representing the two main alloying elements arranged in order of decreasing percentage (or alphabetically if percentages are equal). A-aluminum B-bismuth C-copper D-cadmium E-rare earth F-iron G-magnesium H-thorium K-zirconium L-lithium M-manganese N-nickel P-lead Q-silver R-chromium S-silicon T-tin W-yttrium Y-antimony Z-zinc. [9]

The second part indicates the amounts of the two principal alloying elements. It consists of two numbers corresponding to rounded-off percentages of the two main alloying elements and arranged in the same order as alloy designations in the first part [9]

The third part, distinguishes between different alloys with the same percentages of the two principal alloying elements. A- first compositions, registered ASTM B- second compositions, registered ASTM C- third

compositions, D- high purity, registered ASTM E- high corrosion resistant, registered ASTM X1- not registered with ASTM

The fourth part, indicates condition (temper). It consists of a letter followed by a number (separated from the third part of the designation by a hyphen). F- as fabricated O- annealed H10 and H11- slightly strain hardened H23, H24, and H26- strain hardened and partially annealed T4- solution heat treated T5- artificially aged only T6- solution heat treated and artificially aged T8- solution heat treated, cold worked, and artificially aged [9].

Mg-Al-Zn system is the most principal materials in Magnesium casting alloy used in ambient temperature [6]. It has been found that addition of 3% Aluminum improves the extrudability of the alloy [10]. Although, it is easier to cast Aluminum alloys that have 5%- 6% due to the wide freezing range. However, this will affect the extrudability due to the increased hardness [10]. The role of Zinc in Magnesium alloys is to increase the strength of the Magnesium. However, Zinc decreases the ductility and increases the hot shortness [10]. Also, It is has been reported that Zinc have effects to accelerate the corrosion rate.

During the late 1990's the most Magnesium alloys used in the metal forming were processed by extrusion and forging [11]. The most typical extrusion alloys are AZ61 (Mg-6Al-1Zn), ZK60 (Mg-6Zn-0.6Zr), while forging alloys are AZ80 (Mg-8Al-0.5Zn) and ZK60.

Recently, as reported in [12] AZ31(Mg-3Al-1Zn) is the common alloy used in metal working. According to Busk et.al AZ31 can be extruded faster than AZ61 (Mg-6 Al-1 Zn) and ZK60 (Mg-6 Zn-0.5 Zr) [13]. However, AZ31 alloy does not meet some specific properties and production requirement of the extrusion process for selected shapes that have been commonly used in the automotive industry.

In early 21st century, General Motors has developed and introduced a new Magnesium alloy AM30 [10] which provides a good combination of ductility, strength, extrusion speed and corrosion resistance. Table 1-2 shows the chemical composition of standard AZ31 and new AM30 alloys presenting their chemistry. The amount of Zinc in AM30 is significantly reduced from 1.05 % to 0.16% to improve the ductility.

Table 1-2. The Chemical Compositions of Magnesium alloys AZ31 and AM30 (Weight Percent) [10]

Alloy	**Al**	**Mn**	**Zn**	**Fe**	**Ni**	**Cu**
AZ31	3.1	0.54	1.05	0.0035	0.0007	0.0008
AM30	3.4	0.33	0.16	0.0026	0.0006	0.0008

The addition of Manganese is commonly used in Magnesium alloys as an additive [14]. This addition improves the corrosion resistance of Mg-Al alloys. However, it does not change yield strength but it increases the

tensile strength as shown in Figure 1-2. Also, the ductility has increased about 50% AM30 at room temperature [10].

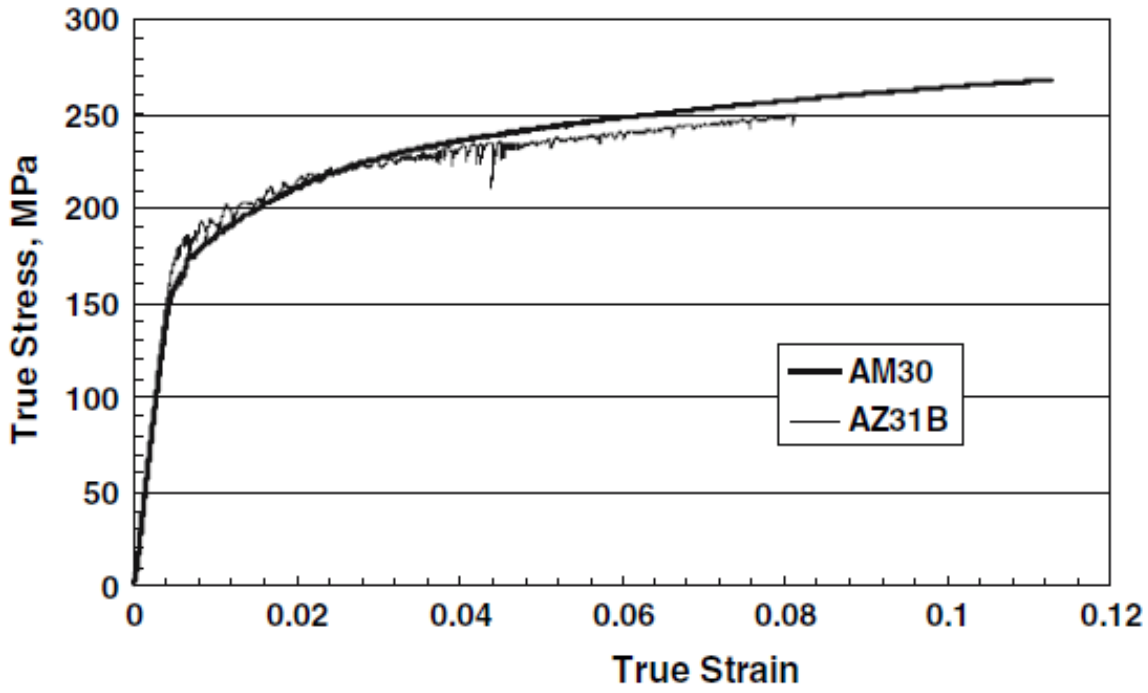

Figure 1-2. Typical tensile curves of AM30 and AZ31 alloy at room temperature [10].

The effect of temperature on the yield strength is shown in Figure 1-3. It can be seen that AM30 exhibits lower yield strength in comparison to AZ31 at different temperatures. However, at room temperature AM30 has higher ductility than AZ31 (see Figure 1-4) which leads to higher extrudability [10].

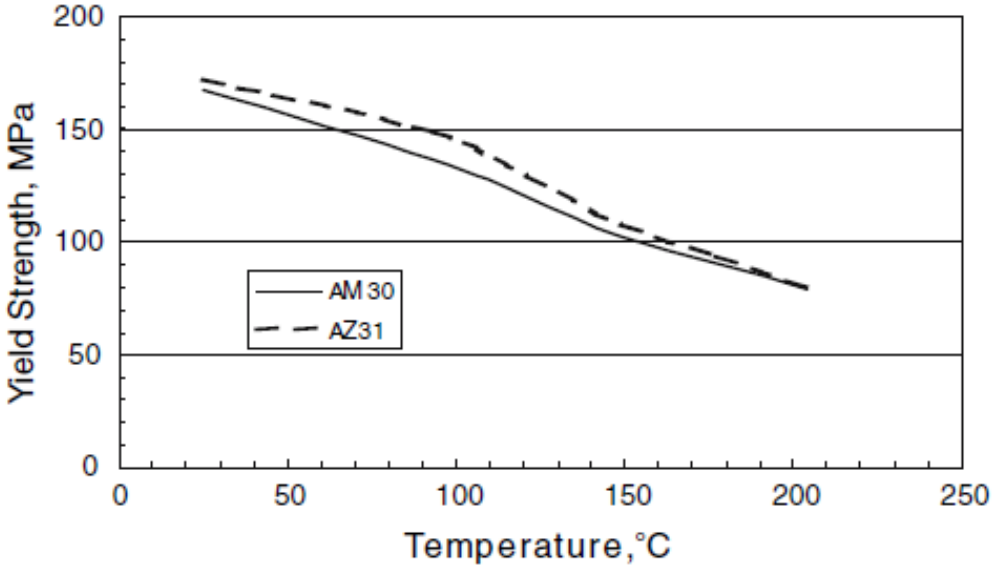

Figure 1-3. The effect of the temperature on the yield strength of AM30 and AZ31 alloy [10]

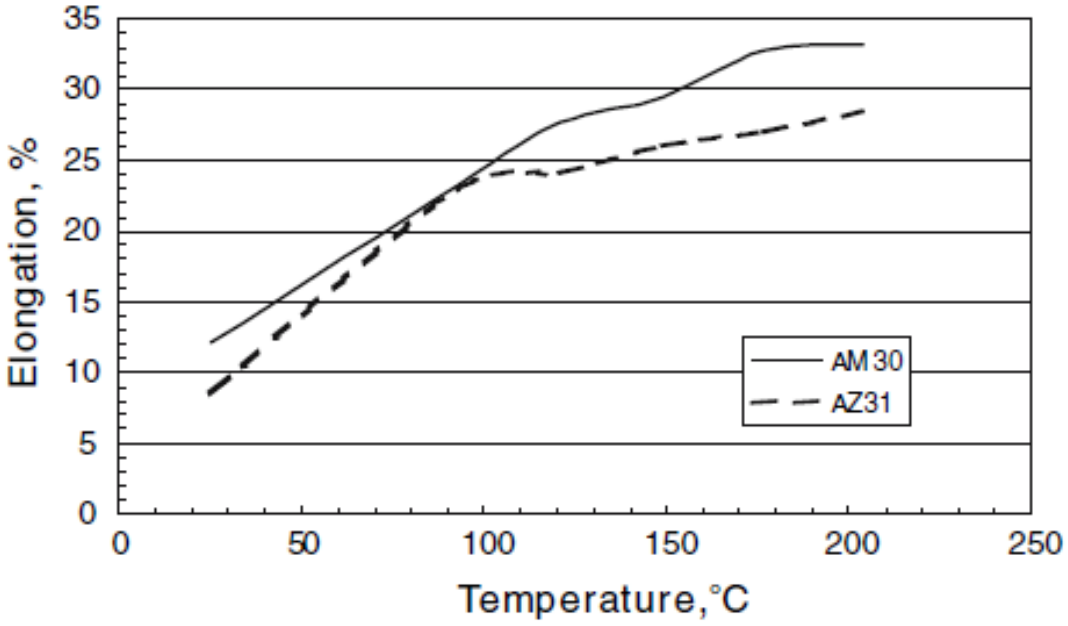

Figure 1-4. The effect of the temperature on elongation of AM30 and AZ31 alloy [10]

1.3 *Extrusion*

Extrusion is a process in which wrought products are formed by forcing a billet through a die opening with a required shape [15]. There are many classifications of the extrusion process based on temperature, lubrication and relative motion between the ram and the billet.

1.3.1 Extrusion Types

In terms of temperature, there is hot extrusion where the process is performed at elevated temperature above recrystallization temperature which is about 0.6 of the material melting temperature on the absolute scale. In contrast, the cold extrusion for most of the metals and alloys is performed at room temperature or close to it. Finally, warm extrusion is performed above the room temperature and below the recrystallization temperature where the process parameters can be optimized to combine the advantages of both cold and hot work. Some materials cannot be formed by cold extrusion especially when the shape is too complex. The hot extrusion process is used to produce different solid and hollow shapes such as rods, bars, tubes, strips and wires.

The second classification is based on the lubrication. As a consequence of that, there are three different types [16].

1) Nonlubricated extrusion process where a flat-face die is used and the billet is pushed inside the container where the dead metal zones are formed between the container and the die as shown in Figure 1-5 a.

2) Lubricated extrusion where a suitable lubricant is used between the billet, the container and the die Figure 1-5 b.

3) Hydrostatic extrusion in which a fluid layer under a pressure would deforms the material and pushes it through the die Figure 1-5 c.

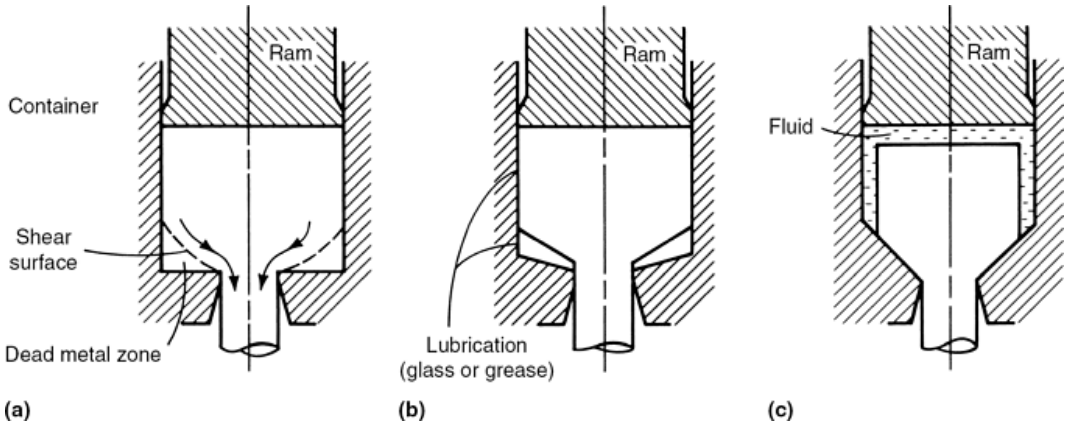

Figure 1-5. Schematic illustrations showing the major difference between (a) nonlubricated extrusion, (b) lubricated extrusion, and (c) hydrostatic extrusion processes [16]

Based on the relative motion between the billet and the tolling, there are three extrusion types. The first type is direct extrusion where the billet is pushed through die in the same direction of the ram as shown in Figure 1-6a. However, in the second type- indirect extrusion- process, the billet is being pushed in the opposite direction by the ram with installed

die as shown in Figure 1-6b. Accordingly, the friction between the container and the billet in the direct extrusion is higher than the indirect extrusion and consequently more energy is required to performed the process (see Figure 1-7). To take advantage of the friction force there is another method called indirect extrusion with active force where the container and the billet are moving with different speeds. This creates a unidirectional metal flow and exploits the friction force [17].

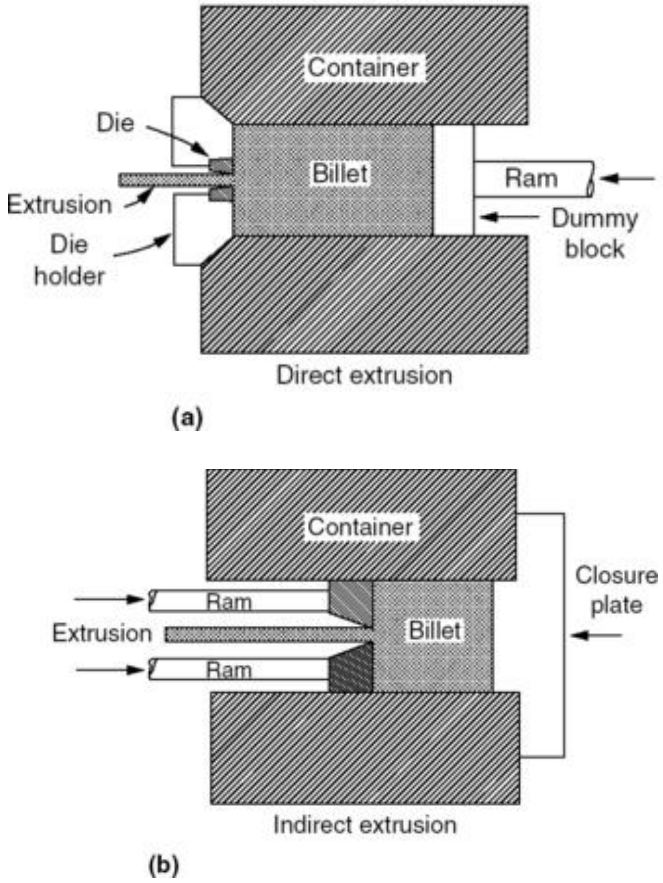

Figure 1-6. (a) direct extrusion and (b) indirect extrusion [15]

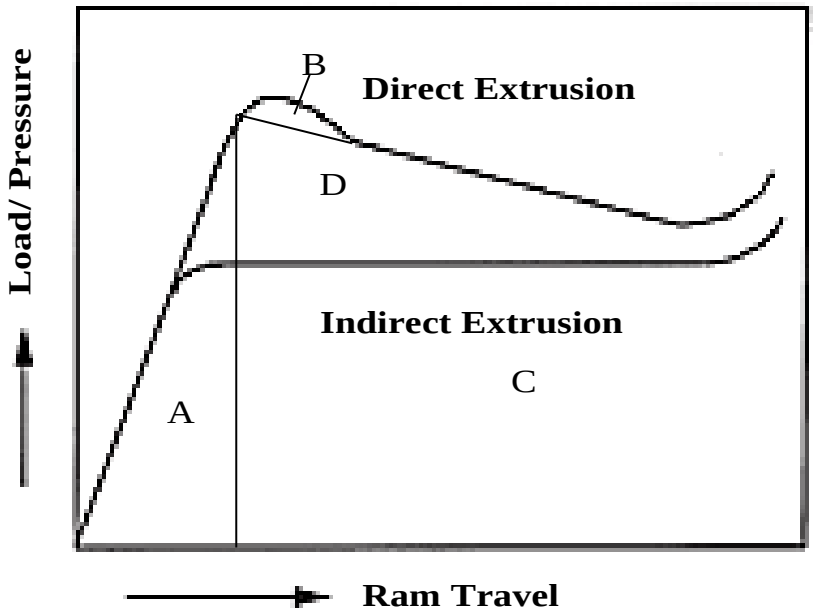

Figure 1-7. Variation of load or pressure as a function of ram travel for both direct and indirect extrusion process. A, work of upsetting; B, work to initiate deformation; C, work of deformation; D, work needed to overcome friction and shearing in direct extrusion. [16][18]

There are different shapes of extrusion profiles. Mainly they are classified in to two types: 1) solid shapes 2) tubes and hollow shapes [18]. The solid shapes are produced by direct or indirect extrusion. It can be seen from Figure 1-7 that indirect extrusion consumes more work to overcome the friction and shearing between billet and container. The typical die configuration by using feeder plate die as shown in Figure 1-8 is used to balance the metal flow and also to make a continuous extrusion. While solid die have a bearing length which control size, shape, finish, and speed of extrusion where (see Figure 1-9) [18].

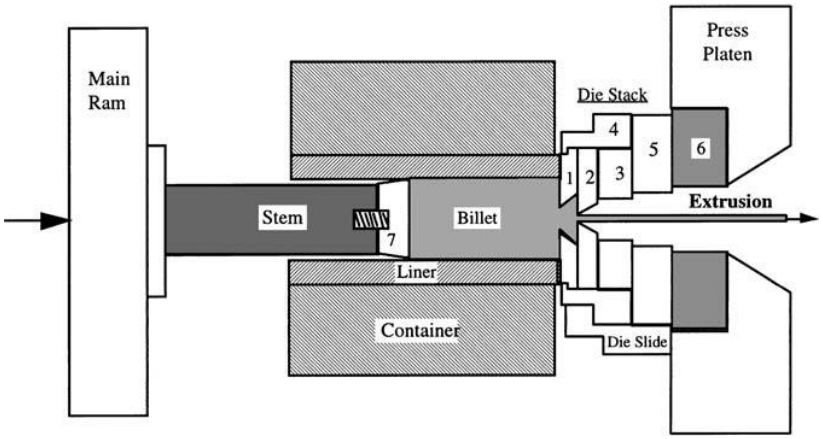

Figure 1-8. Tooling configuration in direct extrusion process with feeder plate die for softer alloy. 1, feeder plate; 2, die; 3, backer; 4, die ring; 5, bolster; 6, pressure pad; and 7, fixed dummy [18]

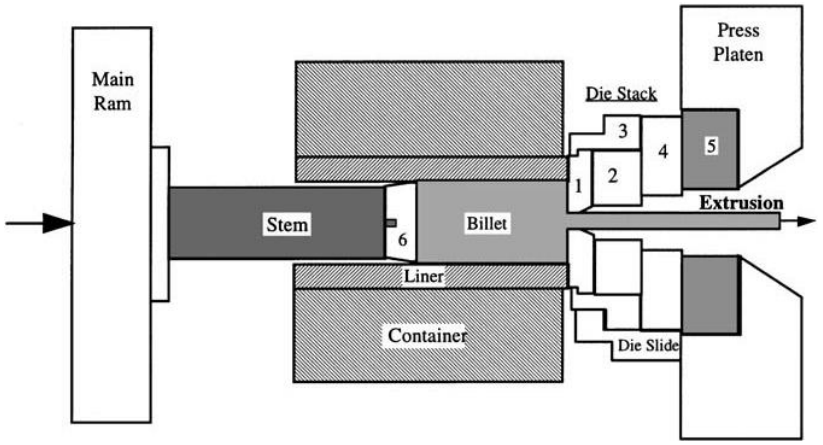

Figure 1-9. Tooling configuration in direct extrusion processing with a solid die for harder alloy. 1, solid die; 2, backer; 3, die ring; 4, bolster; 5, pressure pad; and 6, floating dummy [18]

On the other hand, hollow sections and tubes are extruded by using two different tolling configurations, a die with mandrel or using a porthole die. By using a die with mandrel the material is pushed by the stem and the mandrel inside the container where a seamless tube is formed (see Figure 1-10. However, porthole die is used to extrude a profile with

welding joint occurs in a welding chamber as shown in Figure 1-11. Usually a porthole die is used for more complex hollow sections while a die with mandrel used for simpler shapes such as thick tubes.

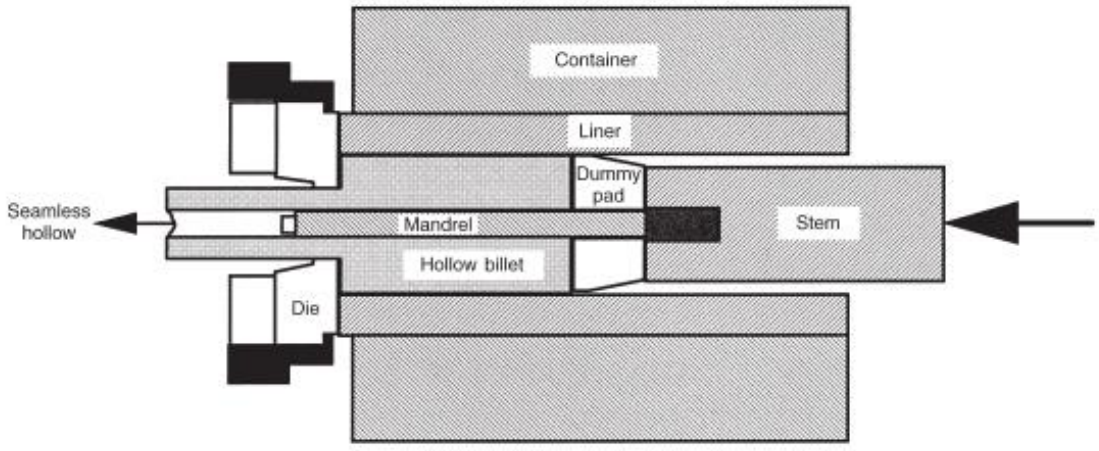

Figure 1-10. A die with mandrel configuration to produce hollow profiles [18]

In a hollow-section extrudate such as shown in Figure 1-11, a billet was extruded through a porthole die presented in Figure 1-12 where billet material is separated by die arms into strands and then re-joined together by high temperature and pressure in the welding chamber within the porthole die. This joining process occurs as longitudinal solid-state bonding and is known as extrusion welding.

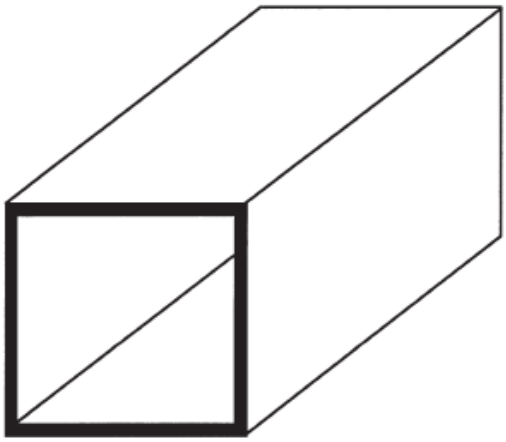

Figure 1-11 Holow-section profile **[18]**

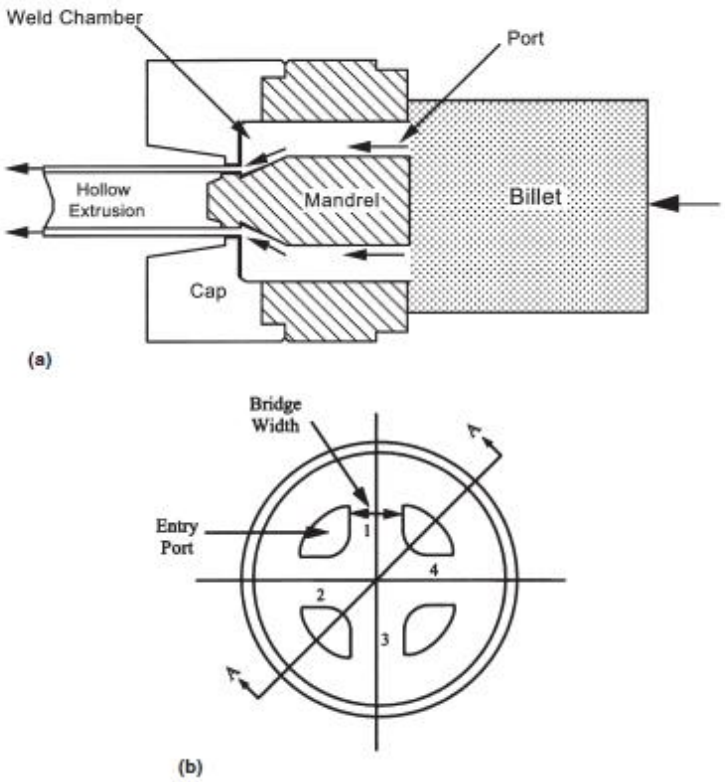

Figure 1-12. Schematic of welding chamber porthole die hollow extrusion. (a) Cross section showing metal flow into port streams and around the mandrel. (b) Billet entrance face of the die set [18]

The solid state bonding occurs when the two metallic surfaces meet together as shown in Figure 1-13 [19]. When the spacing between the atoms is around a crystal lattice, the bond is started to form. With the pressure and the temperature inside the welding chamber, the adhesion between the two surfaces is increased. With more pressure and more temperature, the bond strength is increased because of the more flatten surfaces are appeared which will provide more surfaces contact and therefore more homogenous plastic deformation. This will lead to shearing off the asperities and break the peaks that appear on the two surfaces and form a good seam weld [20].

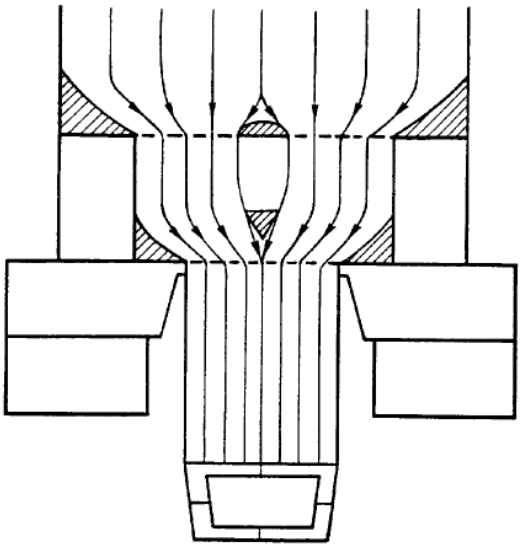

Figure 1-13. The flow through a porthole die [18]

1.3.2 Extrusion Defects

Every product could have some defects that should be avoided during the extrusion process by applying a good quality control. There are many defects that appear in the extrusion profiles such as weak extrusion weld joint, streak, surfaces cracks, die line and blister. These defects could be related to one or more than one of the following extrusion factors: metallurgical variables, billet casting, initial billet and container temperature, extrusion ratio, die design, extrusion speed, extrusion temperature and lubrication system [18]. The quality of the extrusion welding is one major type of defect that is not completely understood. The improper bonding is precisely influenced by the pressure, temperature, velocity of the material inside the welding chamber and the die design. Figure 1-14 shows a defect on the longitudinal extrusion welding.

Making defect free products are the main objective of most extrusion companies. Many important outlines to check the quality of the extrusion process can be summarized in Figure 1-15

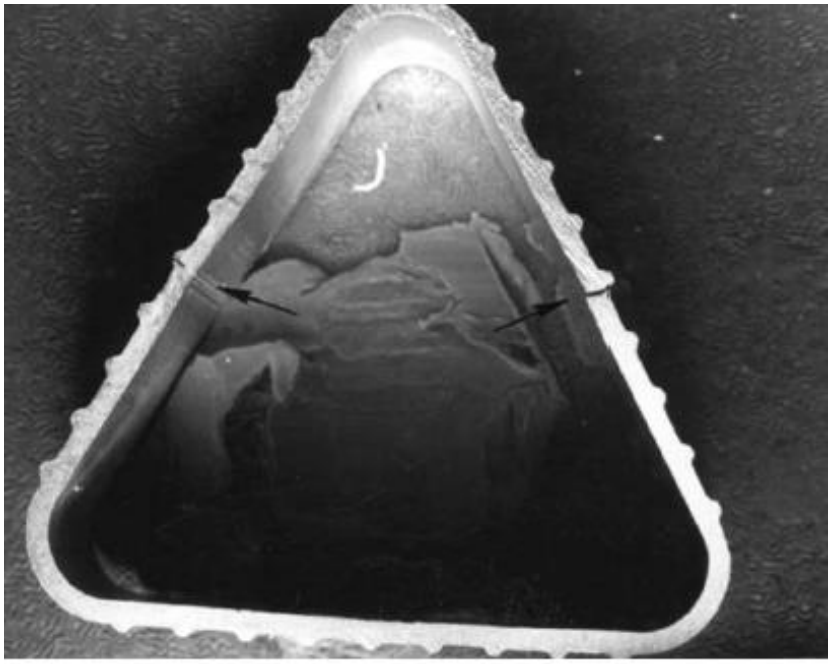

(a)

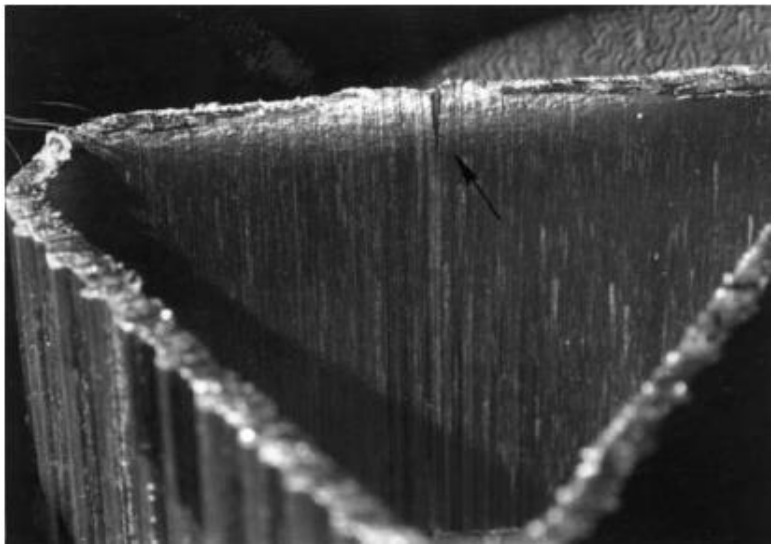

(b)

Figure 1-14. Improper weld joint in hollow shape extrusion (a) Full cross section showing two poor-quality welds (b) Partially bonded joint. [18].

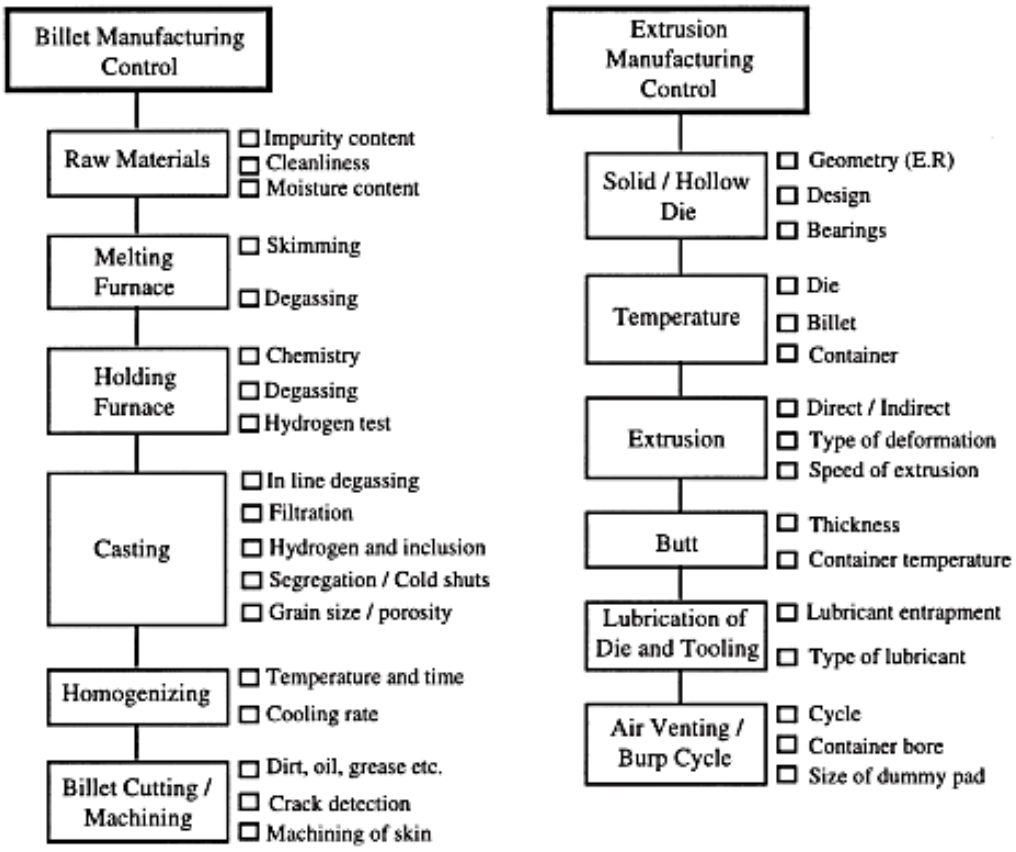

Figure 1-15. Billet casting and extrusion manufacturing control process to eliminate potential extrusion defects [18].

1.4 *Research Objectives*

A strong bonding within the seam welds is one of the most important requirements during the extrusion of many hollow profiles used in the transportation applications. The integrity of the weld microstructure is very substantial to avoid any potential failures during operation. The design of the extrusion die and control of the process parameters play a role in determining the quality of the weld bonding. All of these factors affect the microstructure of the final product and consequently its mechanical properties. Many researchers have attempted to fully understand solid state bonding in different structural materials such as copper and Aluminum. However, there is a lack of sufficient understanding of the extrusion welding in these materials and very limited in hollow Magnesium alloys profiles in terms of the integrity and the quality of the welding microstructure.

In this dissertation three research projects are investigated by using different tools such as microstructure characterization, mechanical testing, thermo-mechanical physical simulation and finite element numerical simulation (see Figure 1-17).

Project 1: Microstructure characterization supported by mechanical testing of the extrusion welding regions in Magnesium alloy AM30 extrudate (see Figure 1-16). The microstructure characterization was conducted using Light Optical Microscopy (LOM), In addition to (LOM)

the electron backscattered diffraction (EBSD) technique was implemented to characterize deformed and welded microstructure.

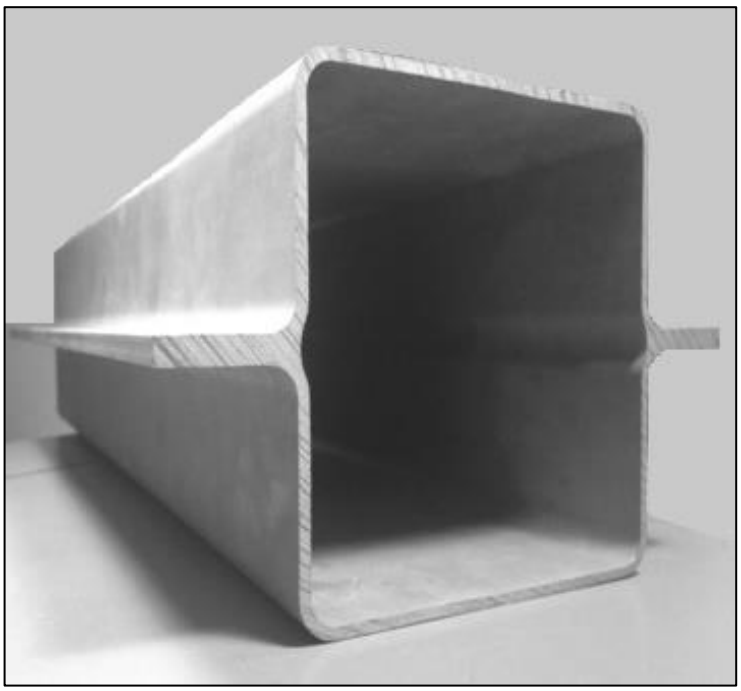

Figure 1-16. Hollow section profile of Magnesium Alloys AM30

Project 2: Finite element numerical simulation of AM30 extrudate to model the different process parameters. The simulation was conducted using HyperXtrude® finite elemt package.

Project 3: Physical simulation of the extrusion welding by using Gleeble 3500 thermo-mechanical simulator. The physical simulation was performed using different strain rate and temperatures.

Based on the results of the previous research work a new qualitative criterion of extrusion welding has been proposed as contribution to the field. The previous mentioned analyses have provided better

understanding of material response to processing parameters and assist in selecting the processing windows for good practices in the extrusion process. In addition, the presented study will contribute to better understanding and evaluating the quality of the solid state bonding and joining of Mg alloys and will help avoiding formation of potential mechanical and metallurgical imperfections

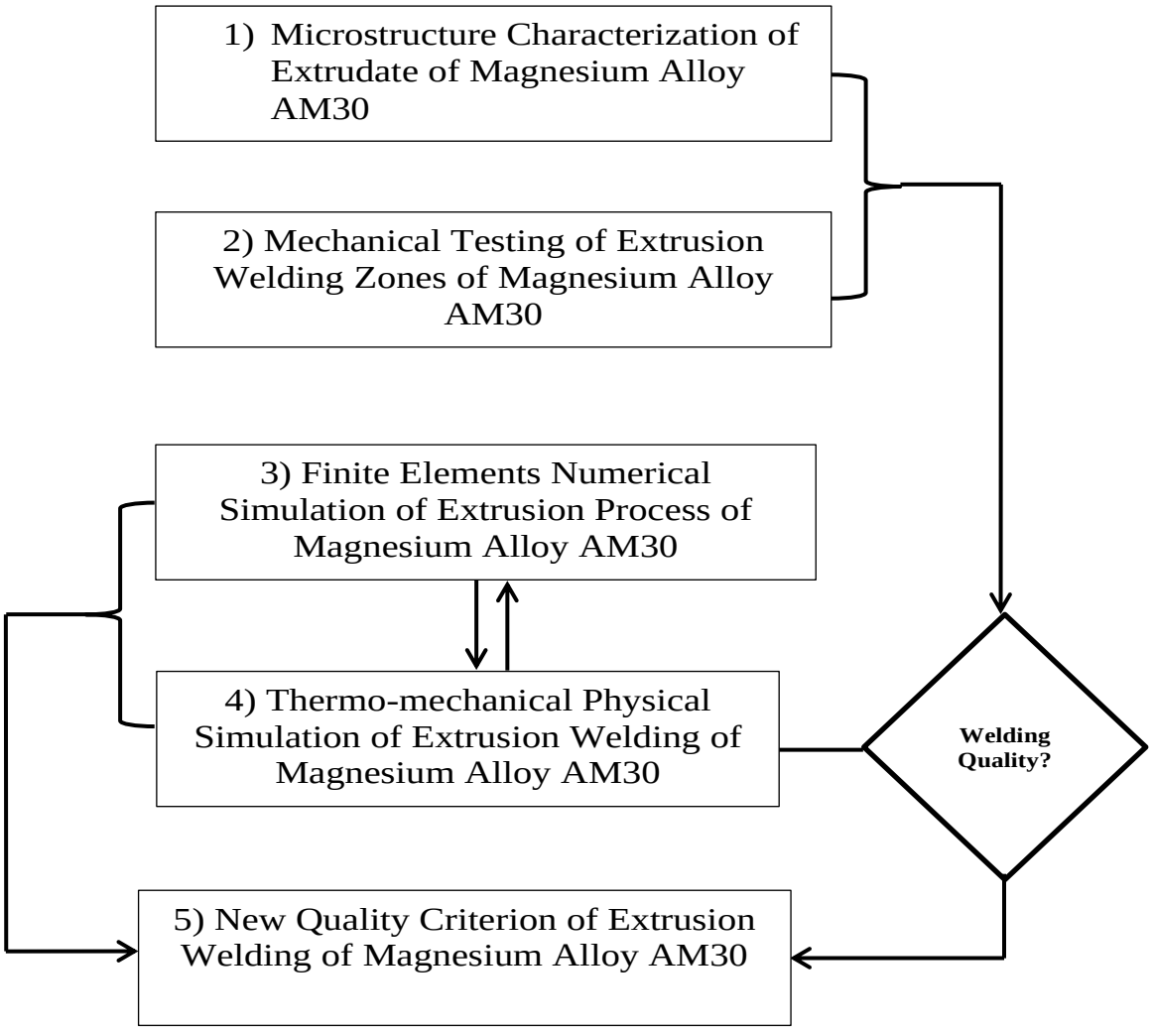

Figure 1-17 Flow diagram of the conducted research

1.5 *Dissertation Structure*

There are six chapters in this dissertation describing an integrated approach of analyses including microstructure characterization, mechanical testing, numerical simulation and experimental physical simulation.

Chapter 1: Introduction of the research field including motivation and a brief summary about Magnesium and Magnesium alloys including more information for Magnesium alloy AM 30, which is the subject of this research. In addition, brief background of extrusion process and extrusion welding as well as extrusion defects are presented. This chapter is finished with a presentation of research objectives.

Chapter 2: Microstructure characterization of industrial AM30 extrudate profile is provided. An introduction to the laboratory techniques that have been used is presented as well as a literature review of the previous studies. On the subject of different techniques for sample preparation are discussed. Accordingly, microstructure characterization micrographs and mechanical testing micro hardness results are presented. At the end of the chapter a discussion of the results is delivered.

Chapter 3: Numerical simulation of a double hat Magnesium alloy AM30 extrudate is presented. The finite element method and the software used for the research are introduced. Then, extrusion modelling setup for AM30 as well as flow stress model are described. After that, the results of the hot extrusion for different process conditions are presented in form of

contours plots. Accordingly, the influence of different ram speeds and temperatures on the localized state variables - temperature, strain rate and normal pressure on weld zone has been compared and discussed. The results of this chapter are used as guide lines for design of experiments of the physical simulation. Also, the presented results are used for establishing of a new criterion for the extrusion weld integrity.

Chapter 4: Physical simulation of extrusion welding of Magnesium alloy AM30 is the focus of the presented research. An introduction to the thermo-mechanical physical simulator Gleeble 3500 is presented. Also, several studies of physical simulation of extrusion welding have been reviewed. Then, experiment setup, measurements and analysis of normal pressure that ensure weld integrity are discussed.

Chapter 5: New criterion for evaluation extrusion welding quality is proposed. A review and comparison of existing criteria have been provided. Then, the methodologies of the criteria are discussed. Different process conditions have been applied to evaluate their extrusion welding quality.

Chapter 6: Summary, Conclusion and future studies.

This chapter summarized the work that has been done so far and presents the research results conclusion for each research topics. Finally, future studies have been recommended for further investigations and analyses.

2 Microstructure Characterization of AM30 and Mechanical Testing

2.1 *Introduction*

Understanding the microstructure evolution of the extruded hollow section profiles is very important. In other words, the microstructure of the profile such as grain size and crystallographic orientation influence the mechanical properties of the final product. Many factors affect the evolution of the microstructure of the extrusion of hollow section profiles such as die design and the geometry of the container, porthole die, welding chamber and the bearing land length. In addition, the final product will be affected by the extrusion process conditions such as the billet temperature, container temperature, ram speed and pressure, all of which will affect the strain, strain rate and stress. Moreover, any subsequent heat treatment procedure could be applied to the extrudate such as annealing or quenching or a combination of more than one method. In this research, the objective is to focus on the integrity of the welding area of an extruded industrial hollow section profile of Magnesium alloy AM30 in terms of microstructure characterization and mechanical testing of the areas in the extrudate as shown in Figure 2-1.

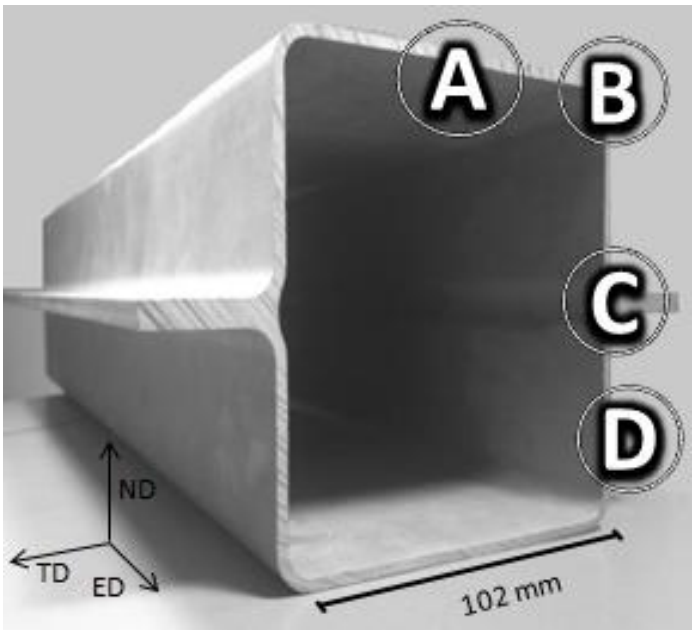

Figure 2-1. Investigated extrusion welding locations of the AM30 profile

2.2 *Literature review*

M. Engelhard et al. [21] have conducted extrusion experiments that focused on the Aluminum alloys AA 6060 and AA 6082. Microstructure characterization and mechanical testing of different samples with different billet temperatures and extrusion speeds are reported. Also, H. Matsuoka et al [22] have studied Aluminum alloy AA 6061 hollow extrudate sections with seam welding and without welding. Many tensile tests were conducted to compare the tensile strength. The results showed that the samples with welding have lower tensile strength than the non-welding samples. The metallographic investigation by Electron Backscatter Diffraction (EBSD) technique showed recrystallized grains in the welding region however, the non-weld part was the un-recrystallized one having

subgrains. Another study by Loukus et.al [23] investigated the seam welding and charge weld in Aluminum alloy AA6082-T4 (see Figure 2-2). They compared different tensile samples located at the weld location with different orientation 0˚, 45˚, 90˚ and offset to the tensile axis. Also, for comparison purposes a sample where taken from no weld regions. The result showed that the sample with weld 45˚ had the lowest tensile strength than samples in 90˚ and 0˚ orientations. In terms of the fracture, result showed that samples with weld exhibits a ductile fracture.

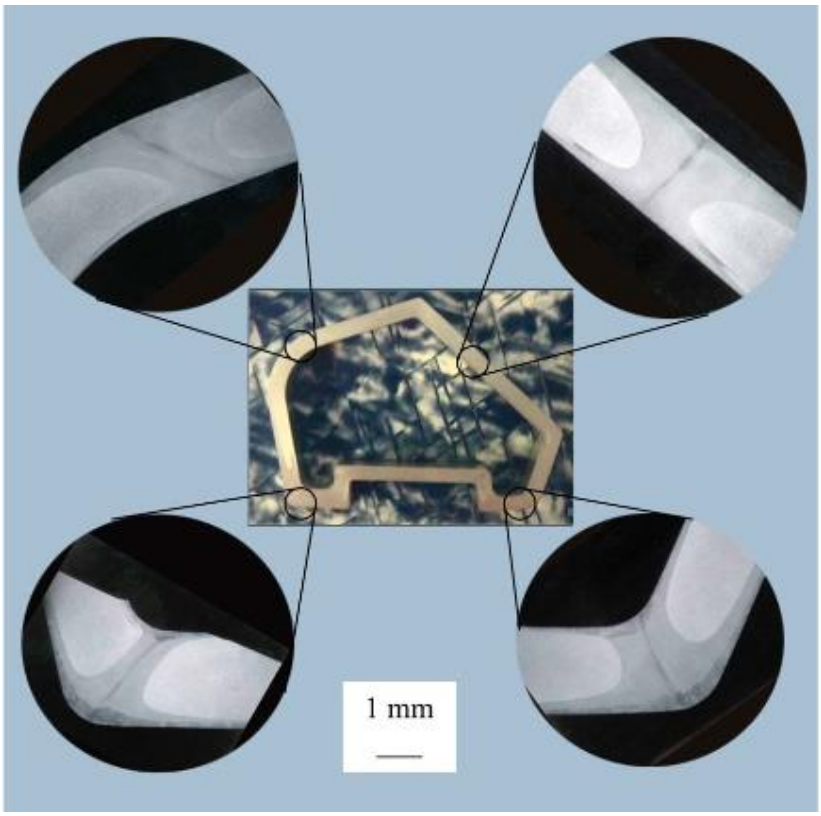

Figure 2-2. Micrographs of polished and etched A-pillar cross-section revealing the weld regions [23]

Furthermore, Nanninga et.al [24] have studied the effect of the presence of extrusion welding in fatigue life. The results showed 60% drop of the fatigue life in samples that have welds in comparison to the sample without welds.

Here at Lehigh, Van Geertruyden, Claves and Misiolek [25] have studied the crystallographic orientation map of the welding regions in Aluminum alloy AA6063 extrudate by using Electron Backscattered Diffraction. The results in Figure 2-3 show that the grains on the side of the welding region have the same texture as the extrusion direction <100>. However, inside the weld a random texture and <111> which could affect the strength and the quality of the weld integrity with the no weld regions.

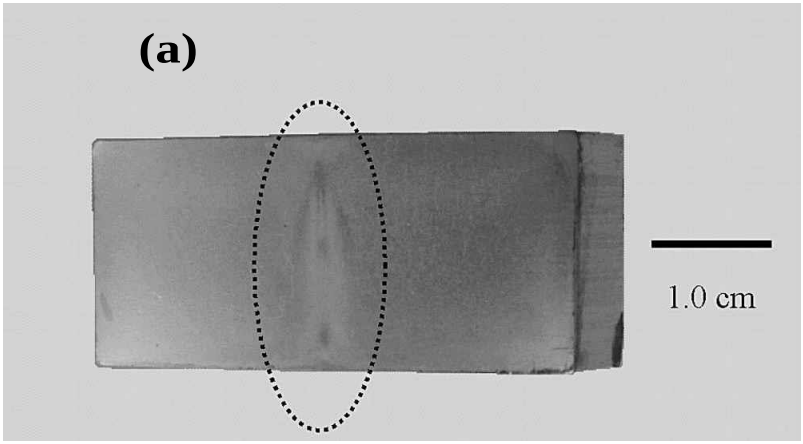

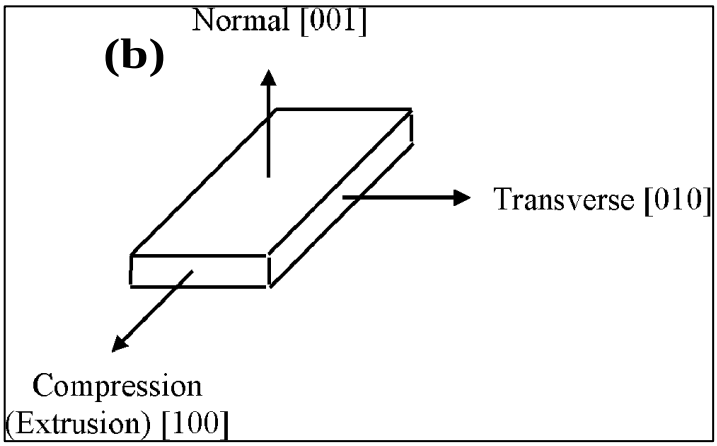

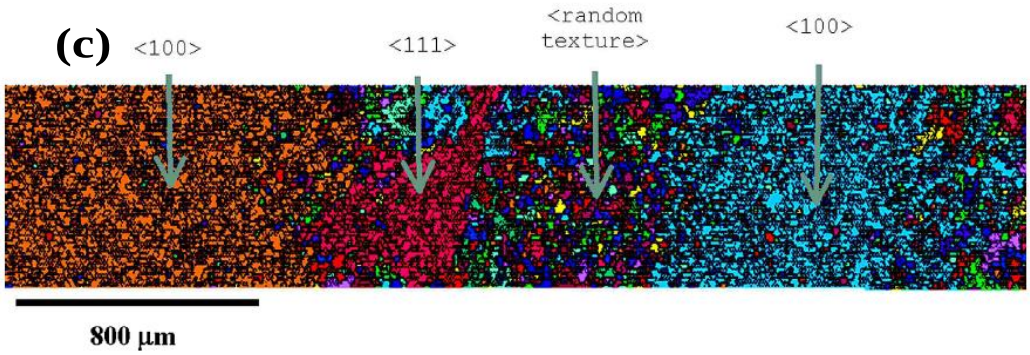

Figure 2-3. (a) Cross section of extrudate with the weld region in the center region, (b) notation of sample directions used EBSD analysis. (c) Grain map generated across the weld region showing the texture of the various regions. (Grain map is used courtesy of TexSEM Laboratories) [25]

For Magnesium alloys, Sikand et al. [26] have studied the microstructure and the mechanical properties of AM 30 tube extruadtes by using two different dies, a conventional conical dies with mandrel and port holes dies. The tubes fabricated using porthole die showed significant refinement in microstructure with improved mechanical properties, outside

the seam-joint portion, compared to the tubes fabricated using conical die with a mandrel.

In the early stage of the investigation of Magnesium Alloy AM30 here at Lehigh University, Brian F. Gerard and Wojciech Misiolek [27] have mechanically tested the same profile shown in Figure 2-1 and microstrucaturlly characterized it. The samples were cut as shown in Figure 2-4 for four different extruded sections (A, B, C, and D) and different orientations with respect to the welding region perpendicular (M), in the same direction (P) and offset to the welding region (S).

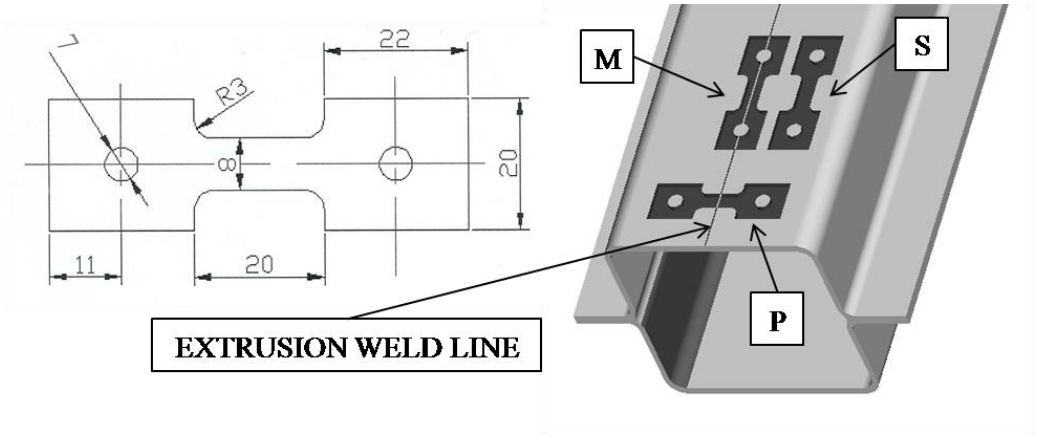

Figure 2-4. Tensile bar dimensions (mm) and locations within the AM30 double-hat extrudate. The thickness of the tensile bars is 2.54mm [27]

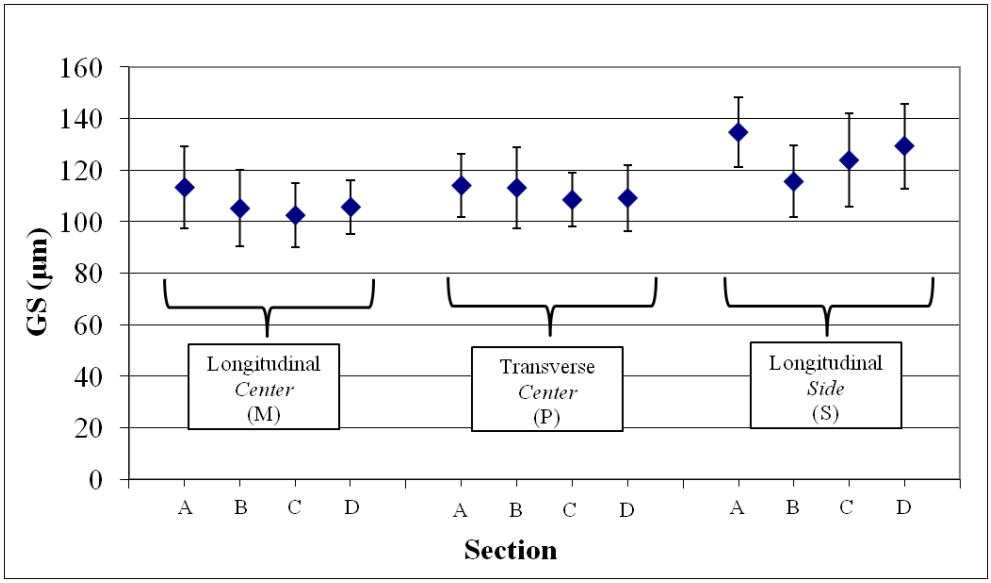

Figure 2-5. Grain size of each section (A-D) for each orientation (M, P, and S) measured using the ASTM-E112 three circle method [27]

The grain size of different samples is shown in Figure 2-5. By averaging each section, the grain size in location M is 107±14µm, S 126±17µm and P 111±13µm. The results show that the sample orientation has a strong influence on engineering stress-strain curves. The P orientation samples have a yield point significantly below that of the samples in the extrusion direction (M and S) [27].

2.3 *Microstructure characterization of Magnesium alloy AM 30*

During the investigation, a microstructure characterization was conducted by using a Light Optical Microscopy (LOM) -Olympus®- (see Figure 2-6) of the regions that contain an extrusion welding. Furthermore, an analysis was performed by using Electron Backscatter Diffraction

(EBSD) - Hitachi 4300SE/N (see Figure 2-7) to study the crystallographic orientation map in the extrusion welding regions within the profile in comparison to the pre-extruded billet.

Figure 2-6. Light optical microscopy -Olympus®, Nikon

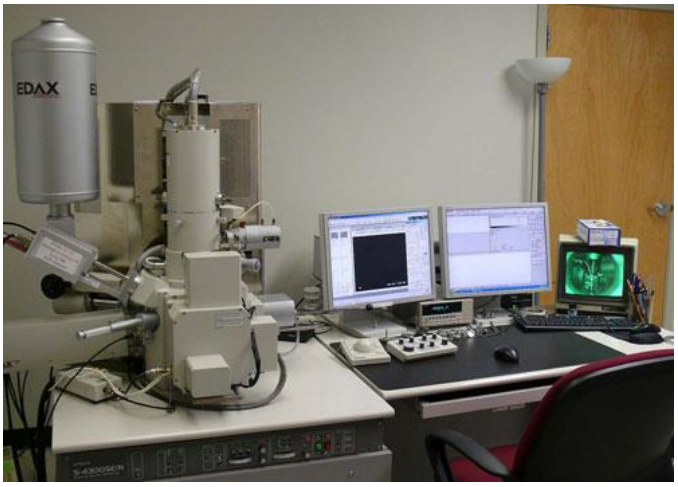

Figure 2-7. Electron Backscatter Diffraction in Scanning Electron Microscope -Hitachi 4300SE/N

2.3.1 Metallographic sample preparation

Metallographic sample preparation of Magnesium alloys can be challenging; these alloys are relatively soft and can be easily scratched during sample preparation. Polishing can induce twin deformation in the material, leading to difficulties in properly etching to reveal the microstructure. Some of the intermetallic particles from these alloys can be pulled from the sample by the polishing action and contaminate the polishing cloths, causing additional scratches. Furthermore, water should be avoided during the final polishing because Magnesium alloys have a tendency to stain when exposed to water [28]. As reported by Brian Gerard [27] a new technique is used for the preparation of AM30 samples for both Light Optical Microscopy (LOM) and Electron Backscattered Diffraction (EBSD). Due to the symmetry of the profile three different extrusion welding areas were investigated as indicated in (A, B and C) the forth location is used as a reference and is marked as (D) (see Figure 2-1).

2.3.2 Sample mounting and grinding

The samples were cut transversely to the extrusion direction in the mentioned location (A, B, C, D). Then, a resin epoxy is used for mounting as well as a vacuum was pulled any trapped air in the mounts. The mounted samples were labeled then ground by standard Silicon Carbide grinding papers (320, 400, 600) grit for 60 seconds each. Ethylene glycol was used as a lubricant instead of water to avoid and stain. Between each

step cotton and ethanol spray were used to clean the samples followed by air drying. The 600 grit grinding were performed twice to make sure that samples didn't have any contamination from the previous steps that could leave some small particles and consequently scratch the samples [27].

2.3.3 Mechanical polishing

In this step, alcohol based 6µm diamond suspension was used for 6 minutes on a Struers DP-Dur cloth and alcohol based lubricant in automatic polishing machine. It was set to a pressure equal to 50 N which considered a low pressure to not introduce any deformation twins. The samples were cleaned by ethanol spray and cotton followed by air-drying.

After the 6µm step, hand polishing was performed using an alcohol based 3 µm diamond spray on a Struers Mol cloth for two minutes and moderate pressure. Then the samples were dipped in ethanol and ultrasonically cleaned for 20 sec followed by ethanol spray and cotton then air drying. The final step of mechanical polishing was performed in Nap cloth for 3 minutes using 1 µm diamond spray with medium pressure. The same cleaning steps were used as in 3 µm [27].

2.3.4 Chemical polishing

Many chemical polishing solution were reported in the literature however most of them left a stain in Magnesium alloys [27]. A combination made of 8mL nitric acid (conc.), 12 mL hydrochloric acid

(conc.) and 100 mL ethanol were used for 8-10 second [29]. The solution left a white film over the surface, which can be ultrasonically cleaned by dipping the sample in methanol for 20 sec. After that, a methanol spray was used and followed by air-drying. The polished samples showed very flat surface if the exact time is maintained. However some samples showed a slight wavy surface. Most of the scratches have been removed but some will show up after the etching step.

2.3.5 Etching

For the sample that be used for Light Optical Microscopy (LOM), a solution of acetic picral (2g picric acid, 5mL acetic acid, 10mL H_20, 100mL ethanol) was used for 5 sec [30]. A brown film has appeared on the etched surface. After that, the sample was ultrasonically cleaned by dipping the sample in ethanol for 20 sec. Followed by ethanol spray and air-drying. Another etchant solution was used for Electron Backscattered Diffraction (EBSD) a solution of 5mL HNO_3, 15mL acetic acid, 20mL H_20, and 60mL ethanol for 4 sec [31]. Then, sample was ultrasonically cleaned by dipping the sample in ethanol for 20 sec. Followed by ethanol spray and air-drying.

2.4 *Micro hardness testing*

Micro hardness tests were performed to different regions. In this work, the focus was on the hardness profiles for three samples: A- sample from the pre-extruded billet, B- sample from location (A) in Figure 2-1 which contains a weld region, C- sample from location (C) in Figure 2-1 which contains another weld region. The samples were cut, ground and polished (6 µm, 3 µm , 1 µm) to ensure the flatness of the tested regions. The tests were performed according to ASTM International E384-08a Standard Test Method for Microindentation Hardness of Materials. A 300 gf used for 15 sec by vickers indenter in LECO M-400 Hardness Tester shown in Figure 2-8

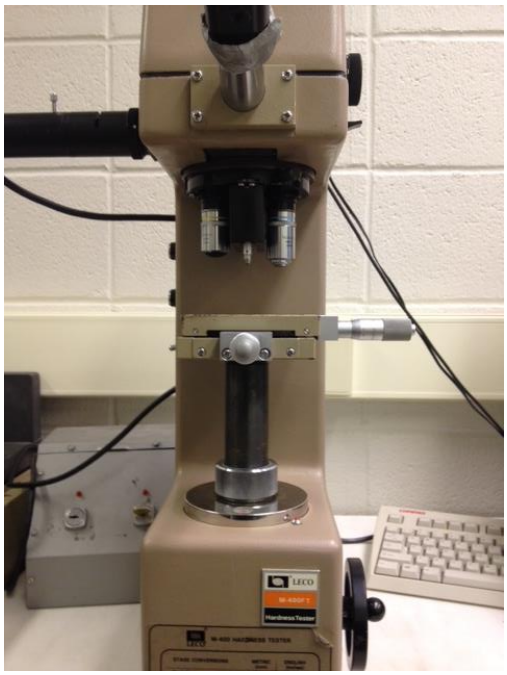

Figure 2-8. Micro hardness tester LECO M-400

2.5 *Results*

2.5.1 Light optical microscopy results

Polarized Light Optical Microscopy (LOM) was used to analyze the microstructure of the extrudate in each of the four locations "A" through "D" shown in Figure 2-1 . Figure 2-9 shows the difference in grain sizes between the middle of the image where the extrusion welding has taken place and the rest of the extrudate near the edge of the image representing less modified alloy microstructure in the welding chamber. Figure 2-10 is a magnified image that was captured in the middle of the specimen in location A (see Figure 2-9), which shows good extrusion weld integrity with no visible weld line [28].

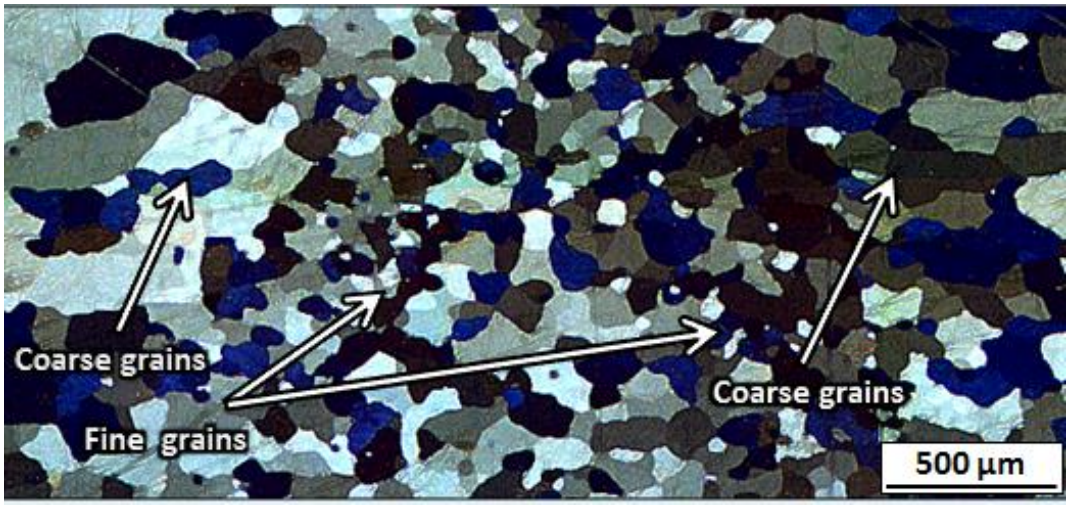

Figure 2-9. Polarized LOM mosaic image of location (A) of the extrudate **[28]**

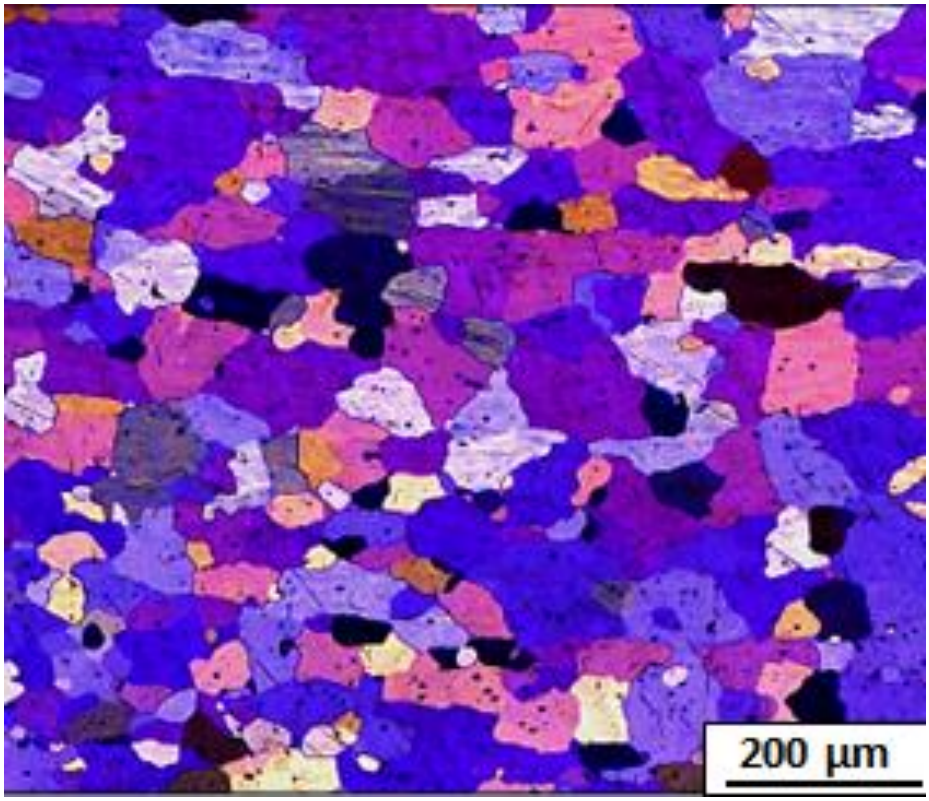

Figure 2-10. A good welding integrity in location (A) **[28]**

On the other hand, Figure 2-11 and Figure 2-12, from locations B and C, respectively, both show different types of extrusion welding with a curved weld line. The presence of the line is most likely due to the oxidization of the individual strands' surfaces during extrusion, or insufficient heat for grain growth of the recrystallized grains. These welding lines could be straight or tortuous depending on the velocities of the two neighboring strands, their surface roughness, and the level of applied stresses [28].

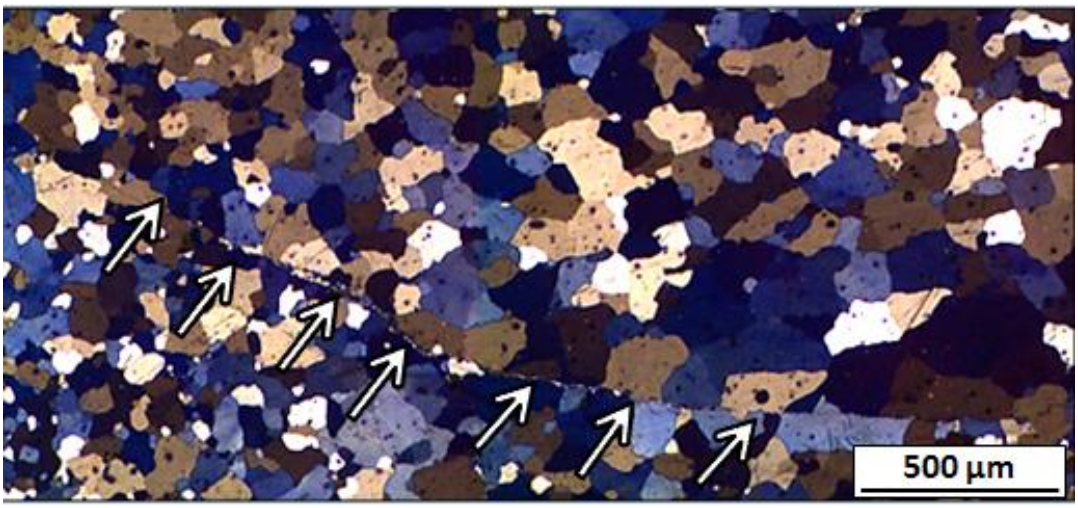

Figure 2-11. LOM mosaic image shows curved weld line in location (B) **[28]**

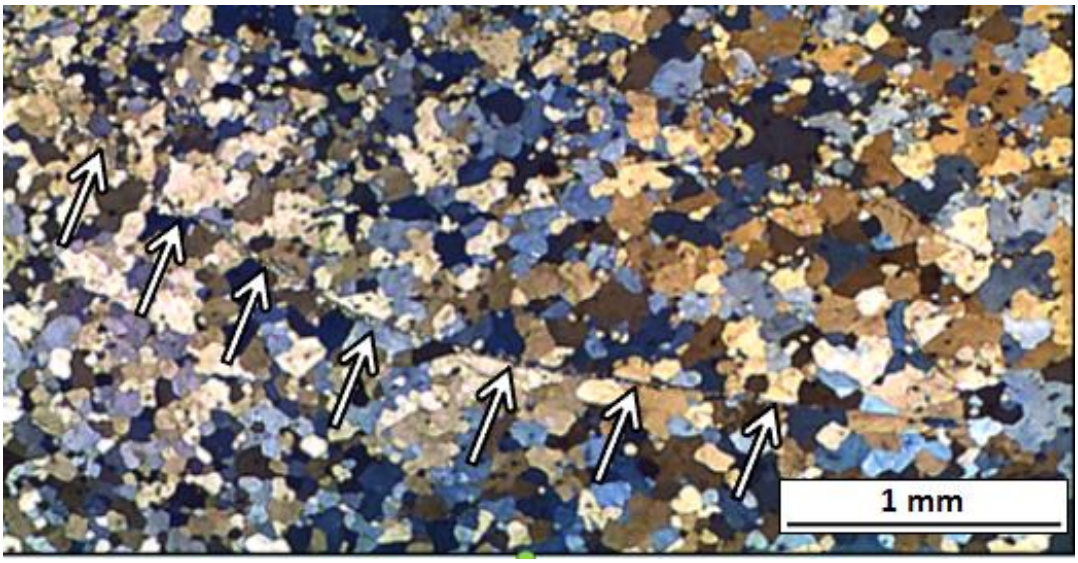

Figure 2-12. LOM mosaic image shows curved weld line in location (C) **[28]**

Some coarse grains along the extrusion weld are shown in Figure 2-13. In contrast, ‘‘necklacing’’ of small grains appears along the extrusion weld lines in Figure 2-14, which could be representing the newly recrystallized grains [28].

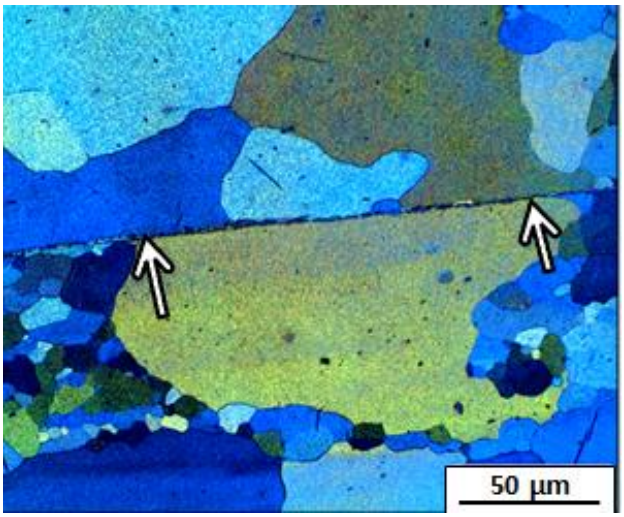

Figure 2-13. Straight extrusion weld line in location (B) **[28]**

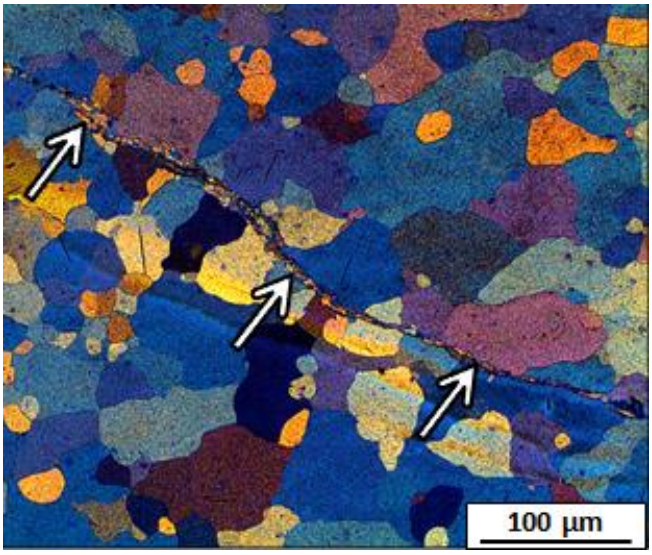

Figure 2-14. Tortuous extrusion weld line in location (C) **[28]**

In location (D), the grains were elongated during the extrusion process toward the thiner section of the profile (see Figure 2-15). Near the edge of the profile, deformation bands were observed due to the high

deformation represented by high local extrusion ratio. Also, Figure 2-16 shows different grain sizes structure near the corner of location (B).

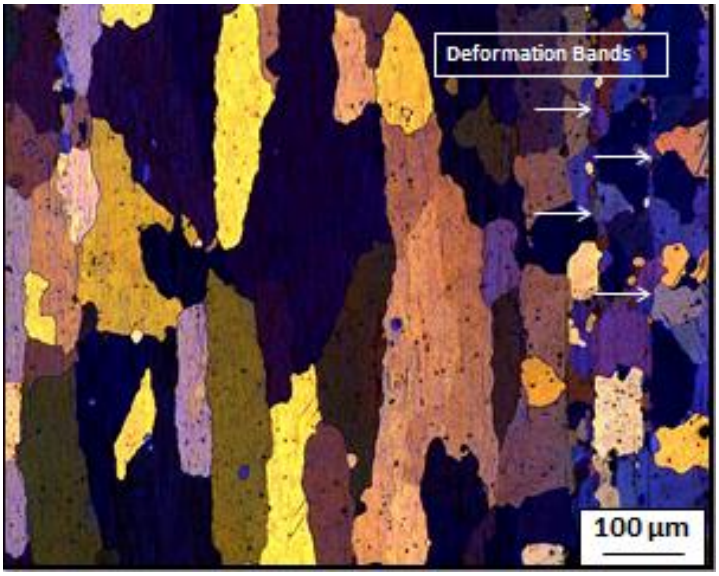

Figure 2-15. Polarized LOM image of elongated grains with a deformation lines in location (D)

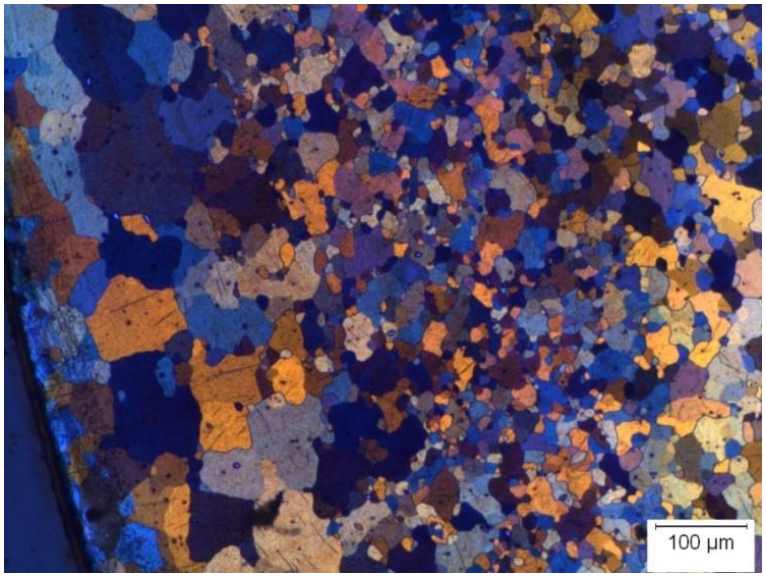

Figure 2-16. Polarized LOM image of the corner edge in location (B)

2.5.2 Electron Backscattered Diffraction (EBSD) results

Electron Backscatter Diffraction (EBSD) was carried out to compare the grain orientation maps between two types of extrusion welds observed using LOM and the grain orientation maps of the pre-extruded billet. Also, average grain sizes were obtained using E112 − 13 Standard Test Methods for Determining Average Grain Size – Intercept Method.

The grain orientation map of the pre-extruded billet is shown in Figure 2-17. It shows a random orientation but majority of the grains have ⟨1000⟩ orientation with average grain size 5.3μm. The grain orientation map for the good integrity extrusion welds without weld line type observed in the AM30 extrudate at location (A) (See Figure 2-1) is shown in Figure 2-18. It shows a fairly strong $\langle 2\bar{1}\bar{1}0\rangle$ orientation with average grain size of 93 μm. In contrast, the extrusion welding with a weld line at location (C) exhibits $\langle 10\bar{1}0\rangle$ orientation as shown in Figure 2-19 and Figure 2-20. The average grain size around the weld line is approximately 32 μm however, the grains along the weld line show fine grains structure with average size from 2 μm to 6 μm. The difference in crystallographic orientations in various types of welds could be due to the dynamic recrystallization during the extrusion. However, this much more complex metallurgical phenomenon needs further in-depth investigations.

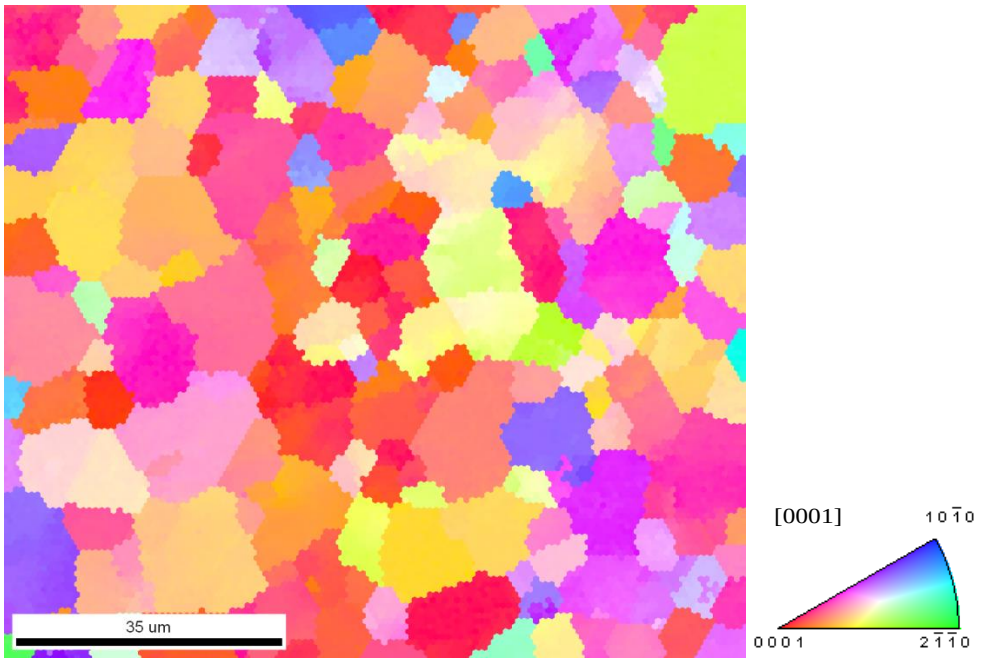

Figure 2-17. EBSD orientation map for the pre-extruded billet of AM30

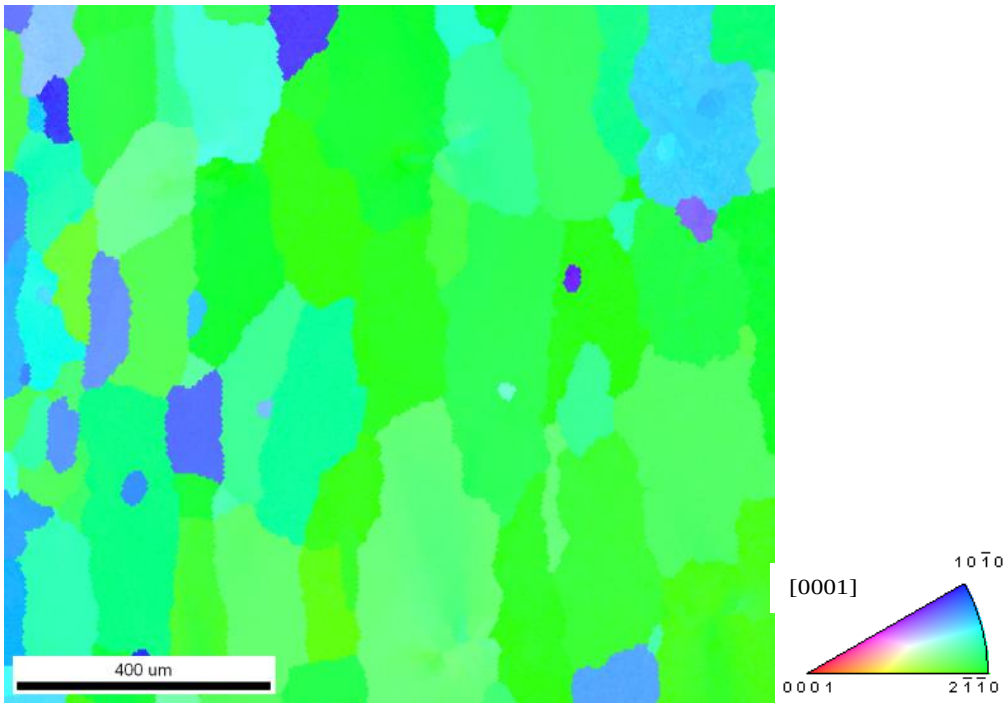

Figure 2-18. EBSD orientation map from location (A) of AM30 extrudate with good weld integrity

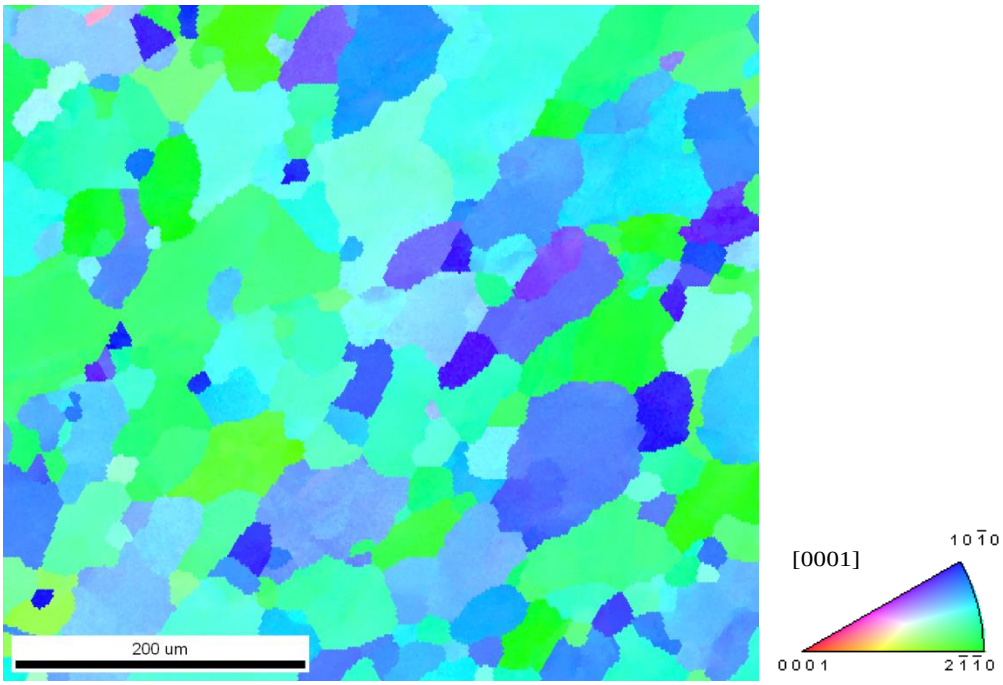

Figure 2-19. EBSD orientation map from location (C) of AM30 extrudate with a weld line

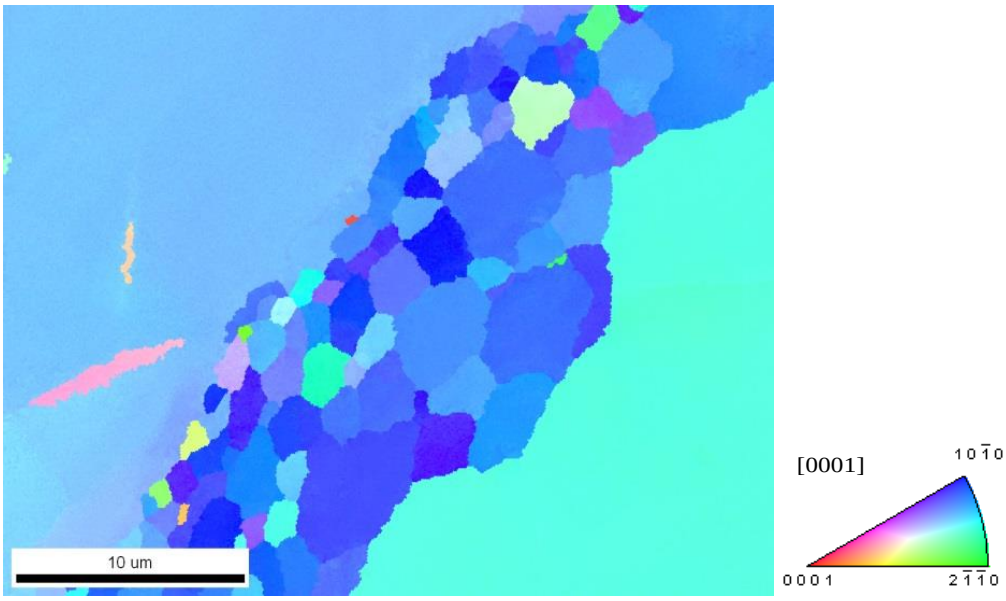

Figure 2-20. A magnified EBSD orientation map for the welding line in location (C) of AM30 extrudate

2.5.3 Micro hardness test results

Micro hardness tests were conducted to evaluate the homogeneity of the microstructure. Three samples were tested to compare the hardness values. The first sample was cut from the pre-extruded billet and was prepared to micro hardness test. Twenty five indentations are used to establish a hardness profile. The distance between the indentations was 1 mm. The values were averaged as shown in Figure 2-21. The average value shows consistent values between 50-52 HV. The second sample was cut from location (A) good weld integrity without weld line. Fifty indentations throughout the thickness of the profile were measured. The distribution was along 4 mm including the weld region with 1mm distance between indentations.

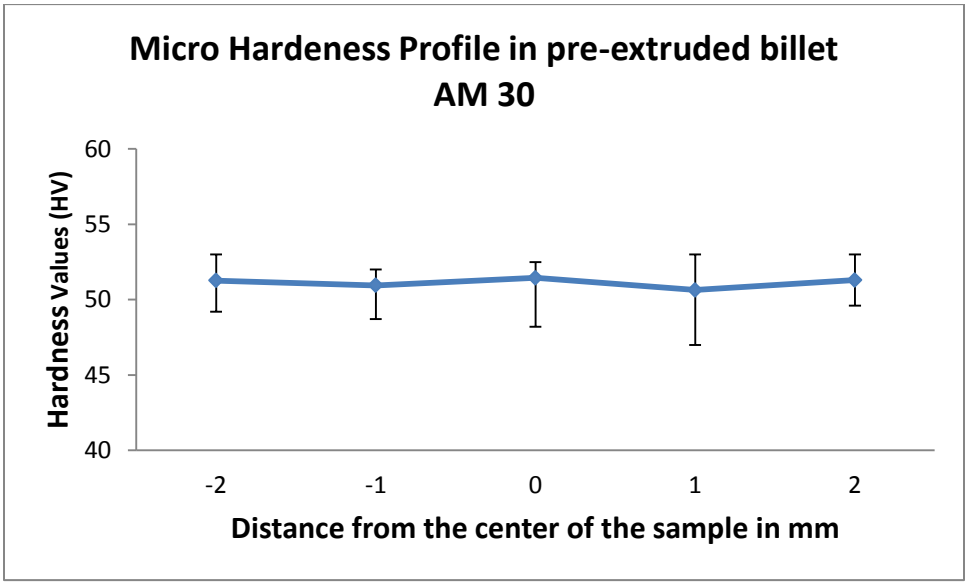

Figure 2-21. Micro hardness profile in pre-extrused billet AM30

The reference value (0) indicates the middle of location (A) where the good weld was observed. Then 25 indentations were measure along 2 mm on both side of the center of the weld. The averaged values indicate a consistency of hardness values between 45-48 HV (See Figure 2-22).

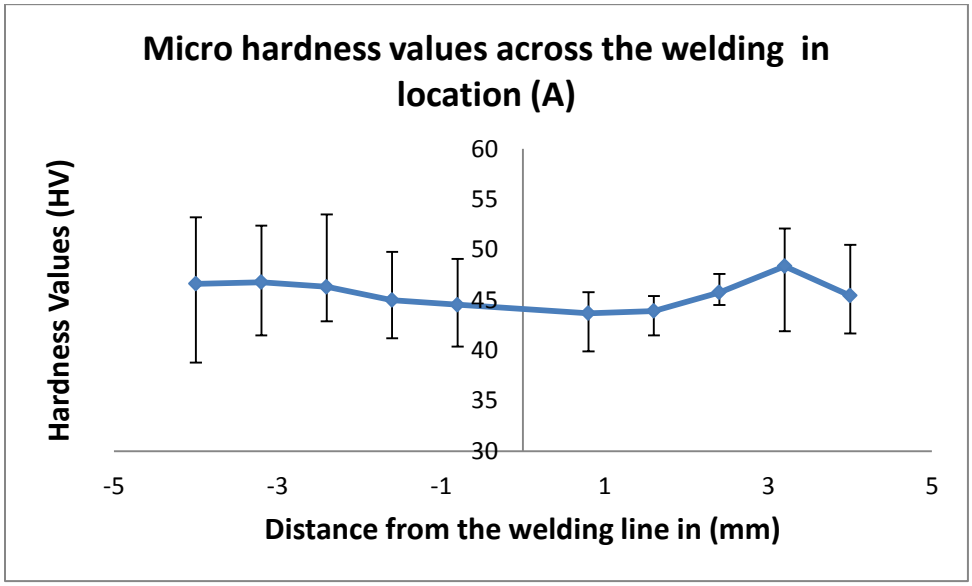

Figure 2-22. Micro hardness profile across the good weld in location (A)

The third sample was cut in location (C) where the extrusion weld line was observed. A total of 35 indentations were measured and averaged. The reference value (0) in Figure 2-23 indicates the weld line. The distance between the indentations was 300µm and the hardness profile show consistency with average values between 49-51 HV.

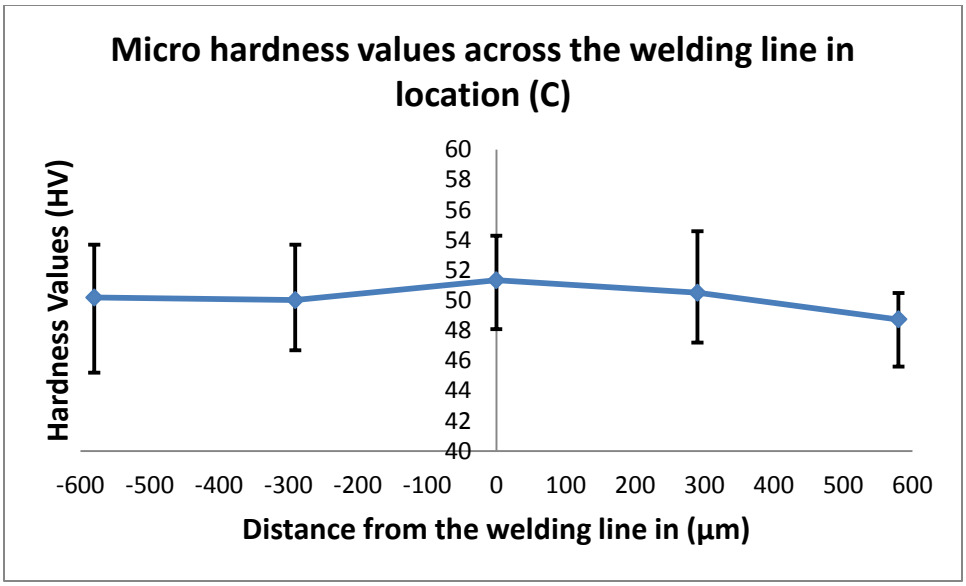

Figure 2-23. Micro hardness values across the welding line in location (C)

2.6 *Discussion*

Two types of extrusion welding in the double hat profile were observed for locations (A) and (C) presented in Figure 2-9 and Figure 2-12. Good weld integrity can be associated with lack of any distinctive weld line as presented in a micrograph for location (A). However, in location (C) an extrusion welding with a distinctive line was observed at the edge of the extrudate and suddenly disappeared in the middle of analyzed area (C). As reported in literature [26] a dynamic recrystallization can occur during the hot extrusion of Magnesium alloys especially in the welding chamber where a high deformation is expected due to the material splitting and its welding. This high amount of strain could be a driving force for a dynamic recrystallization in the welding chamber and at the metal interfaces.

The dynamic recrystallization at the metal interface leads to a necklace grain structure [10]. With normal pressure levels above the critical value at the interface, the solid state bonding is promoted inside the welding chamber. Depending on the amount of deformation work at different location and consequent transformation to heat, coarse grains could appear along the welding chamber up to the exit of the die [10][26].

The numerical simulation results for "double hat" of Magnesium alloy AM30 will be introduced in Chapter 3. The temperature distribution within the portholes and welding chamber (See Figure 2-24) shows a temperature gradient within the welding chamber and different values at locations (A) and (C). Accordingly, after the formation of the recrystallized grains, the increase of the temperature within the welding chamber caused grain growth and the presence of coarse grains at location (A) which formed good weld integrity. However, the weld line was observed at the left edge of location (C) and the "necklacing" of small recrystallized grains appeared around the weld line where the temperature was lower than the temperature at location (A) based on the numerical simulation results shown in Figure 2-24. It has been concluded that the dynamic recrystallized grains were not exposed to enough heat to cause the grain growth.

The hardness values at location (A) ranged from 45 to 48 HV and are shown in Figure 2-22. However, the hardness values at location (C)

(See Figure 2-23) were in the range of 49 to 51 HV. The difference in hardness values between the two locations (A) and (C) can be attributed to the difference in average grain size which was observed using the EBSD technique. Per EBSD results, the grain size average was 2 µm to 6 µm in the weld line region and 32 µm around the line at location (C) (See Figure 2-19 and Figure 2-20) while the average grain size at location (A) was 93 µm (See Figure 2-18).

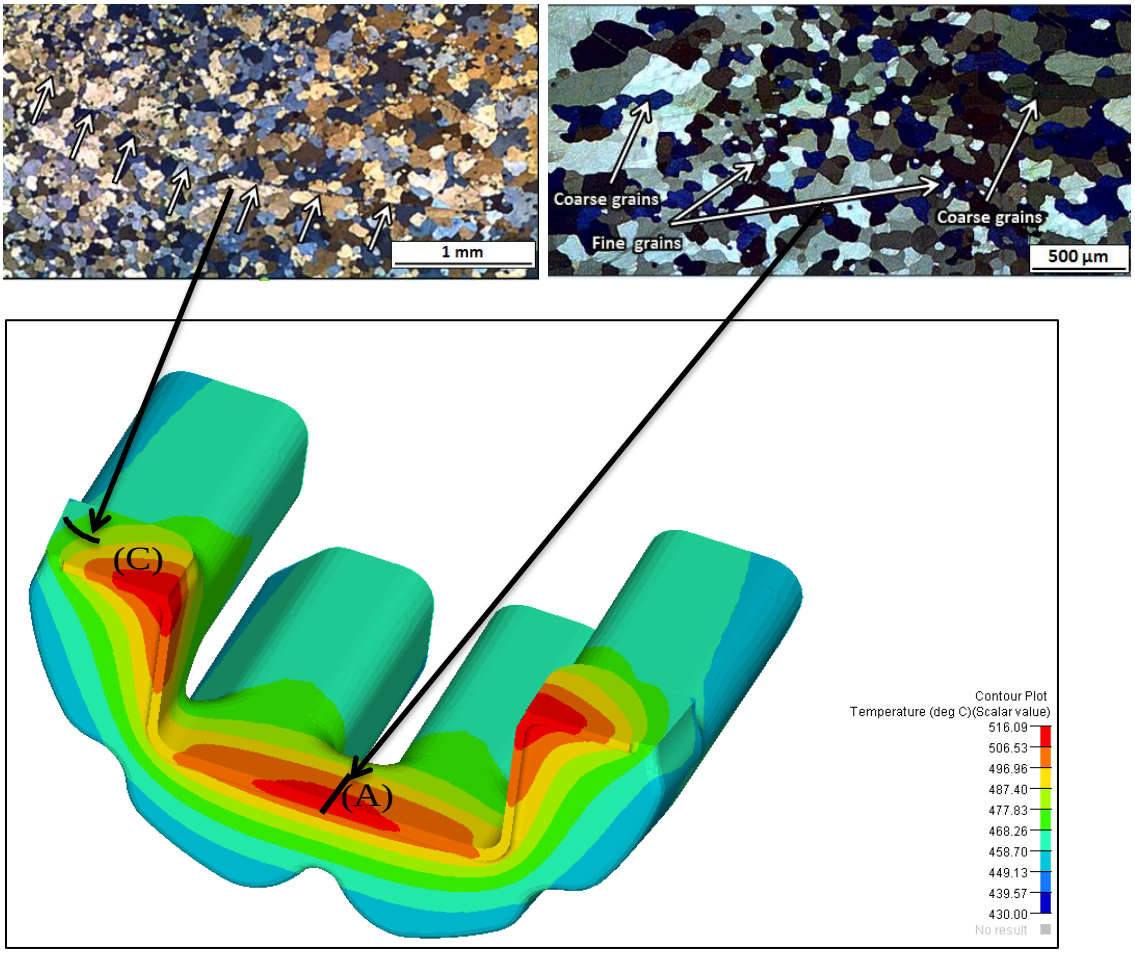

Figure 2-24. Finite element model prediction of Temperature distribution within portholes die and welding chamber at ram speed 1.3 mm/sec and billet temperature 430°C and associated weld micrographs at location (A) and (C)

3 Numerical Simulation of "Double Hat" Magnesium Alloy AM30 Extrudate

3.1 *Introduction*

Engineering problems can be solved using analytical, numerical or experimental methods. The analytical method is a classical approach for simple problems and can be more accurate than the numerical methods. In contrast, the experimental method allows actual measurements of actual process parameters however; it is time consuming beside the cost of the set up and execution. Because of the above mentioned limitations, the numerical methods have been used as an approximation technique, for solving complex mathematic problems, especially in engineering field.

One of the numerical methods is finite element analysis (FEA), also known as finite element method or finite element modeling (FEM). Originally, it was developed within the aerospace industry from 1940's to 1950's. Subsequently it has been adapted to the most areas of engineering by 1960's [32]. FEA provides an alternative solution of differential equations with appropriate boundary conditions or minimizing a function by equivalent set of simultaneous algebraic equations. Basically the method uses discretization or meshing (elements and nodes) to reduces the degrees of freedom of an object from infinite to finite [33]. This simplification makes calculations at a limited (finite) number of points and then interpolates the results for the entire domain (surface or volume).

FEA can be used in different application and analyses such as linear, nonlinear, buckling, thermal, dynamic and fatigue analyses.

In addition, finite element method is used for the numerical simulation of the metal deformation. Several deformation software packages are available, such as QFORM™, LS-DYNA™, DEFORM™, HyperWorks ™ and others.

3.2 *HyperWorks™*

HyperWorks™ has been developed by Altair Engineering –a product design company. Altair Engineering has many softwares and modules for modeling, visualization, manufacturing solutions and engineering solutions. HyperWorks™ products are summarized in Table 3-1 [34].

Table 3-1. HyperWorks™ softwares and modules **[34]**

Modeling and Visualization HyperMesh- finite element modeling HyperCrash- CAE pre-processor tool MotionView - multi-body dynamics HyperView - results visualization HyperView Player - visualize 3D CAE models HyperGraph 2D - plotting and data analysis HyperGraph 3D - plotting and data analysis HyperMath - mathematical scripting language HyperStudy - design exploration BasicFEA - simple analysis HyperWorks Desktop	**Manufacturing Solutions** HyperXtrude - finite element solver / user environment Friction Stir Welding - friction stir welding simulation Forging - three dimensional forging simulation Molding - injection molding simulation HyperForm - sheet metal forming simulation **Engineering Solutions** Crash CFD Drop Test NVH Aerospace

HyperXtrude™ is one of the manufacturing solutions modules based on the FEM approach. It is a simulation tool developed to analyze the extrusion process and performance of the extrusion dies. It is considered a powerful tool for engineers to analyze the material flow and heat transfer during the extrusion process which helps to minimize the cost and time consumed during industrial trials [34] . It is based on Arbitrary Lagrangian Eulerian (ALE) algorithm which is a combination of Lagrangian and the Eulerian approach. This approach is very powerful to simulate the extrusion process and avoids the drawbacks of Lagrangian approach which cannot handle the large deformation due the large distortion of the mesh. Consequently the large distortion of the mesh leads to loss of accuracy. Also, ALE allows tracking of the surface interface of flowing material which cannot be achieved by Eulerian approach due to the high computational time especially in simulation of extrusion process [35]. In this approach the mesh is not attached to the material as in Lagrangian approach and not fixed as in Eulerian one. The movement of the mesh is arbitrary, which allows for large deformation and for easier tracking of free surfaces.

The most key features of HyperXtrude™ are [34]:

- Extrusion- specific graphical user interface to prepare model setup analysis

- Library of different types of materials such as metals, polymers, pastes and ceramics
- Computing die deflection and resulting stress
- Ability to model co-extrusion of two or more materials
- Correcting bearing design to balance material flow
- Integrated with HyperStudy™ for optimization of die bearing, portholes and pocket dimensions.

Benefits of HyperXtrude™ include [34]:

- Minimize die design time and cost
- Visualize material flow
- Design robust die assemblies
- Minimize transverse weld scrap
- Reduce cost
- Increase productivity

3.3 *Literature review*

Since the development of finite elements modeling packages for metal deformation, there were many attempts to simulate the extrusion process for better understanding of the metal flow through the different die designs. Different state variables such as extrusion pressure, strain, strain rate and temperature can be track during this complex process. Some researchers have focused on simulation of the hot extrusion of light metals

to optimize the related process parameters for increasing the productivity and minimizing the product defects [35-42].

Several studies were conducted on optimization of hot extrusion of Aluminum and Magnesium alloys. Some of them have concentrated on the extrusion longitudinal welding phenomenon during simulation of hollow sections extrusion. The different criteria for quality of the extrusion welding will be presented in Chapter 5. In this chapter the focus will be on the numerical simulations of extrusion of Aluminum and Magnesium alloy. Jo et al. [36] have studied the effect of billet temperatures, bearing length and product thickness on the welding quality of Aluminum alloys AA7003 hollow section tubes. The metal flow of the product was analyzed by using DEFORM^{TM} simulations and experiments for different billet temperatures of 400°C, 430°C, and 460°C. An extrusion welding quality criterion developed by Plata and Piwnik [37] was applied to evaluate the different parameters. Some conclusions have been highlighted such as extrusion load decrease with the increase in billet temperature, as well as lower billet temperature for improvement of the surface finish of the tube. Donati and Tomesani [38] have modeled extrusion of AA 6082 aluminum alloy to evaluate the influence of extrusion pressure, material flow stress and velocity on the extrusion welding surface. A new modified version criterion has been introduced by Donati and Tomesani and applied to H-shape exturdate. The modified criterion was based on Plata and Piwnik

criterion [37] where they have proposed pressure-time weld quality relationship by taking the time integral of the ratio of contact pressure (P) and effective stress (Q) along the welding path. The time here is the required contact time along a welding path from the start of the material contact until the exit of the die while leaving the bearing land.

$$\int_t \frac{P}{Q} dt \geq C_{cr} \qquad \text{Equation 3-1}$$

While Donati and Tomesani [38] have modified Equation 3-1 by including the velocity factor thus now the integral will be length integral of the ratio of the pressure (p) to the effective stress (Q) should exceeds a critical value (C_{cr}) that should be determined experimentally.

$$\int_t \frac{P}{Q} dt.v = \int_l \frac{P}{Q} dl \geq C_{cr} \qquad \text{Equation 3-2}$$

They found that high values of the integral can be obtained with low pressures and long chamber lengths or for short chambers if high pressures are maintained.

Another study has been performed by Valberg et al. [39] for an Aluminum alloy to analyze metal flow in cases where two neighboring porthole channels at each side of the die bridge are of a different size. They found that the larger porthole had of course more feed and this had a significant influence on the deformation and metal flow. A significant pressure drop was predicted by the DEFORM^{TM}-3D simulation in the welding chamber behind the die bridge. This drop was caused by a heat

generation occurring adjacent to the bridge surface. In addition the strain rate was higher near the bridge in comparison to the metal flow near the side walls.

Liu et al [40] have modeled different FE simulations to determine the conditions for better longitudinal welding quality of Aluminum porthole die extrusion. Different ram speeds ranging from 1, 5, 10, to 15 mm/s and at different billet temperatures of 420, 450, 465, and 480°C were used with different welding chamber height 4, 7, and 10 mm. Donati and Tomesani criterion [38] was applied for the evaluation the welding quality. It has been found from the simulations' results that higher welding chamber and sharper die leg caused better welding quality. In addition, higher ram speed decreased weld quality. Regarding the billet temperatures, it seems that 450 and 465 ℃ can produce good longitudinal welds [38].

An investigation of the effect of ram speed on the extrusion of Aluminum alloys AA6063 was performed by Zhang et al. [35]. Different simulations with ram speeds ranged from 0.1mm/s to 1.5 mm/sec were conducted using HyperXtrude software package. The optimum value of metal flow uniformity for a given die and process conditions has been achieved at the ram speed of 0.3 mm/s. Also, the increase of the ram speed promoted higher weld quality.

The extrusion welding was investigated via numerical simulation for Magnesium alloys. Liu et al. [41][42] have numerically simulated extrusion of Magnesium alloy AZ31 into a rectangular section at various ram speeds and verified their model results by experiments. The results showed that the metal temperature not uniform inside the portholes die and it increased in the welding chamber close to the die orifice. A linear relation between the increase of temperature and ram speed was established. Also, they found that the higher ram speed, the higher the exit temperature. Another study of the same alloy AZ31 were performed by Li et al. [43] . Similar findings were obtained. In addition, the quality of the longitudinal weld Pressure/effective stress remains constant. However, the maximum normal pressure decreased, along with the value of the flow stress within the welding zone. These results showed that the main reason for common defect at the extrudate front end was entrapped air under the bridges within the welding chamber. A dead metal zone was observed at the corners between the die face and the container.

3.4 *Simulation of double hat Magnesium alloy AM30*

In this work, numerical simulation of the hot extrusion of Magnesium alloy AM30 using HyperXtrude^{TM} software was performed. The extruded profile is of the same geometry as the industrial profile that has been characterized in Chapter 2. The objective of this study is to determine the

effect of different ram speeds and billet temperatures on the state variables such as temperature, strain rate and normal pressure within the welding chamber. The results of performed numerical simulation were used to design the physical modeling experiment of extrusion welding which will be discussed in the Chapter 4. In addition, state variables of the performed simulations have been used in the new proposed criterion for evaluating the quality of extrusion welding for Magnesium alloy AM30 and it will be discussed in Chapter 5.

3.4.1 HyperXtrude^{TM} model setup

The 3D geometries of the extrusion tooling such as portholes die and container were designed in Solidworks^{TM} software as shown in Figure 3-1. Then, all the tolling elements were modeled in this extrusion simulation as rigid bodies. Since AM30 has been extruded at elevated temperature, therefore the material behavior depends on the rate of the deformation. Accordingly, the billet, feeder plate with port holes and welding chamber, bearing and extrudate where modeled as visco-plastic material. The tolling elements usually is modeled as rigid because it needs to be not moving during deformation and acts as constrain to the deformed material. In addition, the rigid body model for the tooling elements saves the computational time since the focus of the analysis not include the tolling deflection. All the model components were meshed using HyperMesh^{TM}. Since the model has complex shape geometries, different

shape elements were used in meshing for different locations. Tetra shapes were used in the billet, feeder plate, port holes and welding chamber. While the prism shape elements were used in bearing land and the extrudate.

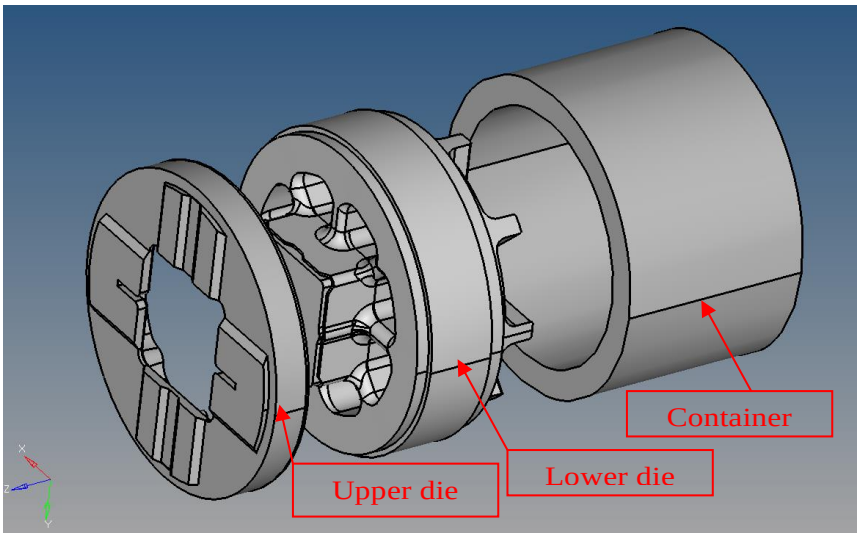

Figure 3-1. 3D geometries of extrusion tooling used in FE simulation

HyperXtrude^{TM} software package has criteria to evaluate the mesh quality. It takes into account the aspect ratio of the neighboring element size or even the side length of an element. The minimum angle was selected to be more than 10° at the same time the maximum angle had to be less than 170°. The element sizes differ depending on their location within the deformed body. For the billet, the element size was selected to be less than 5 mm. However, in the port holes and the bearing land is ranged from 0.5 mm to 2 mm due to the complexity of the deformation in these areas which need smaller elements as well as the high change rate of

state variables. Different mesh densities have been optimized to give good and consistent results in a reasonable time. The total number of mesh elements was around 2 million as shown in Figure 3-2.

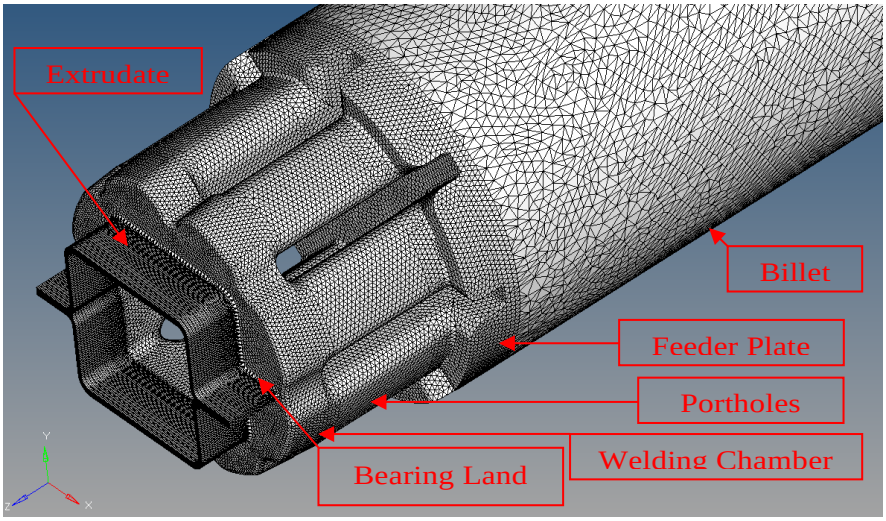

Figure 3-2. 3D mesh model of the different part inside the die and the container

3.4.1.1 Constitutive model of Magnesium alloy AM30

Hyperworks™ has a data base of different types of constitutive model for different materials. However, AM30 alloy is newly modified alloy by General Motors [44] and Hyperxtude™ does not have material model for this specific alloy. However, it has a capability to add data for specific material and fit a constitutive model to be used in a simulation.

There are different constitutive models to describe the behavior of material during deformation but Sine Hyperbolic Inverse law (See Equation 3-3) is the most used model for describing thermo-viscoplastic

behavior of metals during deformation [45]. The constants of the model were taken from [46] and fitted for different strain rates and temperatures using HyperXtrude's material data fitting function.

$$\bar{\sigma} = \frac{1}{\alpha}\sinh^{-1}\left[\left(\frac{Z}{A}\right)^{1/n}\right], \qquad Z = \dot{\bar{\varepsilon}}\exp\left(\frac{Q}{R\theta}\right) \qquad \text{Equation 3-3}$$

Where:

$\bar{\sigma}$: the flowstress (MPa)

Z : Zener-Hollomon parameter,

A: Reciprocal strain factor = 5.92×10^{10} (1/sec)

n: Stress exponent = 7

α: Stress multiplier =0.017 (MPa^{-1})

$\dot{\bar{\varepsilon}}$: Strain rate (1/sec)

Q: Activation energy = 150000 (J/mol)

R: Universal gas constant = 8.314 (J/mol K)

θ: Absolute temperature (K)

All the above constants were used in Equation 3-3 at different temperatures ranging from 600°K to 850°K and at different strain rates ranging from 0.001/sec to 100/sec. The flow stress values (MPa) were plotted as a function of strain rates (1/sec) for different temperatures using logarithmic scale as shown in Figure 3-3.

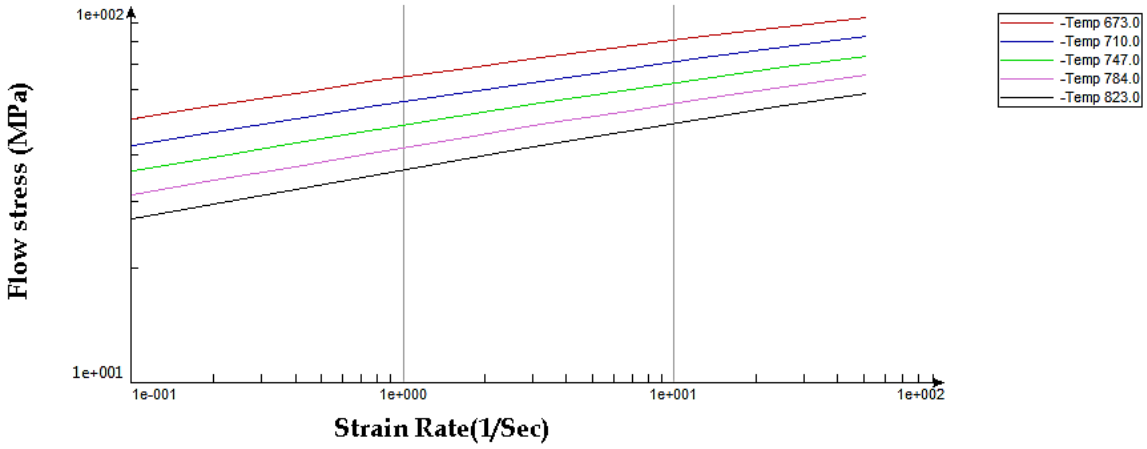

Figure 3-3. Flow stress as a function of strain rate for different temperatures

3.4.1.2 Process conditions and boundary conditions

In HyperXtrude^{TM} software, the process conditions need to be defined and the software is applying the boundary conditions for all model components. The temperatures and ram speeds were selected based on the extrusion force and temperature limit diagrams shown in Figure 3-4 [47]. All process conditions used in simulations are shown Table 3-2.

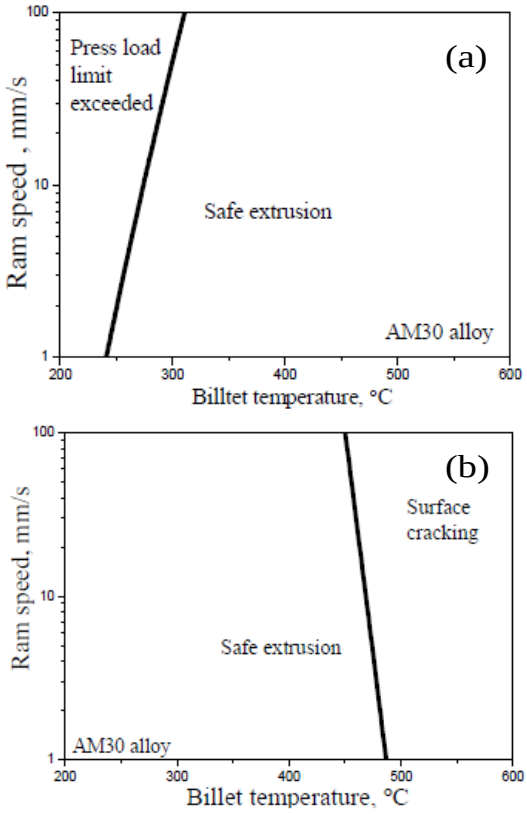

Figure 3-4. (a) Extrusion force limit diagram (b) Extrusion temperature limit diagram of Magnesium alloy AM30 [47]

Table 3-2. Process conditions of the simulation of hot extrusion of AM30

Container Diameter (mm)	215
Billet Length (mm)	500
Billet Preheat Temperatures(°C)	430, 450, 470
Die and Container Temperatures (°C)	430, 450, 470
Ram Speed (mm/sec)	1.3, 2.5, 5
Extrusion Ratio	22.6

3.5 *Results and discussion*

The simulations of the extrusion process of "double hat" Magnesium alloy AM30 were successfully performed for different billet temperatures (430°C, 450°C, 470°C) and ram speeds (1.3 mm/sec, 2.5 mm/sec, 5 mm/sec). The objective of different numerical simulations was to analyze the influence of different billet temperatures and ram speeds on the extrusion weld zone state variables such as temperature, strain rate and normal stresses. Due to the symmetry of the profile, quarter of the simulated profile was chosen to represent two weld zones (1) and (2) as indicated in Figure 3-5**.**

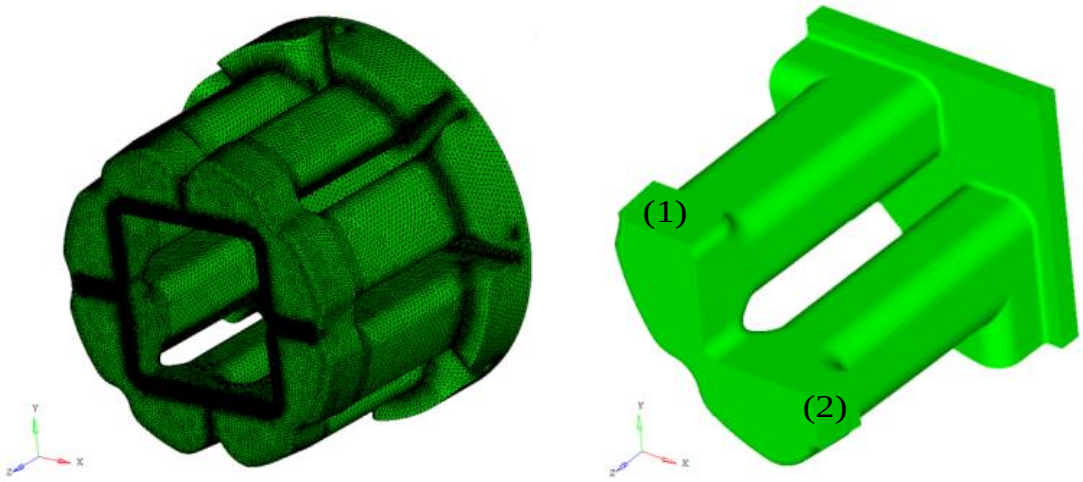

Figure 3-5. The entire mesh model of portholes and welding chamber filling and bearing (left) quarter of the model showing the weld zone (1) and (2) (right).

3.5.1 Temperature, strain rate and normal stress at different ram speeds and different billet temperatures

The general response of the material measured by the state variables such as temperature, strain rate and normal stress within the weld zone (1) to the process conditions will be discussed in this section. However, in-depth comparisons of the influence of different process conditions on weld zone (1) will be discussed in the following sections. Figure 3-6 to Figure 3-10 show contour plots for the state variables of the porthole and weld zones at different billet temperatures and ram speeds. The temperature, strain rate and normal stress within weld zone (1) are labeled a, b, c respectively.

It is well known in the metal forming industry that 90% to 95% of the deformation work is converted to heat. Accordingly, it can be seen in temperature contour plots that the temperature increased during the extrusion process due to the heat generation of the metal deformation. Depending of the thermal conductivity of the deformed material the different temperature change can be observed. In case of Aluminum alloy an increase of the extrudate temperature is observed under typical conditions. However, while extrusion of copper and its alloys we typically observe a drop in extrudate temperature due to the value of K (thermal conductivity), of 401 w/m.k instead of 205 w/m.k at room temperature for Aluminum. Since Magnesium has K =156 w/m.k at room temperature this material will heat up even more during deformation than Aluminum

alloys. The temperature increased as the material moved throughout the container and was increased rapidly at the portholes and welding chamber due to the high strain and strain rate of the splitting of the metal at bridges region and the metal joining at the welding chamber. Also, the friction between the metal stream behind the bridges and between the metal and side walls of the welding chamber and bearing land played a role in increase of the temperature within the weld zone. It can be observed that the temperature was not uniformly distributed within the weld zone. The temperature reached its highest value at the bearing land. In addition, the temperature near the core mandrel was higher than the side walls because of the heat loss from the die to the ambient temperature which was also reported in [41]. Furthermore, the increase of ram speed leads to increase of temperature especially at weld zone.

The contour plots of strain rate (See Figure 3-6 (b) to Figure 3-10 (b)) are showing non uniform distribution especially in the weld zone. This can be attributed to the dimensions of the portholes and welding chamber. The strain rate increased in weld zone towards the bearing land due to the high strain near the exit of the die. Accordingly, the highest value of strain rate was located at the beginning of the bearing land. On the other hand, the lowest strain rate was located at the corner of the side wall and die face which could be a dead metal zone. Also, small strain values can be observed at the beginning of metal joining in the weld zone.

Regarding the normal stress at weld zone (1) (See Figure 3-6 (c) to Figure 3-10 (c)), it can be observed from the contour plots that there was non-uniform distribution of normal stress at weld zone because of the curvatures on the geometry of the welding chamber. After the metal strands were splitted by the arms in the potholes, it started to re-join again at the beginning of the welding chamber. The normal stress was gradually increased until reached its highest value at the beginning of the bearing land which can be attributed to the welding chamber geometry that leads to more normal pressure from the side walls. This observation was also reported by Donati and Tomesani in [38]. The lowest normal pressure can be observed near the side wall of welding chamber where the shear stress was dominant due to the high friction between the metal and side wall and mandrel.

(a)

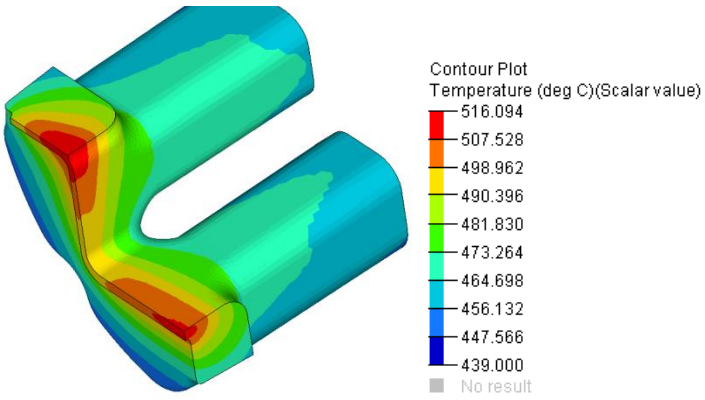

(b)

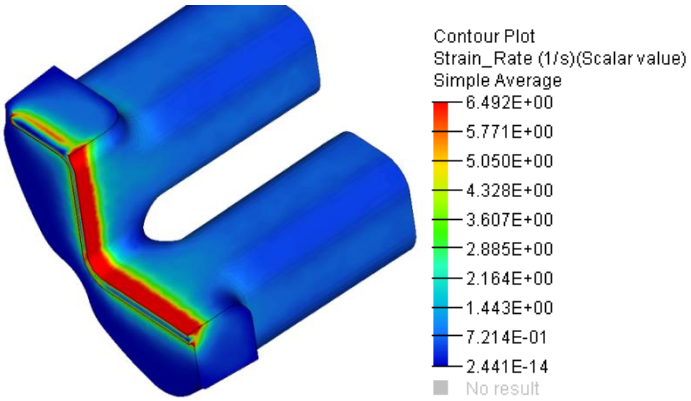

(c)

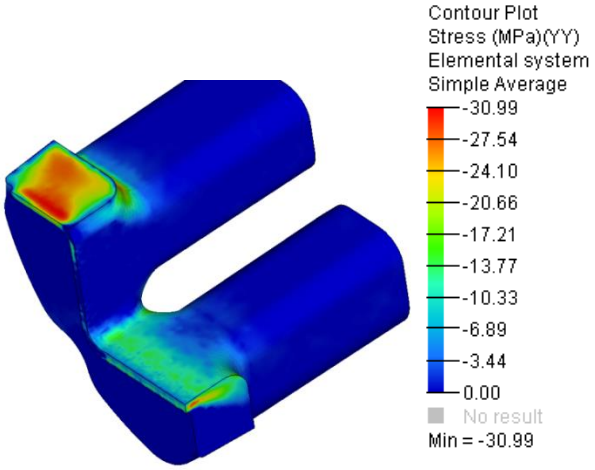

Figure 3-6. Contour plot of two weld zones showing (a) temperature, (b) strain rate (c) normal stress at location (1) for 430°C billet temperature and 1.3 mm/sec ram speed.

(a)

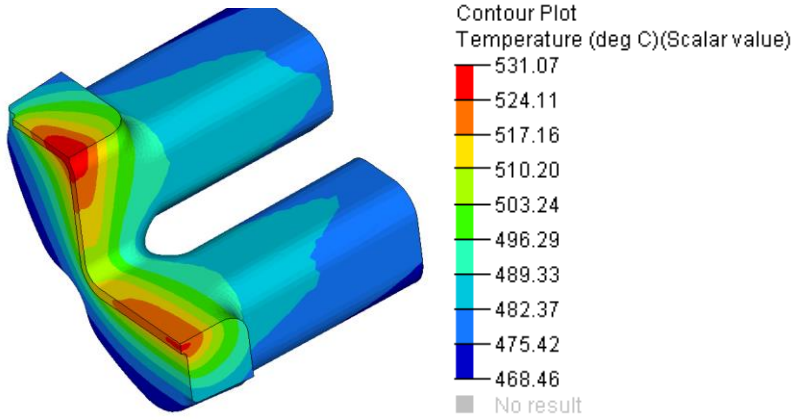

(b)

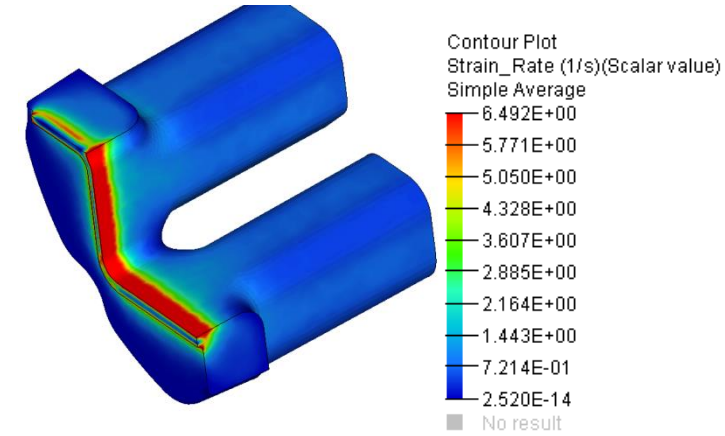

(c)

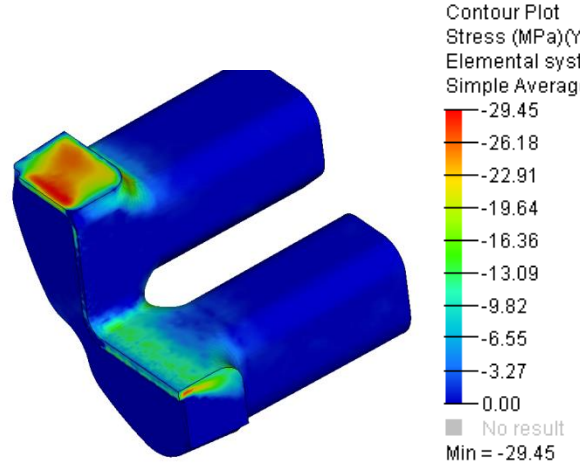

Figure 3-7. contour plot of two weld zones showing (a) temperature, (b) strain rate (c) normal stress at location (1) for 450°C billet temperature and 1.3 mm/sec ram speed.

(a)

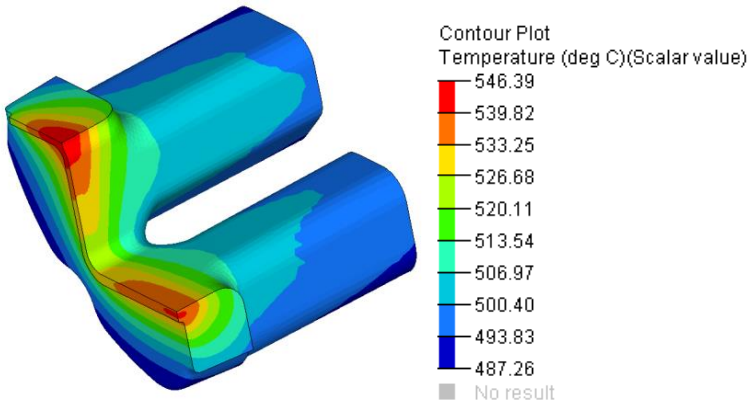

(b)

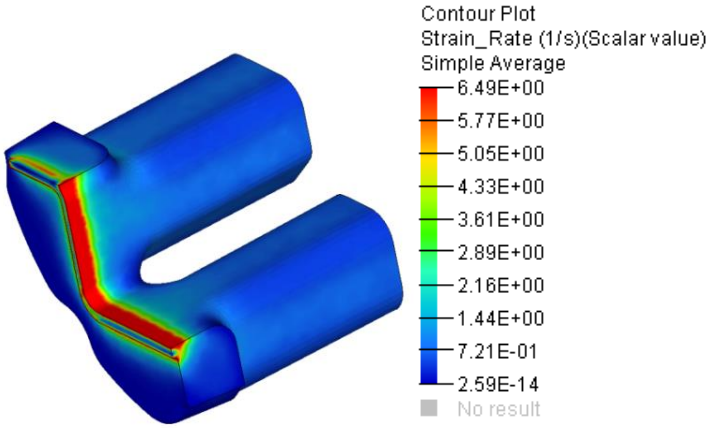

(c)

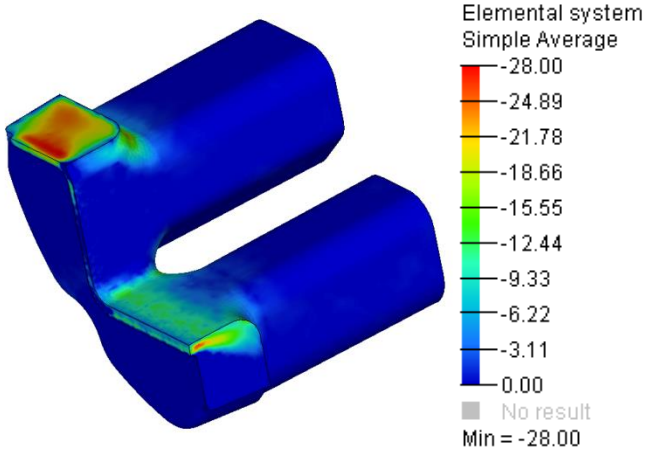

Figure 3-8. Contour plot of two weld zones showing (a) temperature, (b) strain rate (c) normal stress at location (1) for 470°C billet temperature and 1.3 mm/sec ram speed

(a)

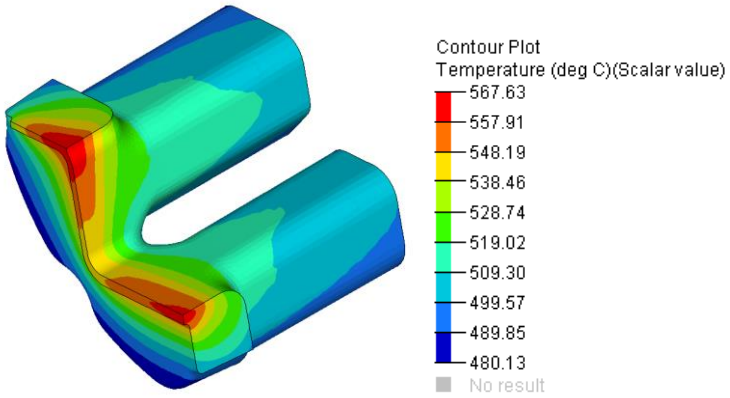

(b)

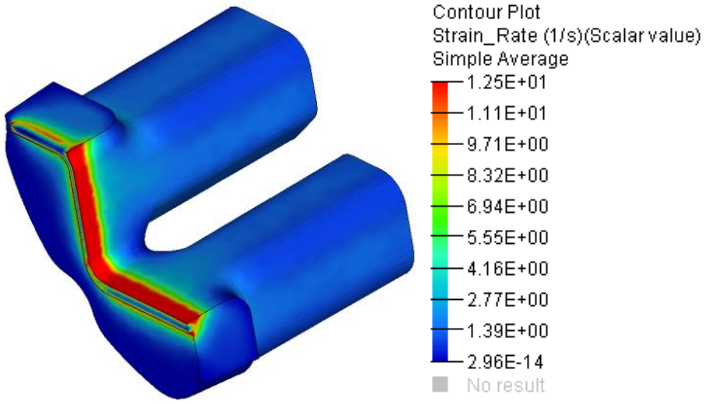

(c)

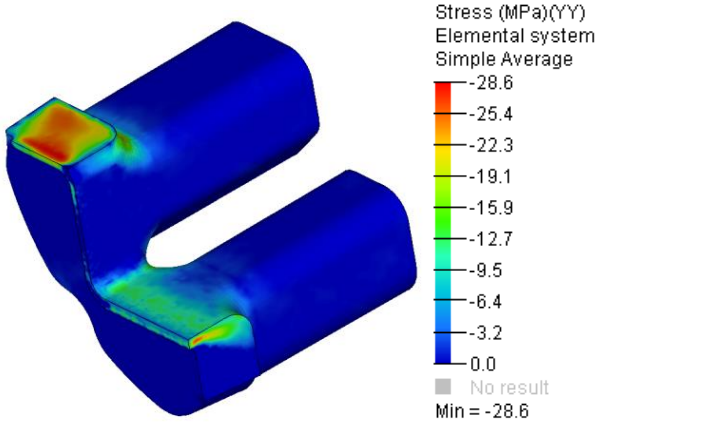

Figure 3-9. Contour plot of two weld zones showing (a) temperature, (b) strain rate (c) normal stress at location (1) for 450°C billet temperature and 2.5 mm/sec ram speed

(a)

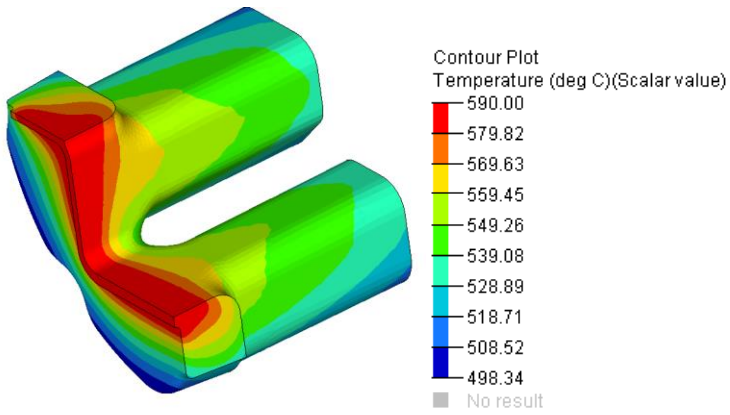

(b)

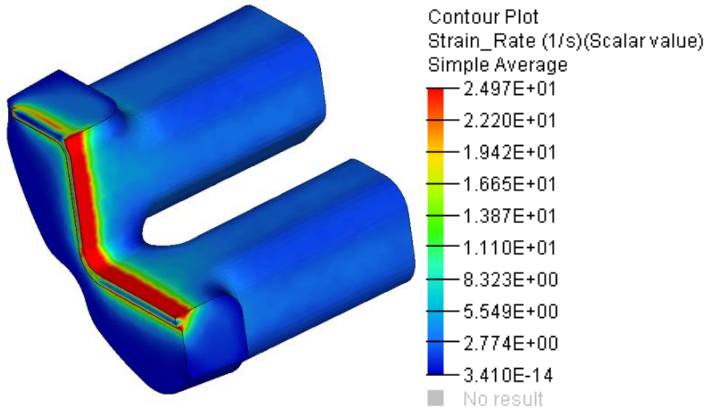

(c)

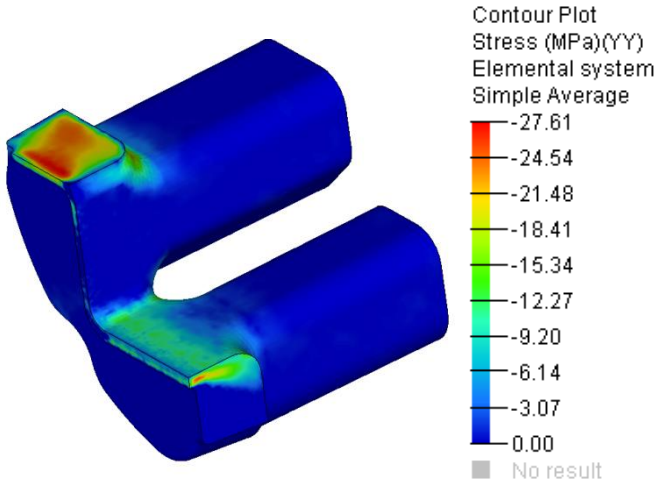

Figure 3-10. Contour plot of two weld zones showing (a) temperature, (b) strain rate (c) normal stress at location (1) for 450°C billet temperature and 5 mm/sec ram speed.

3.5.2 Influence of different billet temperature on weld zone

Temperature, strain rate and normal stress contour plots were presented in Figure 3-11 for different billet temperature (430°C, 450°C, 470°C) and 1.3 mm/sec ram speed. It is obvious from temperature contour plots that the increase of billet temperature had a significant effect on the temperature distribution in the weld zone. The highest temperatures were located at the bearing land and towards the core mandrel. While, the lowest temperatures were located near the side walls of the welding chamber due to the heat loss with ambient temperature. The rise of temperatures on all cases was around 60°C to 70°C. The minimum temperature within weld zone (1) was approximately 450°C in the case of 430°C billet temperature. In contrast, the maximum temperature within the weld zone (1) was around 546°C in the case of 470°C billet temperature.

Regarding the strain rate, there was no effect of different billet temperatures on the strain rate values because the ram speed value was a constant value at 1.3 mm/ sec. On the other hand it can be observed that normal stress decreased when the billet temperature increased due to the softening of the metal with the temperature and subsequent decrease in the required flow stress. The highest value was located near the bearing land in the case of 430°C billet temperature at -31 MPa where the minus sign indicates compresive stress. While in the highest billet temperature at 470°C was

-28 MPa due to the increase of temperature in comparison to other billet temperatures values.

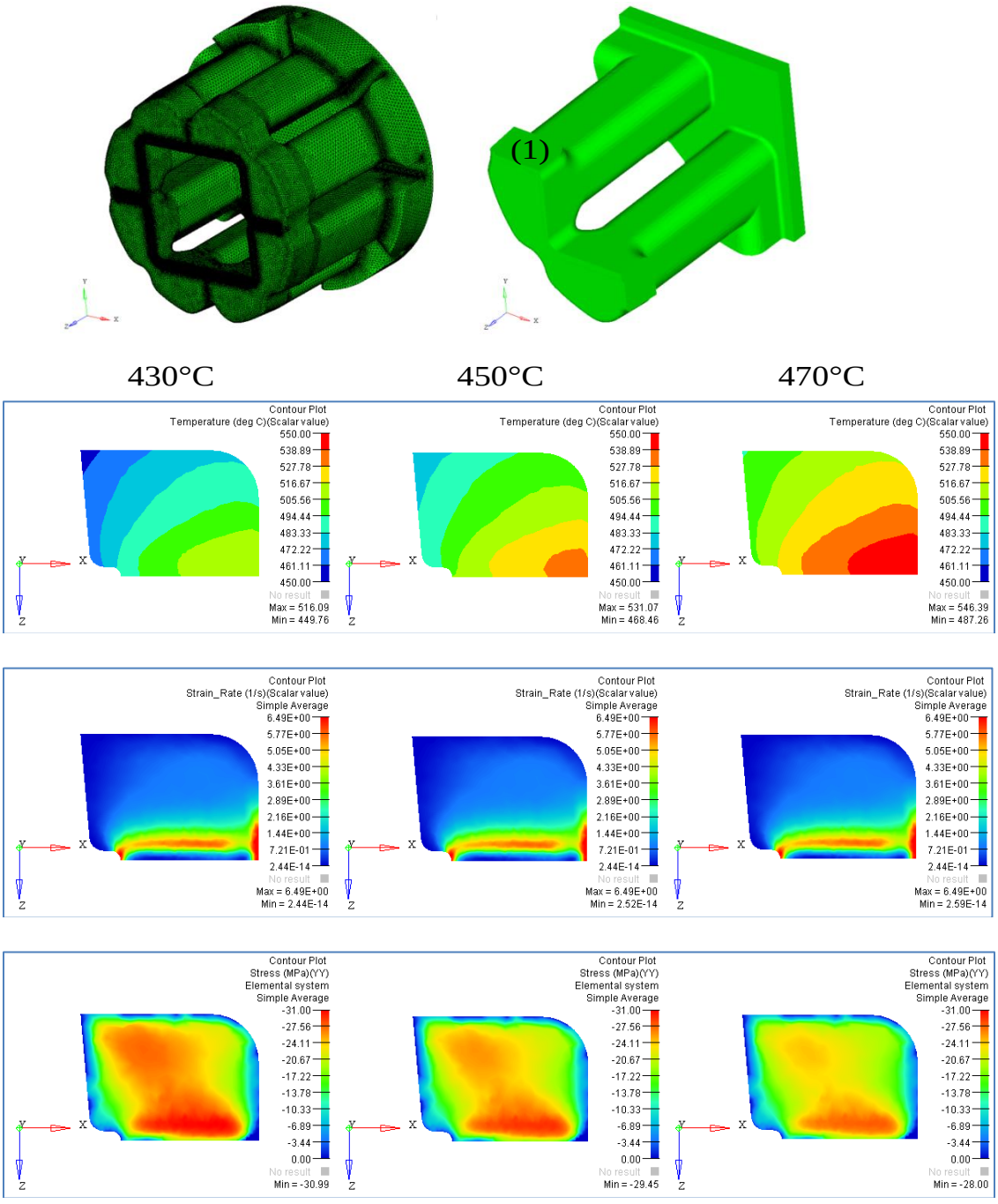

Figure 3-11. Comparison between temperature, strain rate and normal stress at weld zone (1) at different billet temperature (430°C, 450°C, 470°C) and 1.3 mm/sec ram speed

3.5.3 Influence of different ram speeds on weld zone

In the same approach of analysis used in the previous section, temperature, strain rate and normal stress contour plots were presented in Figure 3-12. The billet temperature was constant at 450°C in all cases. From the contour plot of temperature distribution at weld zone, it can be observed that the ram speed had a strong significant influence in the heat generation during the hot extrusion process. The temperatures reached highest values at welding camber. From the presented comparison it can be seen that the difference between the highest and the lowest temperature in weld zone is around 80°C. The highest temperature 612°C was located in bearing land where the ram speed was 5 mm/sec which is 20°C below the melting point of AM30.

As expected and as a consequence of the increased ram speed the strain rate values increased. It can be observed that the highest value of strain rate in the case of ram speed 1.3 mm/sec was 6.5/sec in comparison to 25/sec in the case of ram speed 5 mm/sec.

Regarding the normal pressures, the same behavior of increase of billet temperature was observed with the increase of ram speed where the heat generation increased as well as temperature. Accordingly, the flow stress value decreased and the normal pressure at the welding zone. The highest value was -29.45 MPa in the case of ram speed 1.3 mm/sec while the highest value was in the case of ram speed 5 mm /sec was -27.61 MPa.

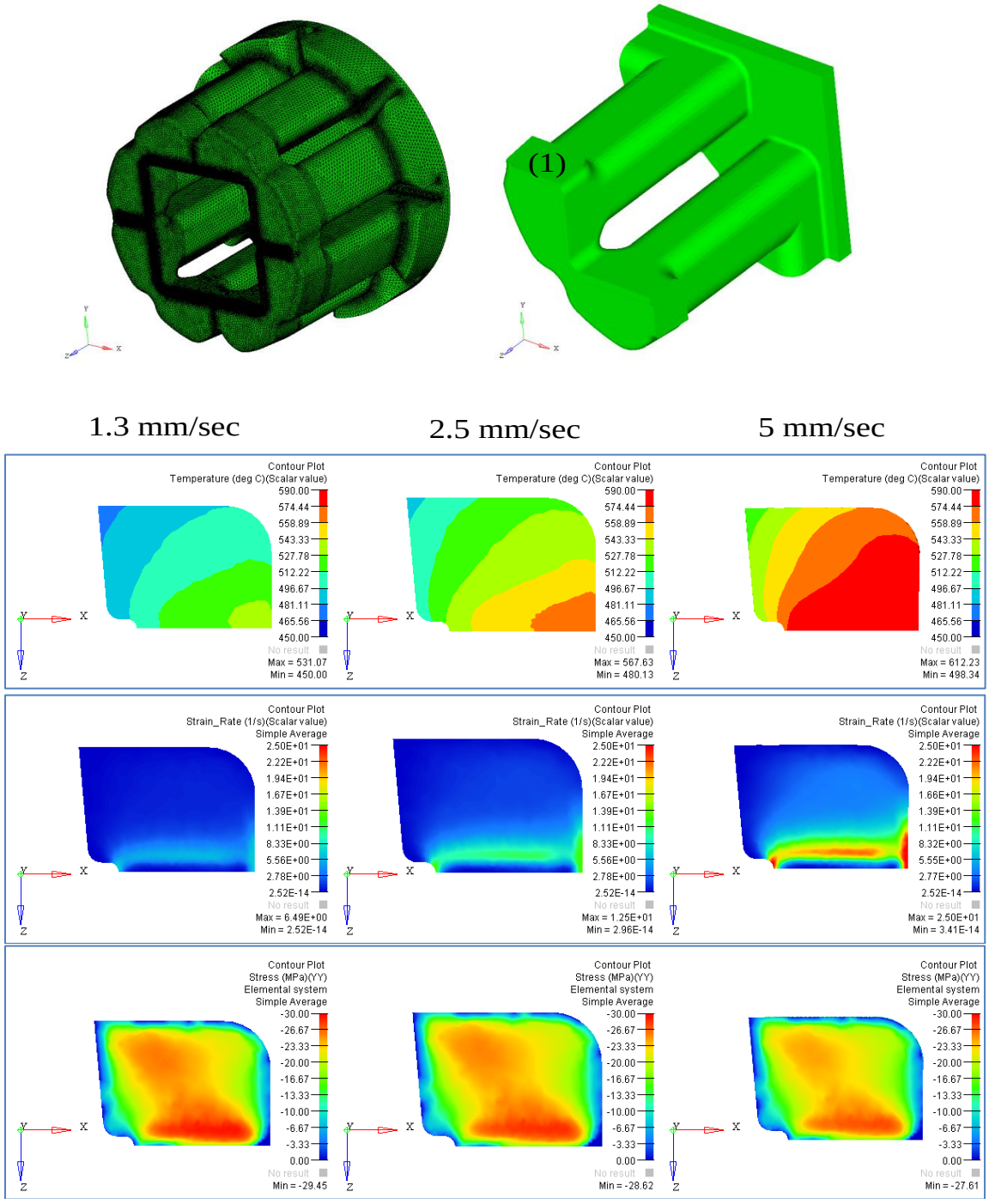

Figure 3-12. Comparison between temperature, strain rate and normal stress at weld zone (1) at different strain rate (1.3 mm/sec, 2.5 mm/sec, 5 mm/sec) and 450°C billet temperature

4 Physical Simulation of Extrusion Welding of Magnesium Alloy AM30

4.1 *Introduction*

There is a lack of fundamental understanding of the optimal extrusion process parameters, which ensure the formation of the sound extrusion weld. In addition, the complexity of the state of stresses, the temperature distribution and the strain rate within the welding chamber complicate further the selection of the optimal process parameters that will yield good extrusion welds. Therefore, many conducted studies reported in literature have been using numerical simulation of extrusion process specifically the extrusion welding. However, these studies need to be verified experimentally in actual laboratory and industrial process which, is time consuming and could be very expensive. Alternatively, some researches have tried to develop methods to evaluate the extrusion welding and relate the process parameter to the integrity of the welding. Those studies will be briefed in the literature review section.

In Chapter 3, 3D numerical simulations for different extrusion process parameters have been presented. The results of the state variables from two different extrusion weld zones have given a big picture of the most important factors that affect the formation of the extrusion welding such as temperature, normal pressure and strain rate. However, there is a need to evaluate those values if they were sufficient to form a weld with

good integrity. In this dissertation, a new criterion for the quality of the weld integrity during the extrusion of hollow section profiles has been introduced based on the combination of inputs from both the numerical simulation and the physical simulations. The physical simulation for different state variables has been conducted on Gleeble 3500 thermo-mechanical simulator to establish the criterion and to help the verification of the obtained results from the numerical simulation step.

4.2 *Thermo-mechanical Simulator- Gleeble 3500*

Gleeble 3500 is a thermo mechanical testing system (See Figure 4-1) and was developed by Dynamic Systems Incorporated (DSI). It is a fully integrated digital closed loop control system [48]. It provides a user-friendly interface based on Windows computer software. It has powerful processors that allow running and analyzing the data from the different thermal-mechanical tests. It has a wide range of materials tests as well as a process physical simulator for conductive materials. The different types of material testing and process simulation were listed in Table 4-1.

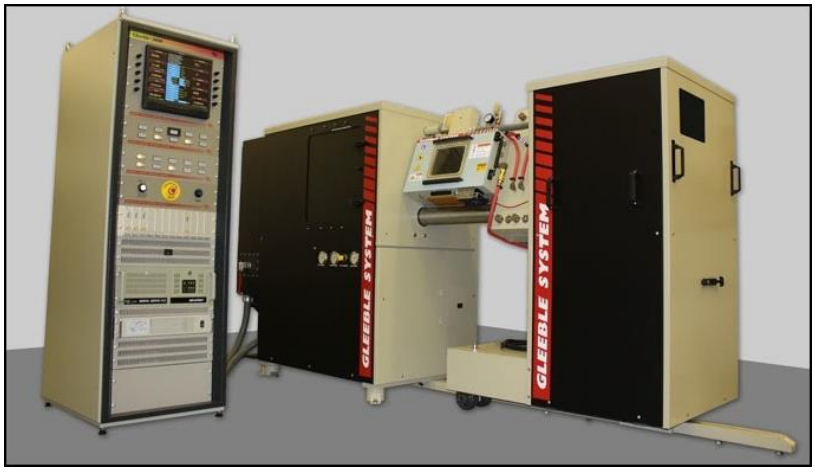

Figure 4-1. Gleeble® 3500 System developed and manufactured by Dynamic Systems Incorporated (DSI)

Table 4-1. Gleeble® 3500 thermo mechanical system for materials testing and process simulation **[48]**

Materials Testing	**Process Simulation**
• Hot/warm tensile testing on many different specimen geometries • Hot/warm compression testing – Uniaxial compression – Plane strain compression – Strain Induced Crack Opening (SICO) • Develop stress vs. strain curves • Melting and solidification • Nil strength testing • Hot ductility testing • Thermal cycling/heat treatment • Dilatometry/phase transformation – On heating and/or cooling – Continuous or non-continuous – Isothermal – Post deformation • Stress relaxation studies • Creep/stress rupture • Fatigue – Thermal fatigue – Thermal/mechanical fatigue	• Continuous casting • Mushy zone processing • Hot rolling • Forging • Extrusion • Weld HAZ cycles • Upset butt welding • Diffusion bonding • Continuous strip annealing • Heat treating • Quenching • Powder metallurgy/sintering • Synthesis (SHS)

4.3 *Literature review*

There have been many attempts to physically simulate the extrusion welding and they were reported in literature. Zasadzinski et al. [49] have used a special testing die to extrude two Aluminum alloys Al-Mg-Si and Al-Mg-Si-Mn through a die with three openings which allowed extrusion of a solid section with a weld in the middle. The weld integrity measured by the tensile strength was tested to evaluate the location of the extrusion weld with a die lay-out under the same process parameters. Different samples were tested from the beginning, middle and end of the extrudates. Generally, the results showed that the mechanical properties of all samples were the same for three extrudates from openings. However, there were slight differences in the mechanical properties between the samples taken from different locations in the beginning, the middle or the end of the extrudate. All Al-Mg-Si samples failed outside of the weld area which is a good indication that the process parameters ensured formation of a weld with good integrity. All Al-Mg-Si-Mn alloy samples failed in the weld area indicating poor weld integrity.

In another study performed by Chakkingal and Misiolek [50] , they introduced new method to evaluate the temperature influence on the weld quality of Aluminum alloy AA6063. The welding physical simulations were conducted on Gleeble thermo mechanical simulator. They used different temperatures between (500 °C -550 °C). Some of the samples

were artificially aged and other samples were solutionized and quenched. The rest of the samples were retained at as welded conditions. Tensile tests were conducted to evaluate the temperature influence on the tensile strength. In conclusions, it was found that there was no significant effect of the temperature on quality of the welds. However, the weld zone was slightly weaker compared to the rest of the tested sample.

The same approach of physical simulation using Gleeble system were used by Edwards et al. [51] where they studied the solid state bonding of three different Aluminum alloys, two from the Al–Mg–Si system - AA6060 and AA6082 as well as AA702 as Al–Zn–Mg alloy [52]. They compressed many samples under different strains, strain rates and temperatures. A new parameter to evaluate the formation of the weld called the surface stretching parameter ω was introduced. It measured the amount of new interfacial surface created during compression. Also, the time of bonding was taken into consideration. Metallography investigations were conducted to evaluate the quality of the bonding for different sample (See Figure 4-2).

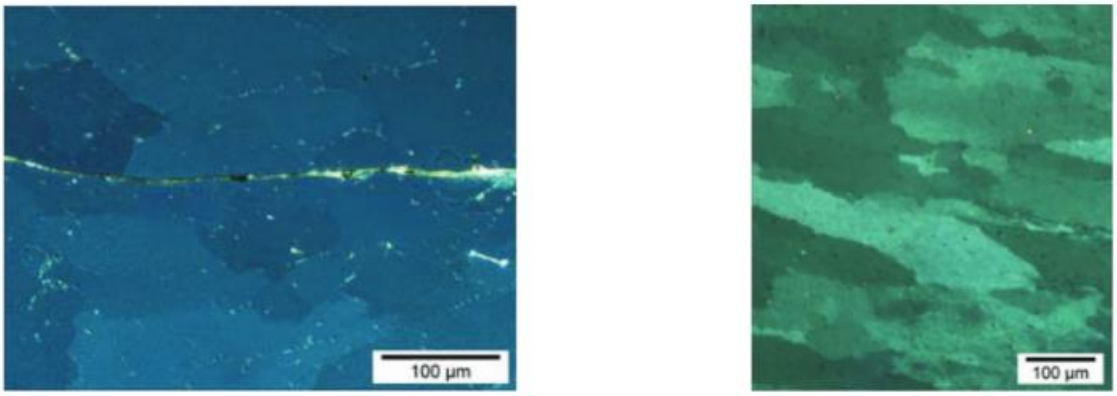

Figure 4-2. Two micrographs for the solid bonding in AA6060 at 560°C with two different strain rates 1/s (left) and 100/s (right) **[51]**

They concluded that the temperature played a role in the bonding formation by decreasing the amount of the required compression stress. In addition, there were no significant differences between the bonding behaviors between the three alloys. However, AA6060 is strongly dependent on the temperature to form the bonding which required less compression stress for the studied value of ω.

In another approach used by Ceretti et al. [53] the extrusion welding was physically simulated in a flat rolling process and compared to the obtained results from the finite element numerical simulation of complex shape hollow section extrudate. They concluded that the bonding formation not only depends on the interface pressure of the two surfaces but also depends on the temperature. Some micrographs presented in Figure 4-3 showing the influence of the temperature on the quality of bonding.

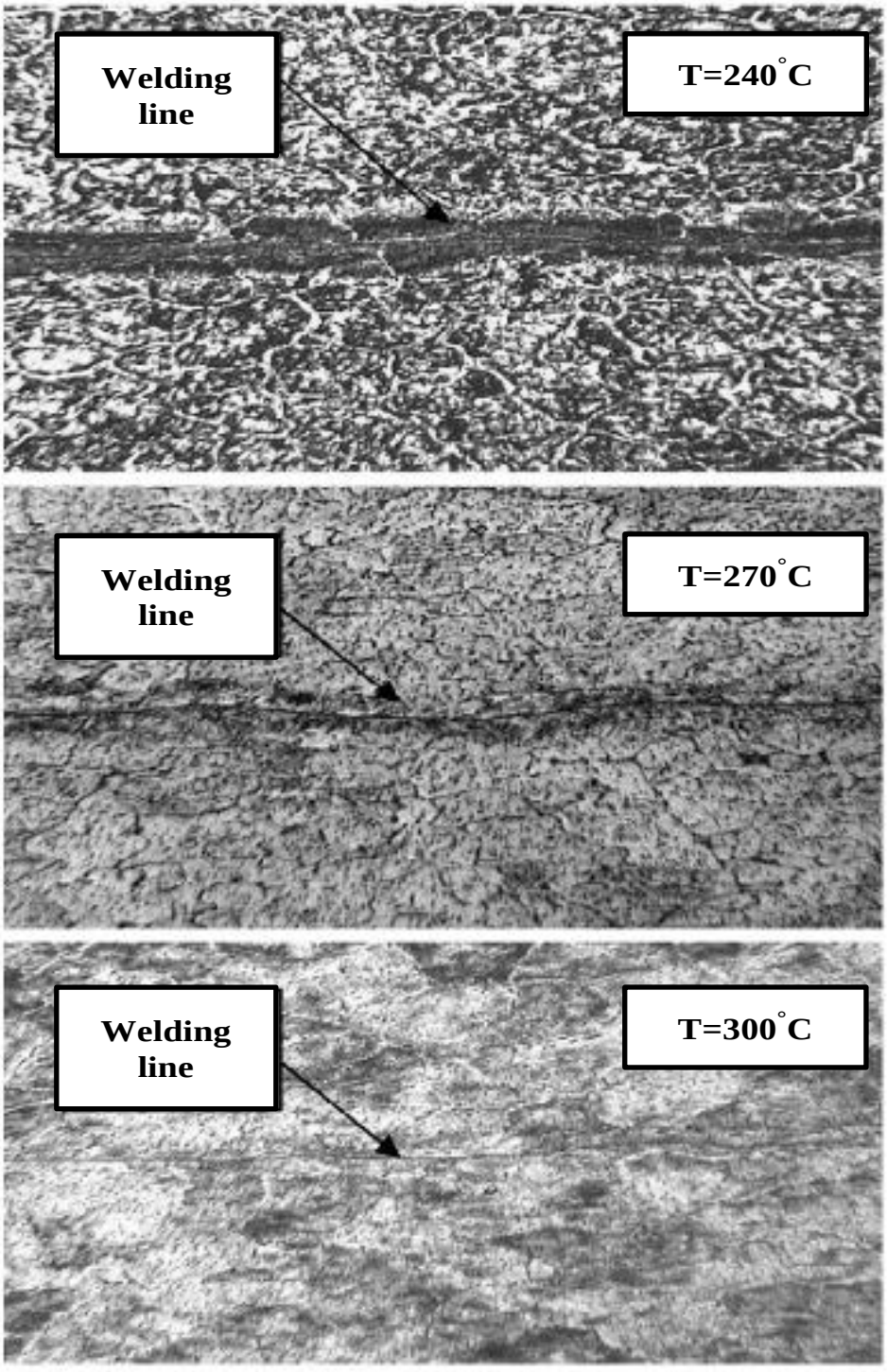

Figure 4-3. Macrographs showing the influence of the temperature on the solid bonding quality at (44% rolling ratio) **[53]**

4.4 *Experiments setup*

The physical simulation part of this extrusion welding research was based on the approach developed by Chakkingal and Misiolek [50] and focused on utilizing thermo mechanical simulator Gleeble 3500. Two cylindrical samples, 8mm diameter × 12 mm height, as shown in Figure 4-4 were placed against each other and uni-axial compression pressure was applied at specific state variables - strain, strain rate and temperature. The state variables for the extrusion process were established in numerical simulation. Then, the same state variables were used to design the physical simulation of the solid state bonding of Magnesium alloy AM 30. The objective of the experiments is to measure the required normal pressure that ensures good welding integrity. Therefore, the experiments were divided into two parts.

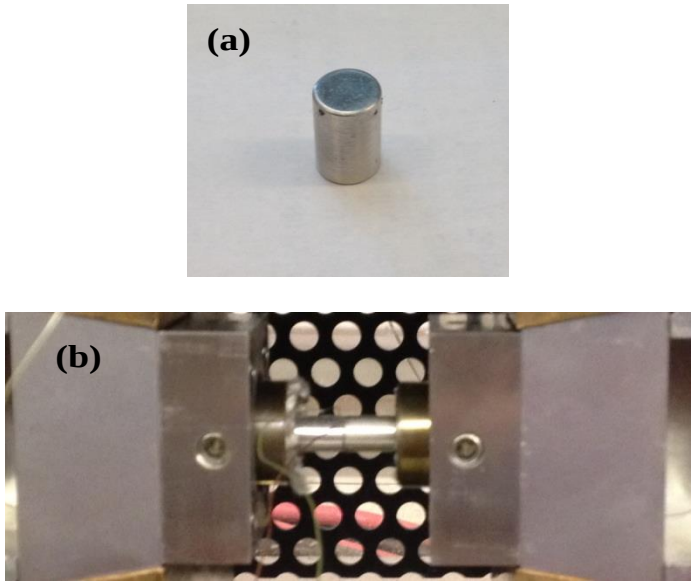

Figure 4-4. (a) A cylinder sample (b) two samples placed against each other inside Gleeble 3500

4.4.1 Evaluation of the different strain values on the formation of the weld

The first set of samples was used to evaluate six strain values (2.5%, 5%, 10%, 20%, 25%, and 30%) of the compressed samples at lowest temperature of 480°C and higher strain rate 20/s. It has been reported in literature [51] [53] that the higher the temperature the higher the quality of the weld. Also, the lower the strain rate the longer the time to form a good weld. So, if the good weld integrity was formed at these values, it is expected to form good welds at higher temperatures and lower strain rates. The microstructure of the interface between the two welded samples was characterized by light optical microscopy (LOM). After that, these samples were mechanically tested by micro hardness tests to evaluate the consistency of the hardness values across the weld line. Finally, one strain value was chosen for the next set of tests to measure the maximum normal pressure that ensures a weld with good integrity.

The samples were machined to the required dimensions then ground and polished down to 6µm using alcohol based 6µm diamond suspension on a Struers DP-Dur cloth and alcohol based lubricant to ensure flatness of the surfaces. A thermocouple was welded as close as possible to the interface between the two cylinders to measure the temperature during the tests. Then, two cylinders were placed between two anvils under a slight force to make sure that the resistive heating through the cylinders can occur (See Figure 4-5). The Gleeble 3500 controls its own temperature,

strain and strain rate very well during deformation using built-in software. The samples were heated to 480°C at a heating rate of 8°C/s. Then the uni-axial compression force was applied at 20/s strain rate while the samples were in vacuum (<10^{-1} Torr) to remove oxygen and to avoid oxidization during heating.

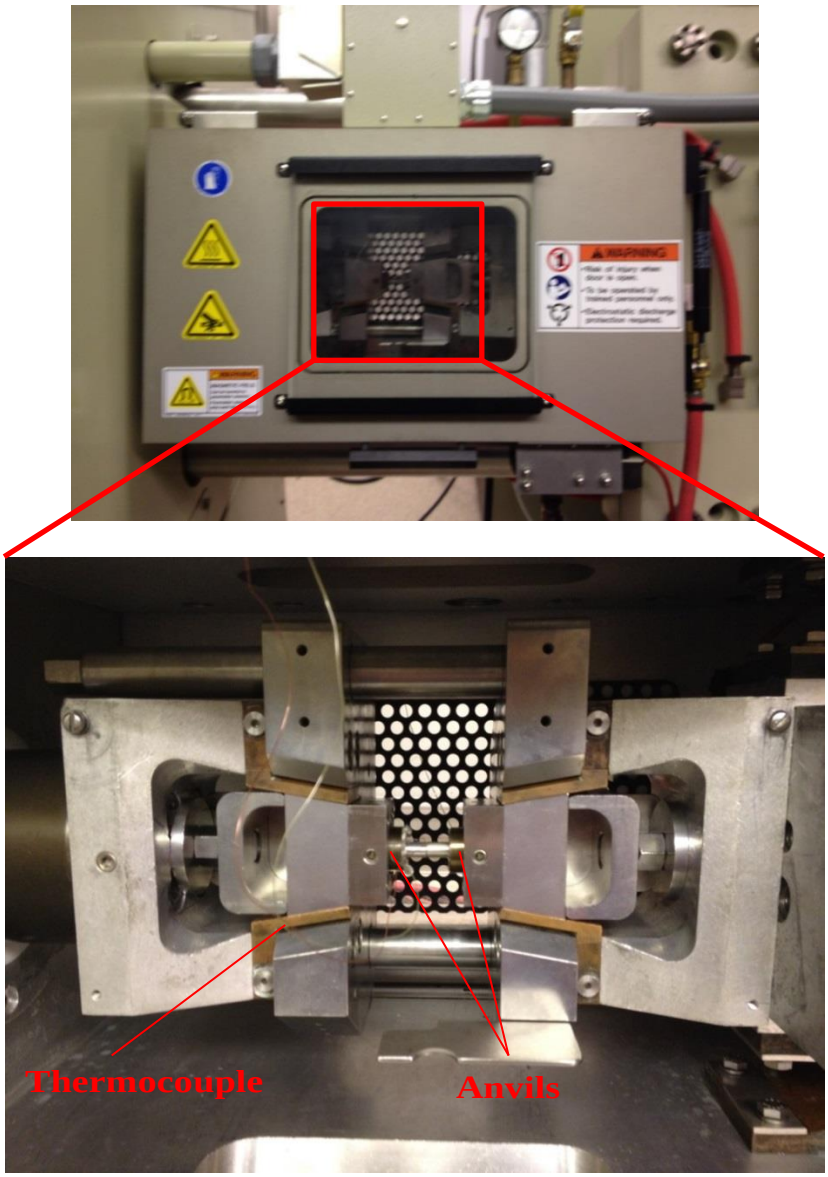

Figure 4-5. The two cylinders with attached thermocouple gripped between the two anvils inside Gleeble 3500

At the point, when required strain was achieved, the heating was discontinued and the force was reduced to its starting value allowed gripping of the welded sample. Then, the vacuum was relieved and the welded samples remained in the test chamber for two minutes to cool down to 70°C. After sample removal, the samples were labeled and stored.

For the evaluation by the light microscopy, the samples were cut by diamond saw perpendicular to the welding interface. Then, the samples were ground, polished and etched using the same previous mentioned procedure in Chapter 2. After that, the samples were polished again to prepare them for micro hardness testing.

4.4.1.1 Microstructure evaluation of the welded samples

Micrographs were taken at the interface of the six samples that represented the different strain values. The objective of the characterization part is to see how the interface looks like in comparison to the characterization of the actual extrudate that was performed earlier and described in Chapter 2. The compressed welded samples at different strains and different magnifications are shown in Figures 4-6 to 4-11.

Sample length	Diameter	Displacement	Strain	Strain Rate	Temp
24 mm	8 mm	0.6 mm	2.5 %	20 1/s	480° C

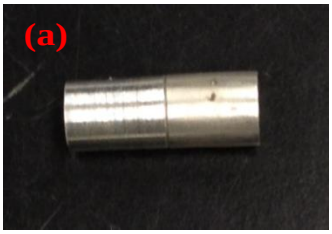

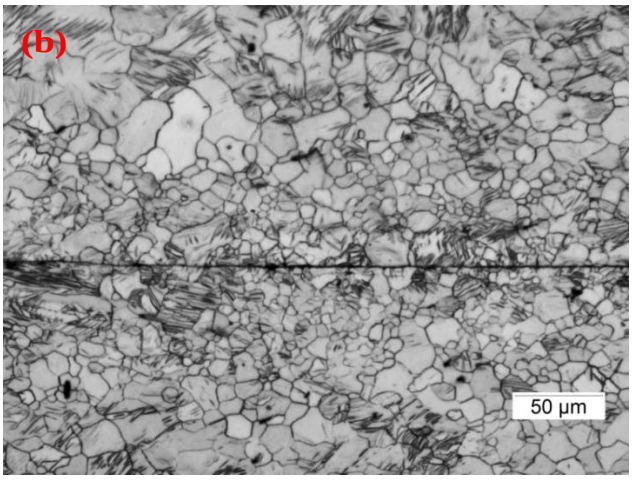

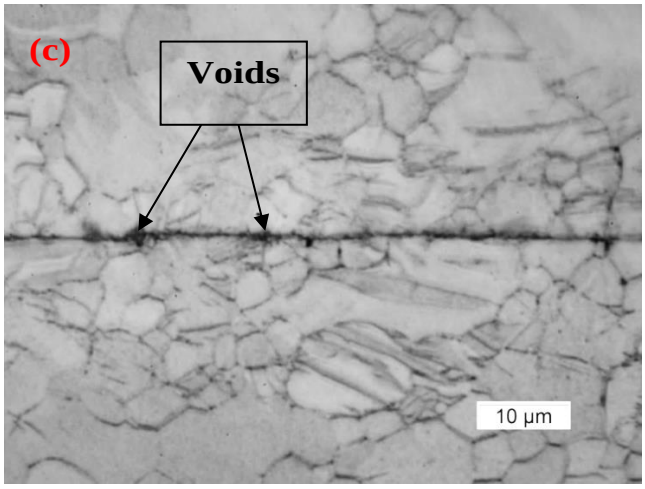

Figure 4-6. (a) The compressed sample at 2.5% strain, 20/s strain rate, 480° C temperature. (b) (c) Micrographs showing the weld at various magnifications

Sample length	Diameter	Displacement	Strain	Strain Rate	Temp
24 mm	8 mm	1.2 mm	5 %	20 1/s	480° C

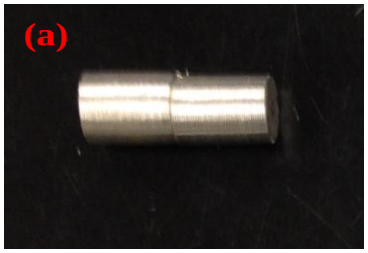

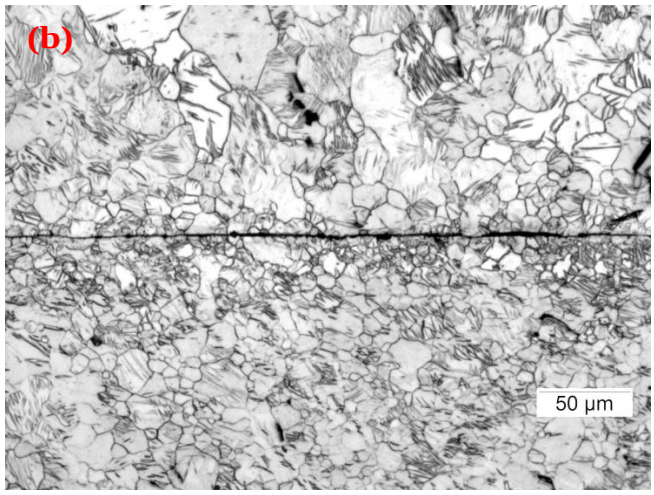

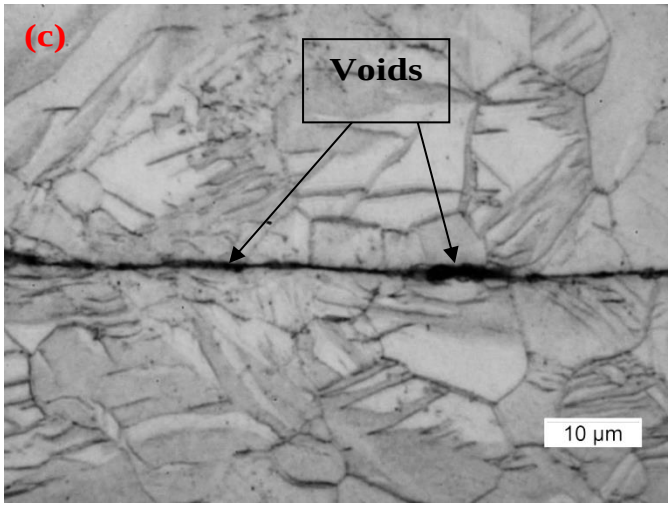

Figure 4-7. (a) The compressed sample at 5% strain, 20/s strain rate, 480°C temperature. (b) (c) Micrographs showing the weld at various magnifications

Sample length	Diameter	Displacement	Strain	Strain Rate	Temp
24 mm	8 mm	2.4 mm	10 %	20 1/s	480° C

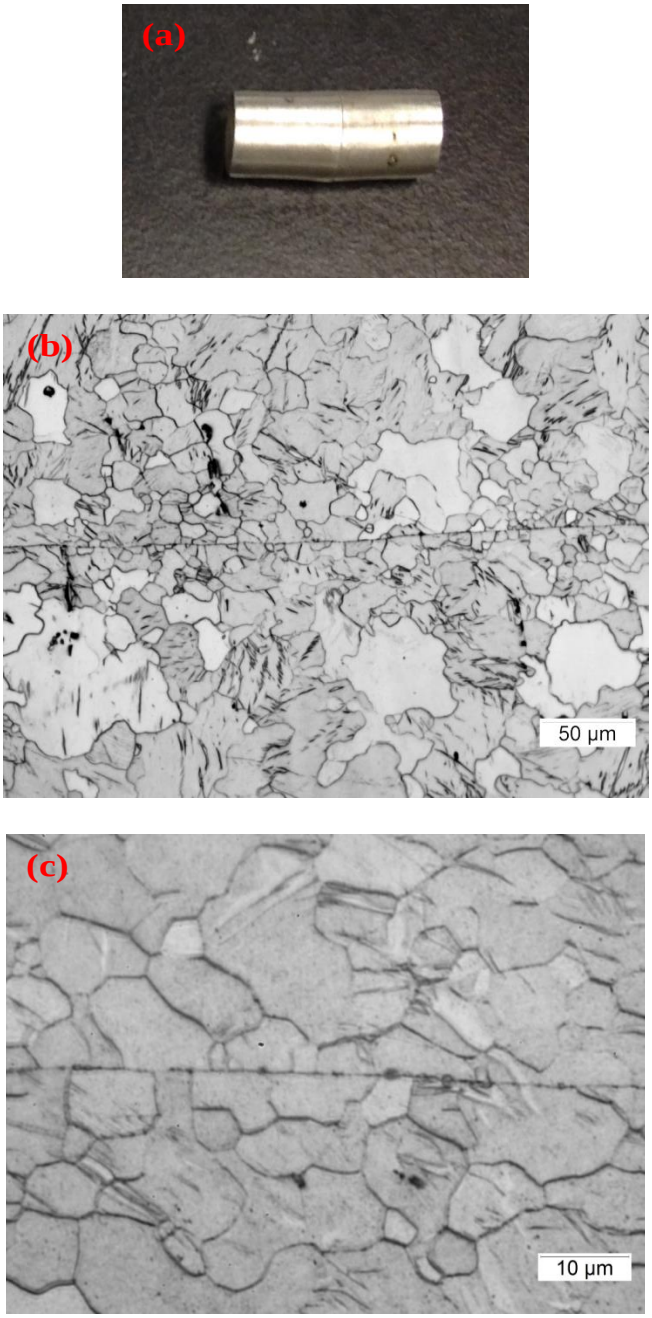

Figure 4-8. (a) The compressed sample at 10% strain, 20/s strain rate, 480°C temperature. (b) (c) Micrographs showing the weld at various magnifications

Sample length	Diameter	Displacement	Strain	Strain Rate	Temp
24 mm	8 mm	4.8 mm	20 %	20 1/s	480° C

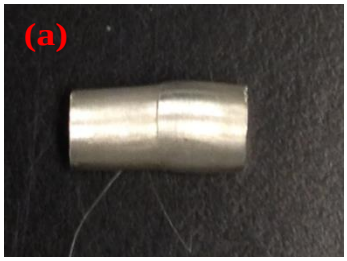

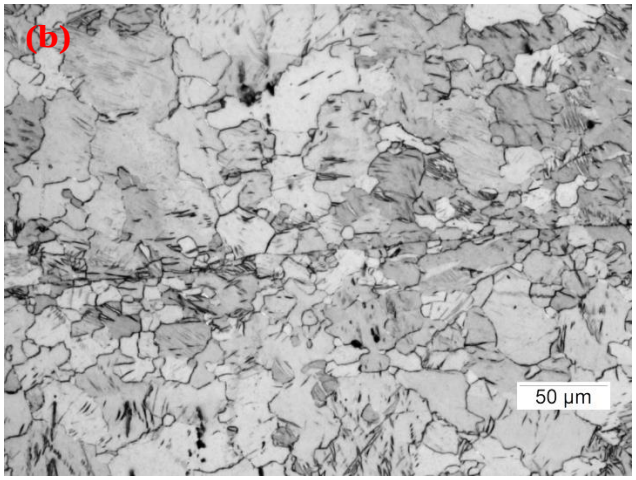

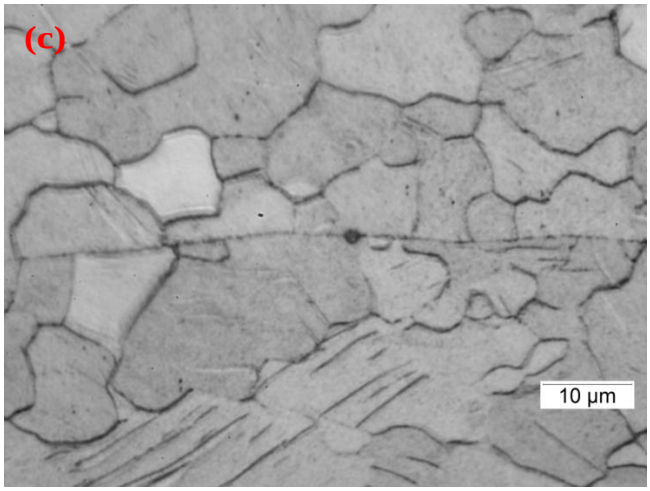

Figure 4-9. (a) The compressed sample at 20% strain, 20/s strain rate, 480°C temperature. (b) (c) Micrographs showing the weld at various magnifications

Sample length	Diameter	Displacement	Strain	Strain Rate	Temp
24 mm	8 mm	6 mm	25 %	20 1/s	480° C

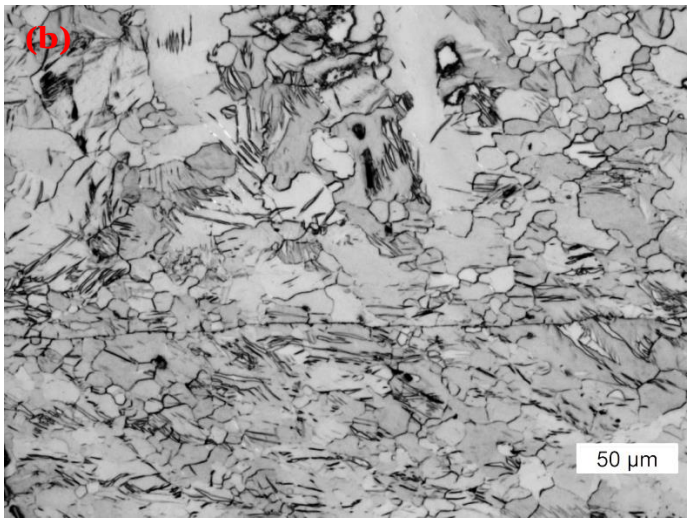

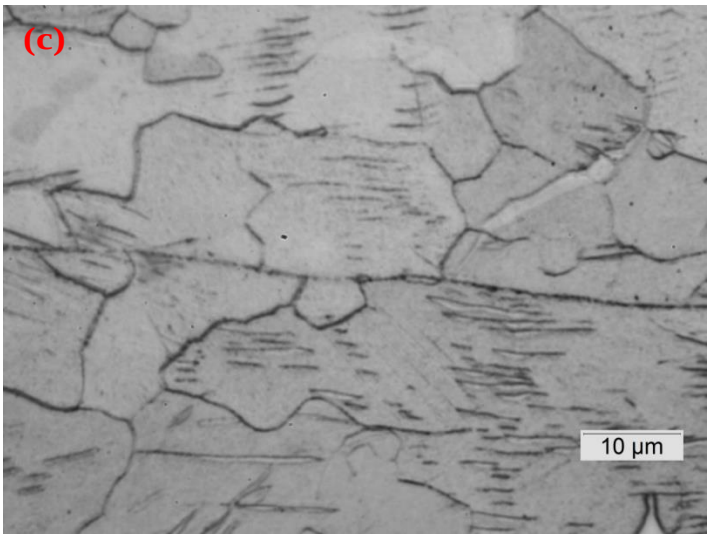

Figure 4-10. (a) The compressed sample at 25% strain, 20/s strain rate, 480°C temperature. (b) (c) Micrographs showing the weld at various magnifications

Sample length	Diameter	Displacement	Strain	Strain Rate	Temp
24 mm	8 mm	7.2 mm	30 %	20 1/s	480° C

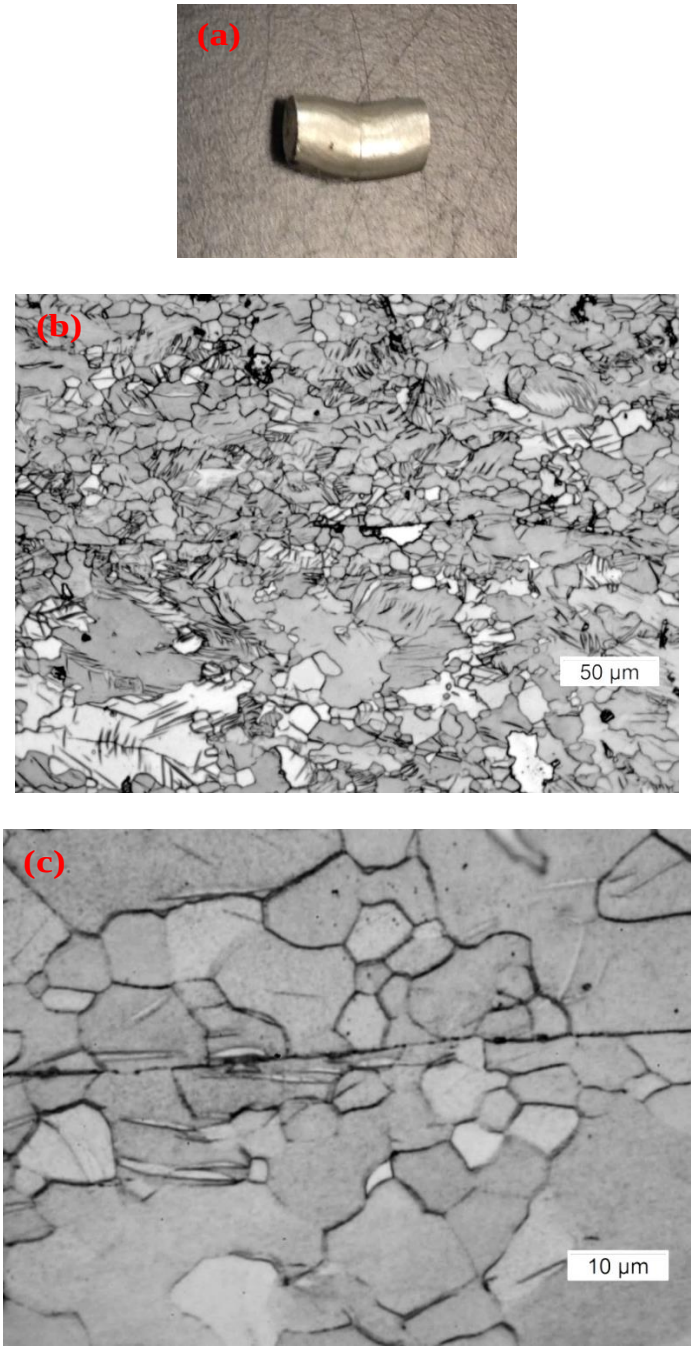

Figure 4-11. (a) The compressed sample at 30% strain, 20/s strain rate, 480°C temperature. (b) (c) Micrographs showing the weld at various magnification

4.4.1.2 Hardness measurements at weld zone

Numerous micro hardness tests were conducted based on the ASTM International E384-08a -Standard test Method for Microindentation Hardness of Materials. The 300 gf load was placed on the indenter for 15 sec. The indentations were placed exactly on the weld line plus additional measurements at 350µm and 700 µm distance from the weld line on both sides. The hardness profile was built taking into account three measurements at every location, which were averaged and plotted as shown in Figure 4-12 to Figure 4-17.

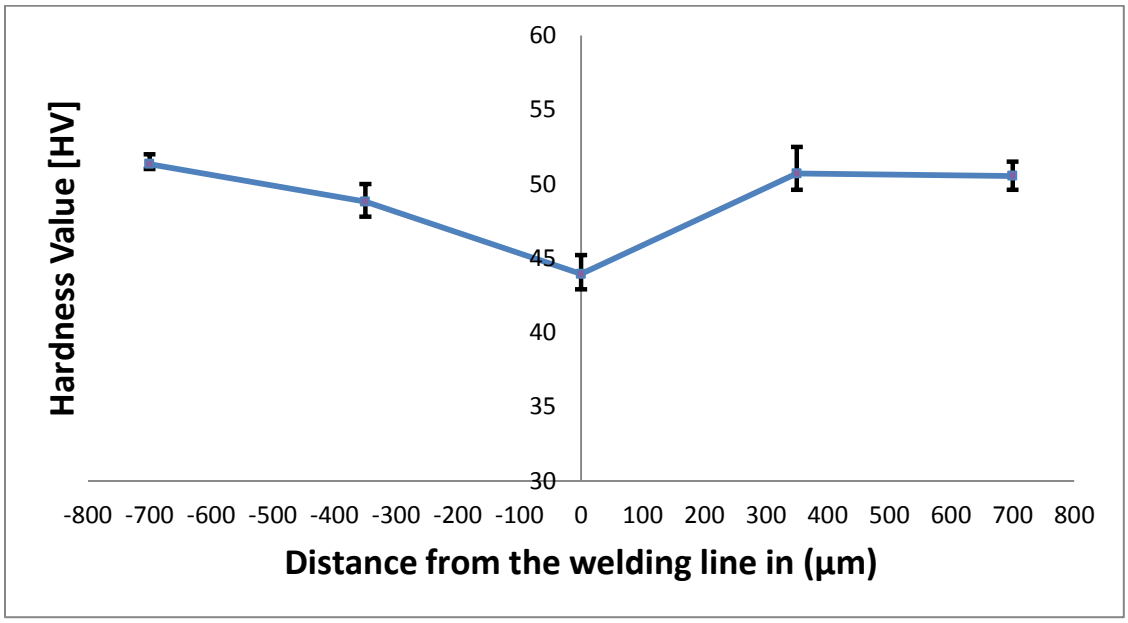

Figure 4-12. Hardness profile across the weld zone of the welded sample at 2.5% strain, 20/s strain rate, 480°C temperature.

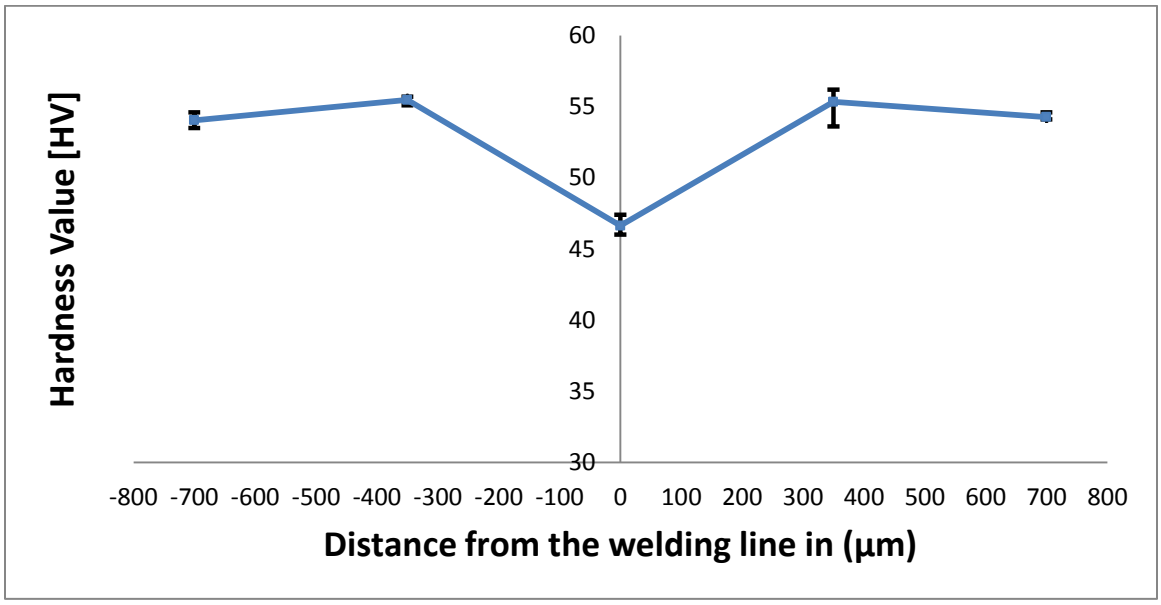

Figure 4-13. Hardness profile across the weld zone of the welded sample at 5% strain, 20/s strain rate, 480°C temperature.

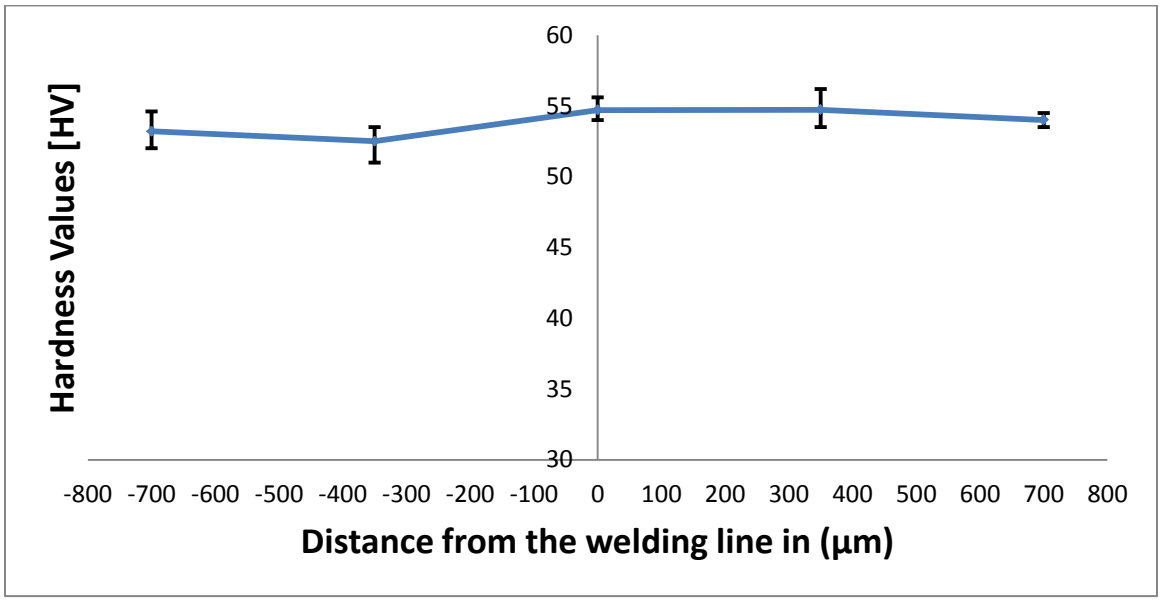

Figure 4-14. Hardness profile across the weld zone of the welded sample at 10% strain, 20/s strain rate, 480°C temperature.

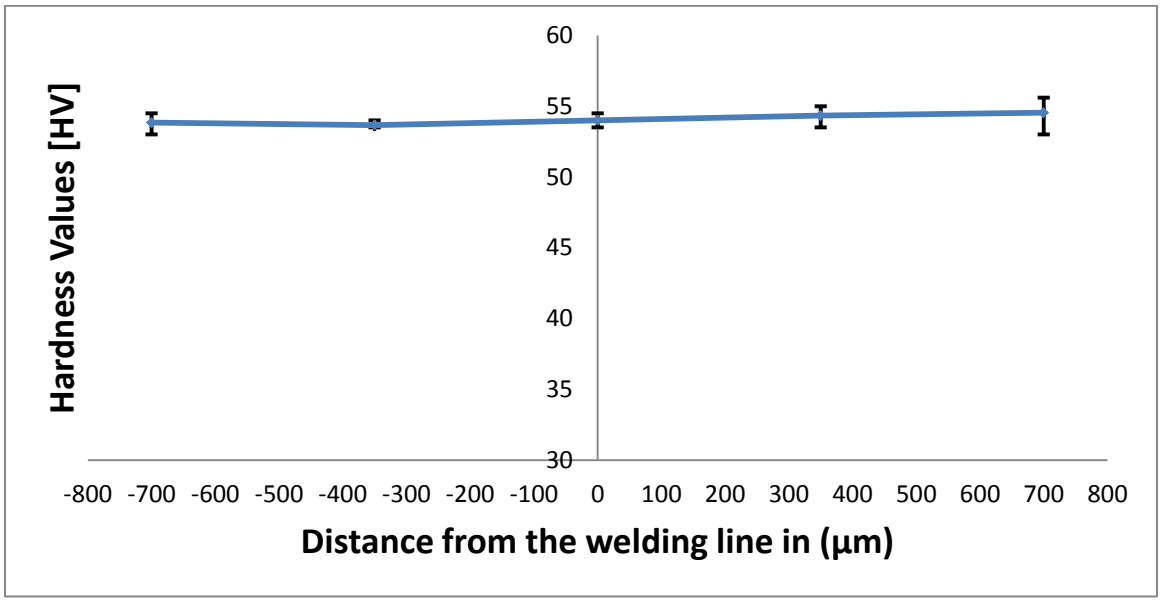

Figure 4-15. Hardness profile across the weld zone of the welded sample at 20% strain, 20/s strain rate, 480°C temperature

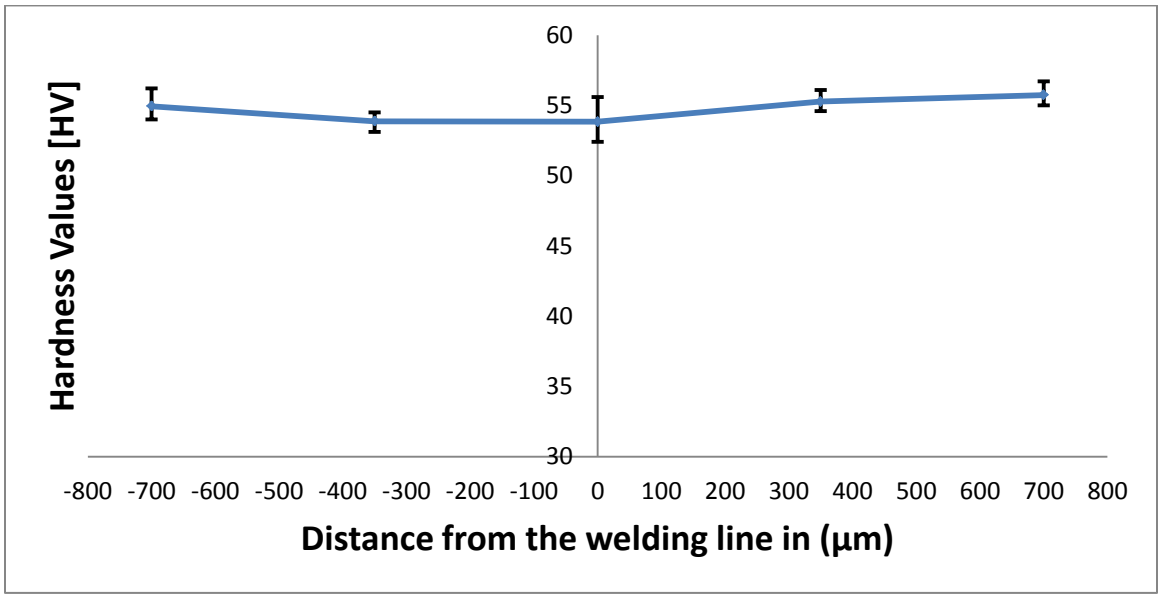

Figure 4-16. Hardness profile across the weld zone of the welded sample at 25% strain, 20/s strain rate, 480°C temperature

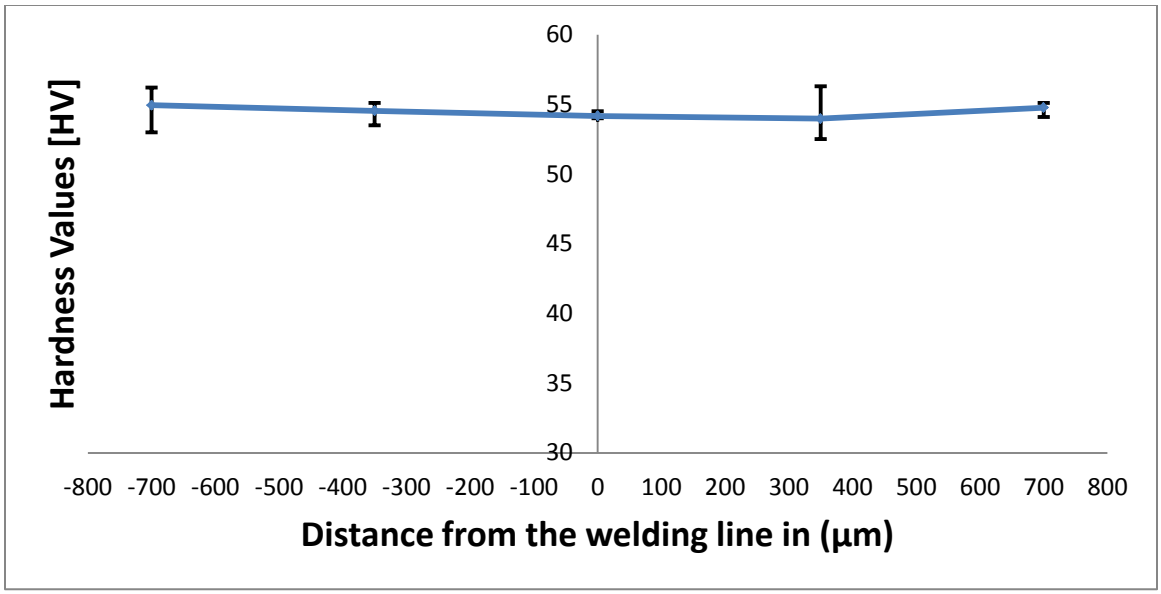

Figure 4-17. Hardness profile across the weld zone of the welded sample at 30% strain, 20/s strain rate, 480°C temperature.

4.4.1.3 Discussion of the microstructure and hardness value results for weld line and its vicinity

The micrographs of different strain values are shown in Figures 4-6 to 4-11. Many voids along the weld line can be seen in Figure 4-6 and Figure 4-7 which represent strain values of 2.5% and 5% respectively. These voids are indication of a weak weld and consequently poor weld integrity. Accordingly, the hardness profiles of the same samples (See Figure 4-12 and Figure 4-13) showing drop in the measured hardness values at the weld line. The hardness values at the weld line for 2.5% strain sample were averaged at 44 HV while the rest of the values are between (48-50) HV. Also, the hardness values at the weld line for 5% strain sample were averaged at 46 HV while the rest of the values are

between (53-55) HV. Therefore, the drop and inconsistency of the hardness values at the weld line can be attributed to the apparent presence of voids at the weld line which is an evidence of poor weld integrity.

Good weld integrity is expected for samples presented in Figure 4-8 and Figure 4-9. There are no voids and the presented microstructure is in a good agreement with the micrographs of the weld line of the actual extrudate that was characterized early in Chapter 2 (See Figure 2-11 and Figure 2-12). In addition, the hardness profiles for the same samples presented in Figure 4-14 Figure 4-15 were consistent across the weld zone in both samples. The hardness values for the 10% strain sample were between (53-55) HV while, in the 20% strain sample was between (54-56) HV. All values were in good agreement with the hardness profiles which were reported in Chapter 2 for the actual extrudate. (See Figure 2-23). Micrographs of the 25% and 30% strain samples look promising at the weld zone as well as the hardness profiles however, both samples started to buckle during compression as shown in Figure 4-10 (a) and Figure 4-11(a). Consequently, an inclined weld line started to form where the shear stresses played a role in the formation of the weld. However, the objective of this experiment was to measure the normal pressure at the interface. Therefore, these higher strain experiments are not fully valuable. Based on the previous results and analyses, 20% strain exhibited the best

strain to ensure good weld integrity and has been chosen for the next set of experiments despite of some challenges during compression test.

4.4.2 Measurements of normal pressure at 20% strain

In the previous section, an evaluation has been performed for different strain values. Based on the analyses, 20% strain has been selected to measure the normal pressure at different temperatures and different strain values. These state variables were chosen according to typical values of the numerical simulation of the extrusion of Magnesium AM30 at the weld zones which was reported in Chapter 3. The objective of the previous set of experiments was to evaluate different strain values whereas the objective of this set of experiments is to measure the maximum normal pressure at 20% strain that ensures good weld integrity for various temperatures and strain rates. Physical simulation experiments for the extrusion weld based on compression of two faced cylinders for three temperatures 480°C, 500°C, 550°C and three strain rates 1/s, 10/s, 20/s were performed. The experiments were performed under the same setup conditions as previous tests.

4.4.2.1 Results and discussion

The normal pressure values were measured during the compression tests for 20% strain at various temperatures and strain rates. All normal pressure values were plotted versus strain in Figure 4-18 to Figure 4-20.

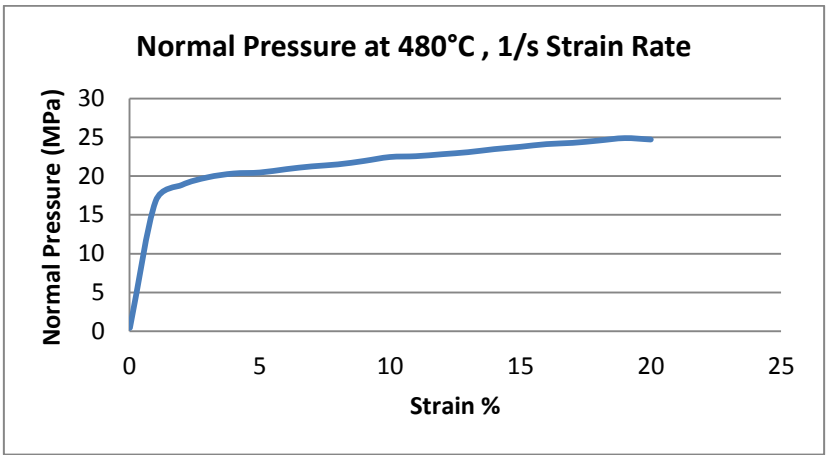

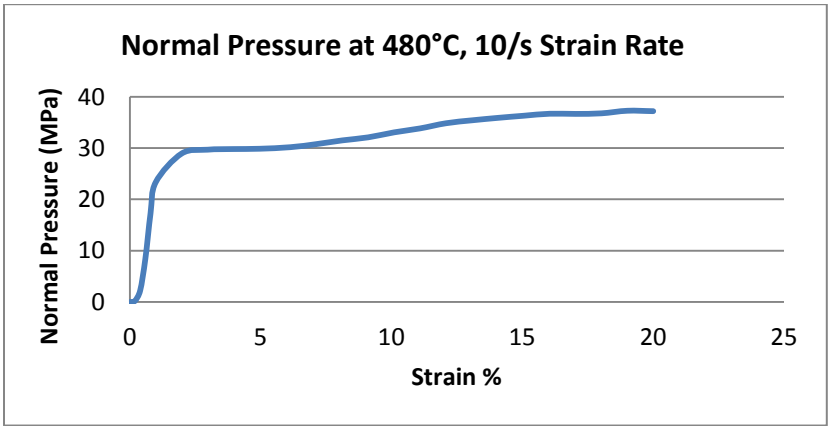

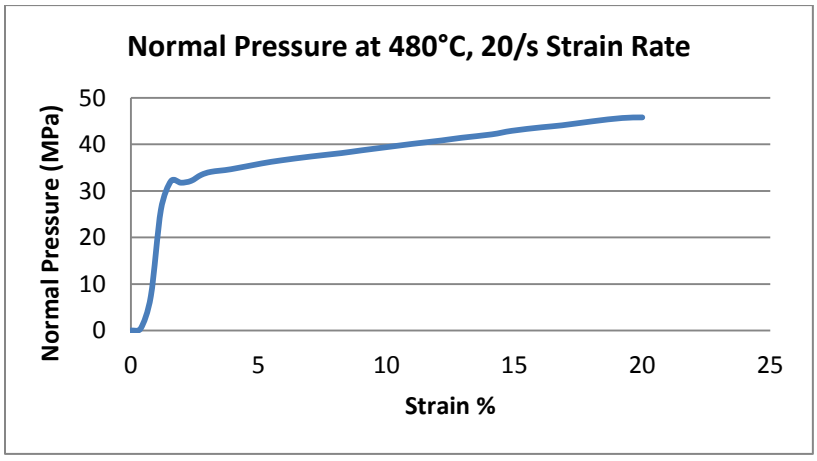

Figure 4-18. Normal pressure vs strain at 480°C, 1/s, 10/s, 20/s strain rates

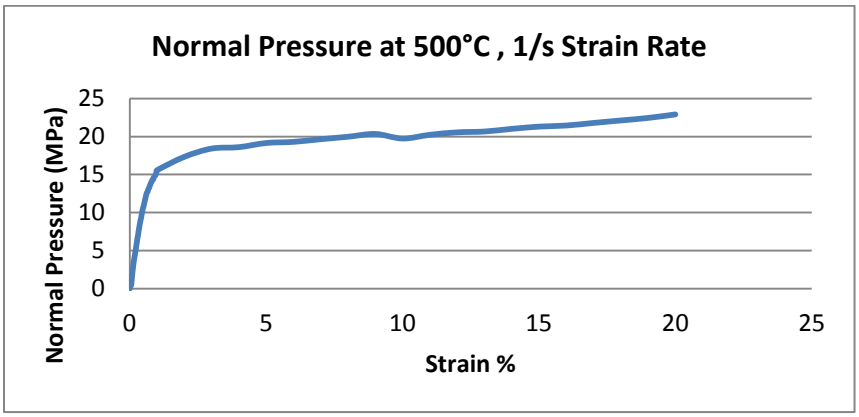

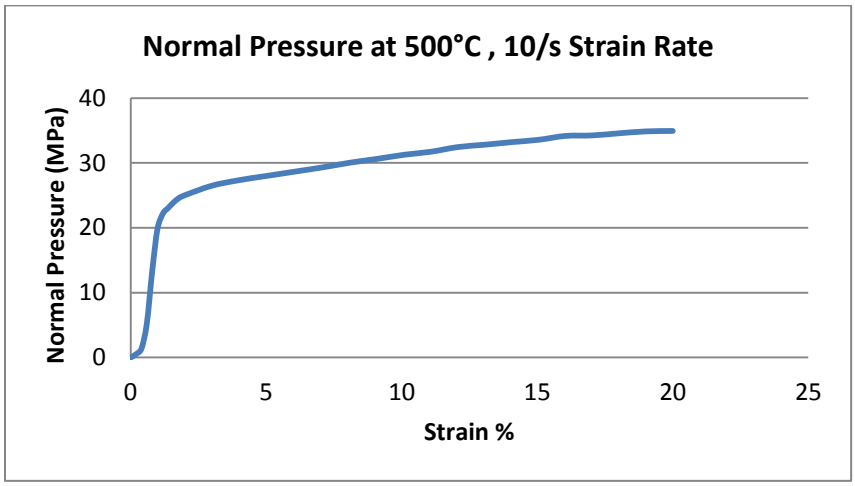

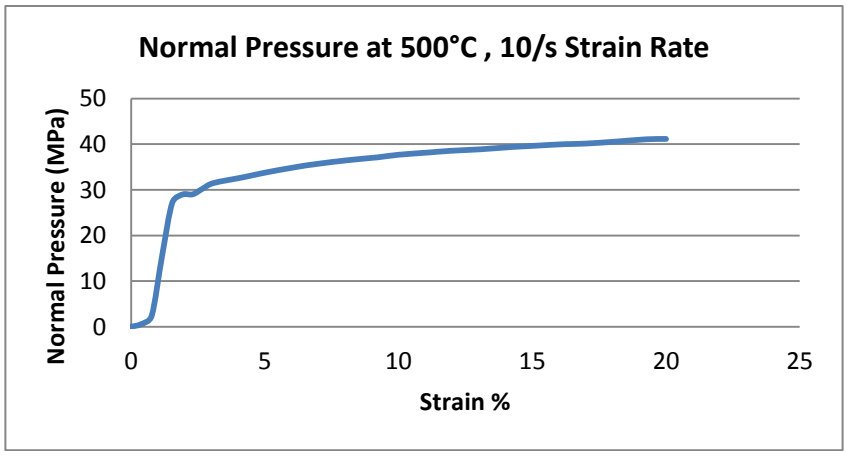

Figure 4-19. Normal pressure vs strain at 500°C, 1/s, 10/s, 20/s strain rates

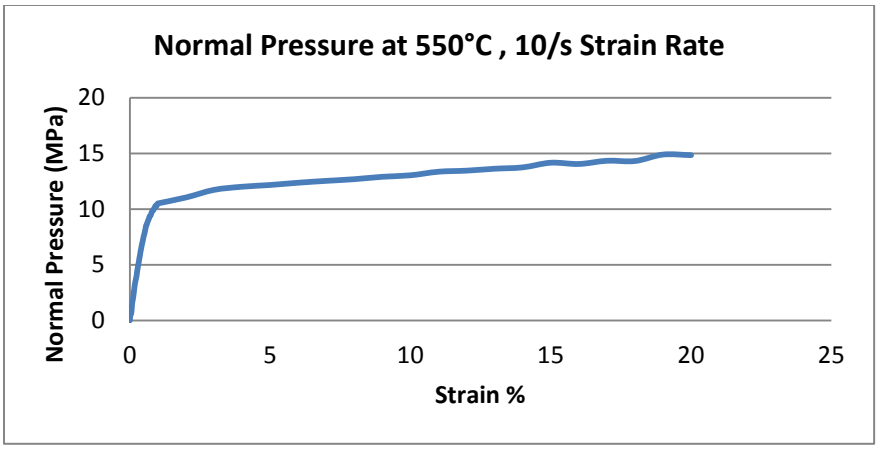

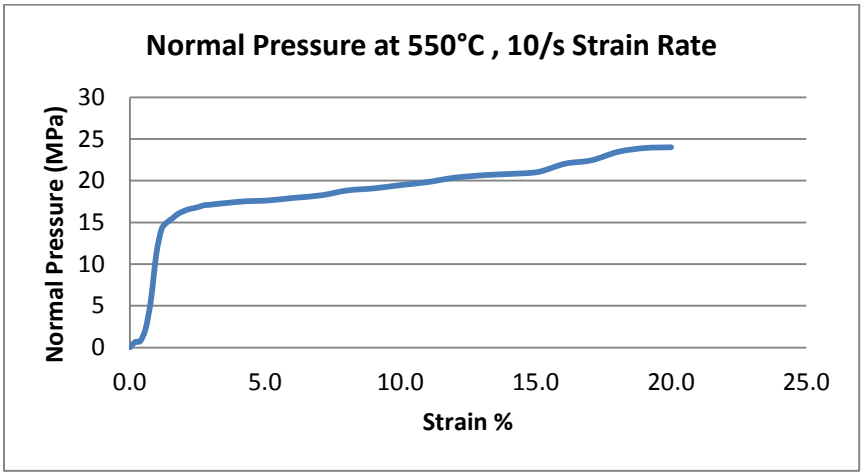

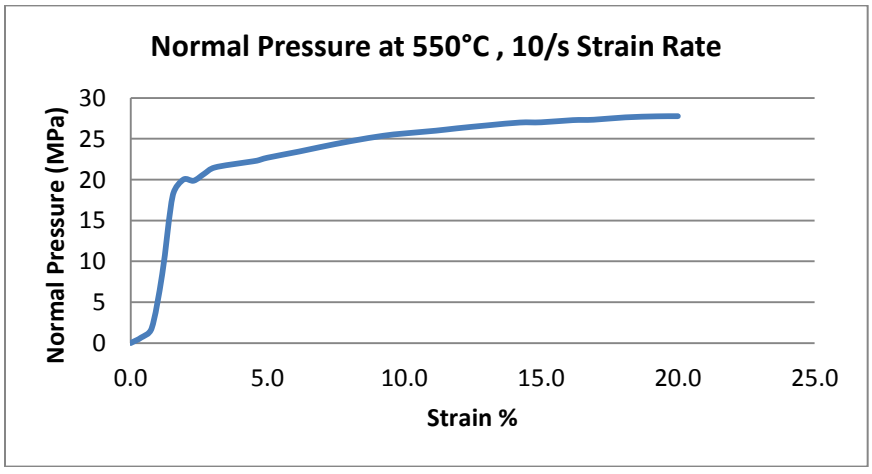

Figure 4-20. Normal pressure vs strain at 550°C, 1/s, 10/s, 20/s strain rates

The behavior of the normal pressure in all of the previous figures was similar to the behavior of the hot compression stress of Magnesium alloys that has been reported in literature [7][31][54][55][56][57][47][44]. The values of compression stresses are in agreement with three studies of modeling the flow stress of Magnesium alloy AM30 [57][47][44]. However, the reported values were at lower temperatures below 450°C. It is well known for metals that the higher temperature the lower the metal strength obtained from the compression or tensile tests. Also, the higher the strain rate the higher the compression stress needed for deformation. The maximum normal pressures values are represented in Figure 4-21. These values will be used for building a new criterion for the extrusion welding quality in Chapter 5.

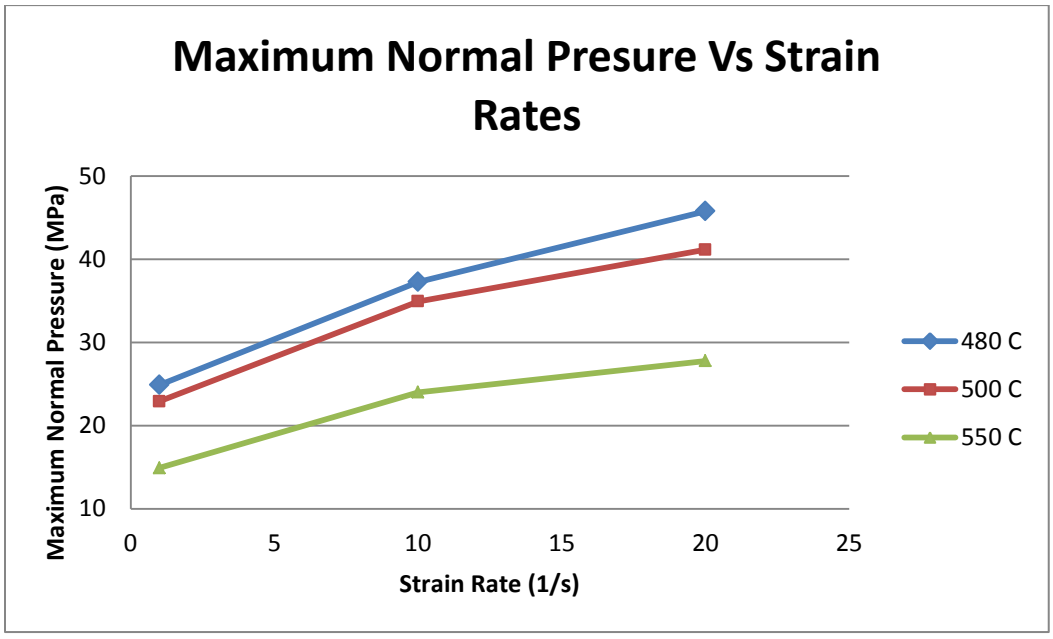

Figure 4-21 Maximum normal pressure as a function of strain rates for temperature 480°C, 500°C, 550°C.

5 New criterion for extrusion welding quality

5.1 *Introduction*

The quality of the longitudinal welds in the extruded hollow shapes is precisely influenced by the pressure, temperature, velocity of the material inside the welding chamber and bearing land geometry of the die. Sound extrusion welding takes place if the necessary pressure value for a given temperature is applied within the welding chamber for a sufficient length of time. In this work a new criteria based on physical and numerical simulation is applied to the hot extrusion of Magnesium Alloy AM30 and its application can be extended to numerous metals and alloys.

The proposed extrusion welding criterion is different than the previous criteria in a few different ways. It is applicable and practical once the peak of normal pressure at the weld interface has been defined in the physical simulation. The previous criteria required an experimental work for each process parameters of the actual extrusion process which is very expensive and labor intensive. However, the proposed physical simulation is relatively simple, practical and does give good predictions for the actual process. In addition, the proposed criterion will help in saving time and expenses in the die design process.

5.2 *Literature review*

Most of studies focused on the seam weld quality are using pressure in weld chamber to quantify weld quality [58]. Donati et al. [38] have summarized the different methods and quantified the welding quality into three categories: 1) maximum pressure by R. Akeret [19] , 2) pressure-time by M. Plata and J. Piwnik [37] and 3) pressure-time-flow by L. Donati, and L. Tomesani [59]. Akert [19] have stated that the maximum pressure inside the welding chamber must be greater than the critical pressure value (P_{Crit}).

$$P_{\max} = \max(P_i) > P_{crit} \qquad \text{Equation 5-1}$$

Where, P_i is the pressure of i-th element inside the weld chamber and P_{Crit} should be established experimentally for a specific profile, which makes this approach not very practical. In another study Bourqui et al. [60] from Alcan have proposed that, the critical value is ratio of pressure inside the weld chamber P_{weld} to pressure at die entrance P_d and it must be greater than 0.5.

$$P_{weld} > 0.5\ P_d \qquad \text{Equation 5-2}$$

Plata and Piwnik [37] have proposed pressure-time weld quality criterion by taking the time integral of the ratio of contact pressure (p) and effective stress (Q) along the welding path. The time here is the required contact time along a welding path from the start of the material contact until it exits the die bearing land.

$$\int_t \frac{P}{Q} dt \geq C_{cr} \qquad \text{Equation 5-3}$$

Donati and Tomesani [38] have modified Plata and Piwnik criterion by including the velocity factor making a new integral of the length integral of the ratio of the pressure (p) to the effective stress (Q) and it should exceed a critical value that would be determined experimentally.

$$\int_t \frac{P}{Q} dt.v = \int_l \frac{P}{Q} dl \geq C_{cr} \qquad \text{Equation 5-4}$$

Both mentioned above criteria need an experimental work effort for every extruded profile shape which is not practical in industry since there is a huge number of an extruded alloy into various shapes.

Parallel to the physical modelling and analyses that has been summarized in the previous chapter; the Finite Element Method (FEM) has been widely used in the extrusion process design and optimization. Numerical simulation by FEM provides information about localized process state variables such as temperature, strain, strain rate and stress which can be properly calculated step by step throughout the entire process. However, solid state bonding such as in extrusion welding was not taken into account in the past by the developers of most FE packages [53][61]. For instance, although DEFORM ™ is one of the most widely used commercial software packages finite element analyses of bulk metal forming processes, it was not capable of predicting weld formation and weld integrity in the extrusion process. Furthermore, it was not capable of generating the local state variables at extrusion welding interfaces. E

Ceretti et al. [62] have discussed this deficiency and developed an automatic procedure algorithm, which has been implemented into DEFORM 2D software. However, the developed method only modifies the simulation of the welding seam and it cannot generate localized state variables. Xu and Misiolek [61] have proposed a new modelling method to overcome this software limitation and has applied it to Magnesium alloy AZ31. A so-called pressure plate was virtually inserted in the interface of the extrusion welding seam by attaching it to the porthole die's short mandrel as shown in Figure 5-1.

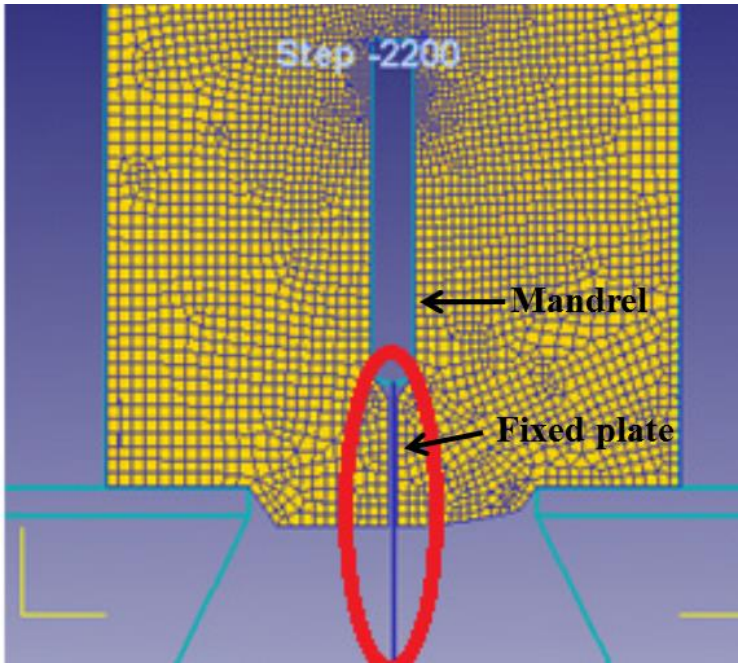

Figure 5-1. The developed model Fixed Pressure Plate in DEFORM^{TM} 2D simulation **[61]**

The pressure plate played a role of a sensor and recorded all the process information at the extrusion welding line. Analytical methods were utilized to study the data collected from this sensor to evaluate the probability of the formation of the sound extrusion welding seam. Furthermore, the Plata and Piwnik [37] criterion, Equation 5-5 , which is the ratio of the normal pressure (P) to effective stress (σ) was employed in this work for data analysis. However, the results showed high noise because of the fixed step number used during the simulation. Accordingly, Alharthi et al. [63] have modified a model proposed by Xu and Misiolek model. The same approach was used but the noise has been minimized. The modified model has a changing number of steps during the ram travel along the pressure plate in the extrusion direction. Also, the average values of state variables were taken for around 700 steps (See Figure 5-2)

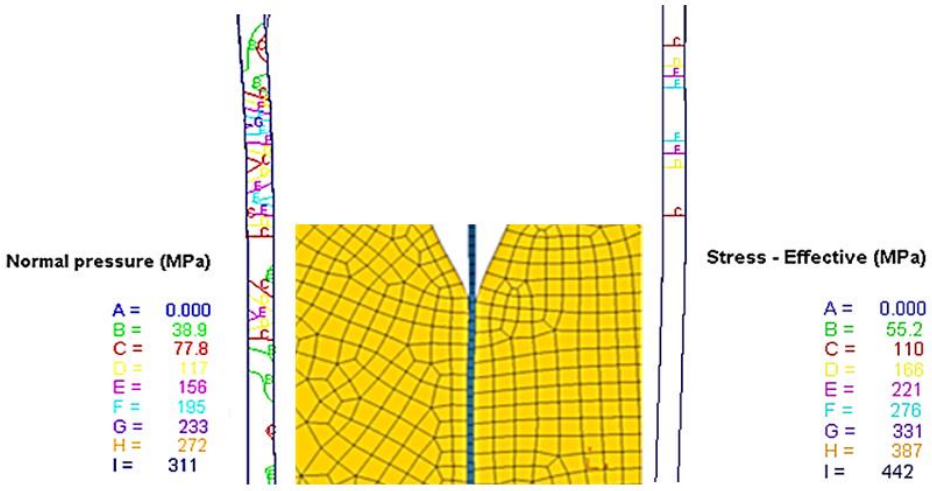

Figure 5-2. The normal pressure and effective stress distribution on the pressure plate between the metal streams at ram speed 1.98 mm/sec and billet temperature 460°C **[63]**

The following conclusions based on the performed numerical simulations by Alharthi et al. [63] and verified by experimental data published in literature [38] have been formulated:

1) Normal pressure and effective stress distributions within the welding chamber and die bearing land is not uniform due the joining of the two metal strands. The normal pressure and effective stress' values decrease along welding chamber and bearing land toward die exit which can be attributed to the complexity of the state of the stress at the beginning of the joining process.
2) In the beginning of the joining of metal streams within the welding chamber, the ratio of normal pressure to effective stress which is related to the welding quality is low, and then it rises clearly for a short distance then stays constant.
3) As the billet temperature increase, the normal pressure and the effective stress decrease in a very similar manner within the welding chamber and die bearing land. However, the P/σ ratio almost remains constant up to the die exit.
4) The normal pressure and effective stress increased with increasing ram speed. However, there is a slight decrease in the P/σ ratio.

5.3 *New proposed criteria for evaluation the extrusion weld quality*

All previous criteria presented in literature [19] [37] [38] [58] [59] were based on the ratio of normal pressure to the effective stress. It was represented that the time integral of this ratio or the length integral should exceeds a critical value (C_{crit}), which should be verified experimentally for actual process making it cost ineffective and time consuming.

As reported in the literature [19] [37] [38] [58] [59], the normal pressure has the strongest influence of the formation of the extrusion welding and in this approach the shear stress was neglected due to its small contribution in comparison to the normal stress. In addition, the ram speed and the temperature have strong influence on weld integrity and should not be neglected.

Basically, the new proposed criteria are based on the numerical simulation of the hot extrusion and the experimental physical modeling of the deformation welding phenomenon. From the results of numerical simulation performed with HyperXtrude^{TM} software, the state variables temperature, strain rate and normal pressure of selected path in the weld zone plane including welding chamber and bearing land (See Figure 5-3) were averaged and compared with the physical simulation results.

In Chapter 4, the maximum normal pressure values that ensured formation of a good weld, which were obtained for different strain rates

and temperatures. The results as well as process conditions are summarized in Table 5-1 for physical simulation tests.

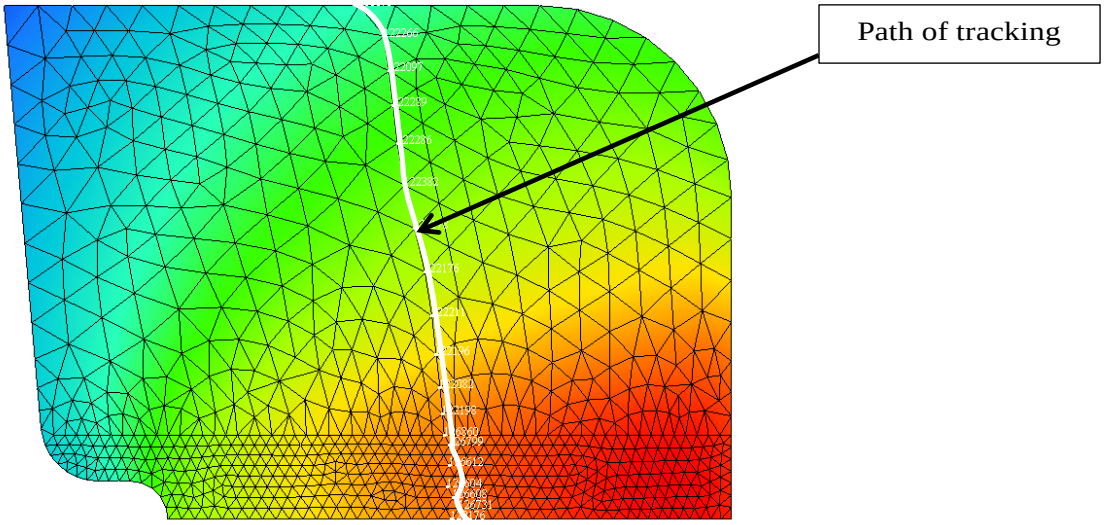

Figure 5-3. The path of tracking the different state variables of temperature, strain rate and normal pressure

Table 5-1. Maximum normal pressure values from physical simulation of extrusion weld for Magnesium alloy AM30 for different strain rate and temperature

Strain Rate (1/s)	Temperature (C)		
	480	500	550
1	24.89 (MPa)	22.90 (MPa)	14.89 (MPa)
10	37.26 (MPa)	34.93 (MPa)	24 (MPa)
20	45.78 (MPa)	41.14 (MPa)	27.76 (MPa)

5.4 *Results and discussion*

The averaged values of temperature, strain rate and normal pressure of selected path were obtained from HyperView™ and are presented in Figure 5-4 to Figure 5-8

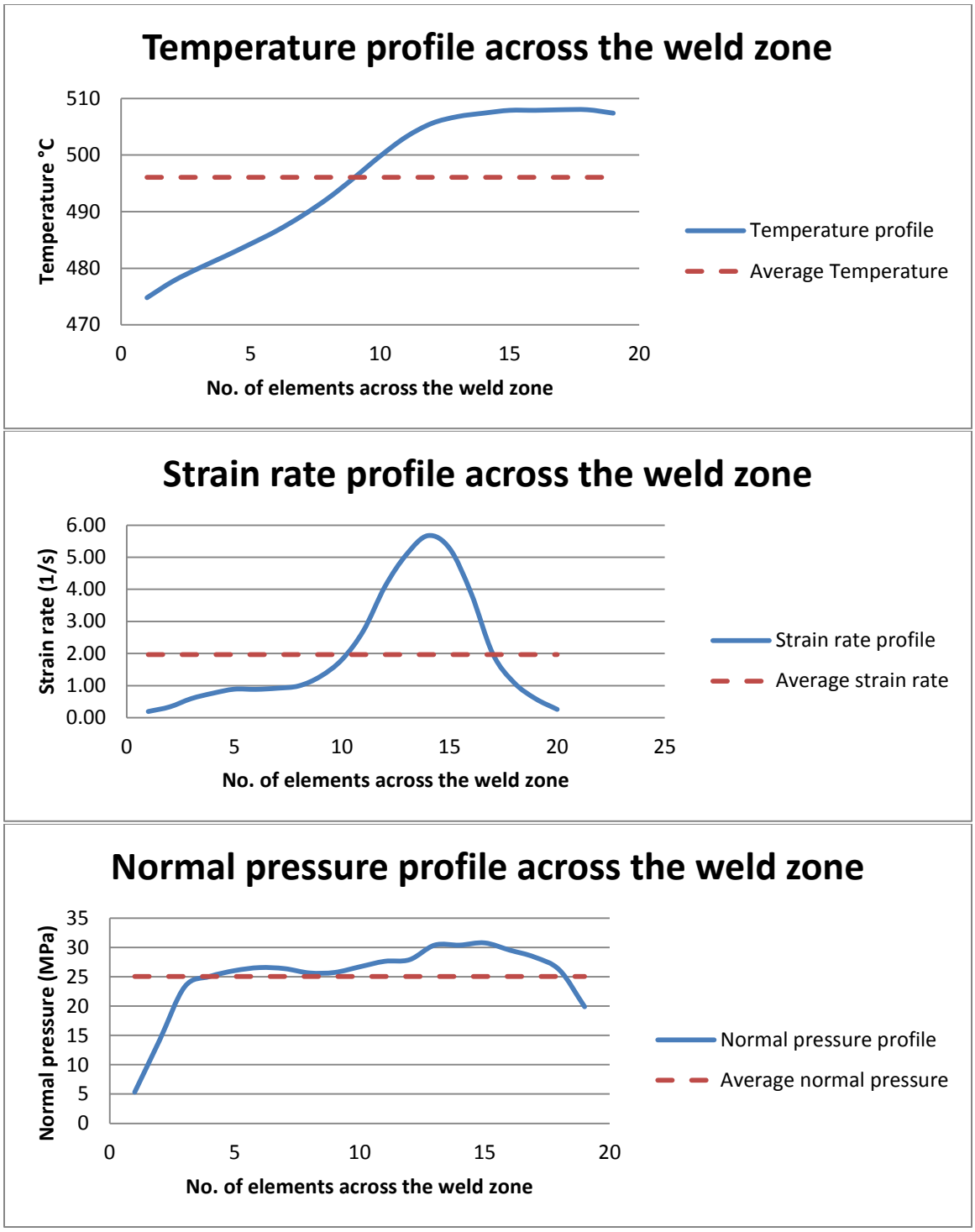

Figure 5-4. Predicted FEM values - temperature, strain rate and normal pressure profiles across the weld zone and their average values for ram speed 1.3mm/sec and billet temperature of 430°C

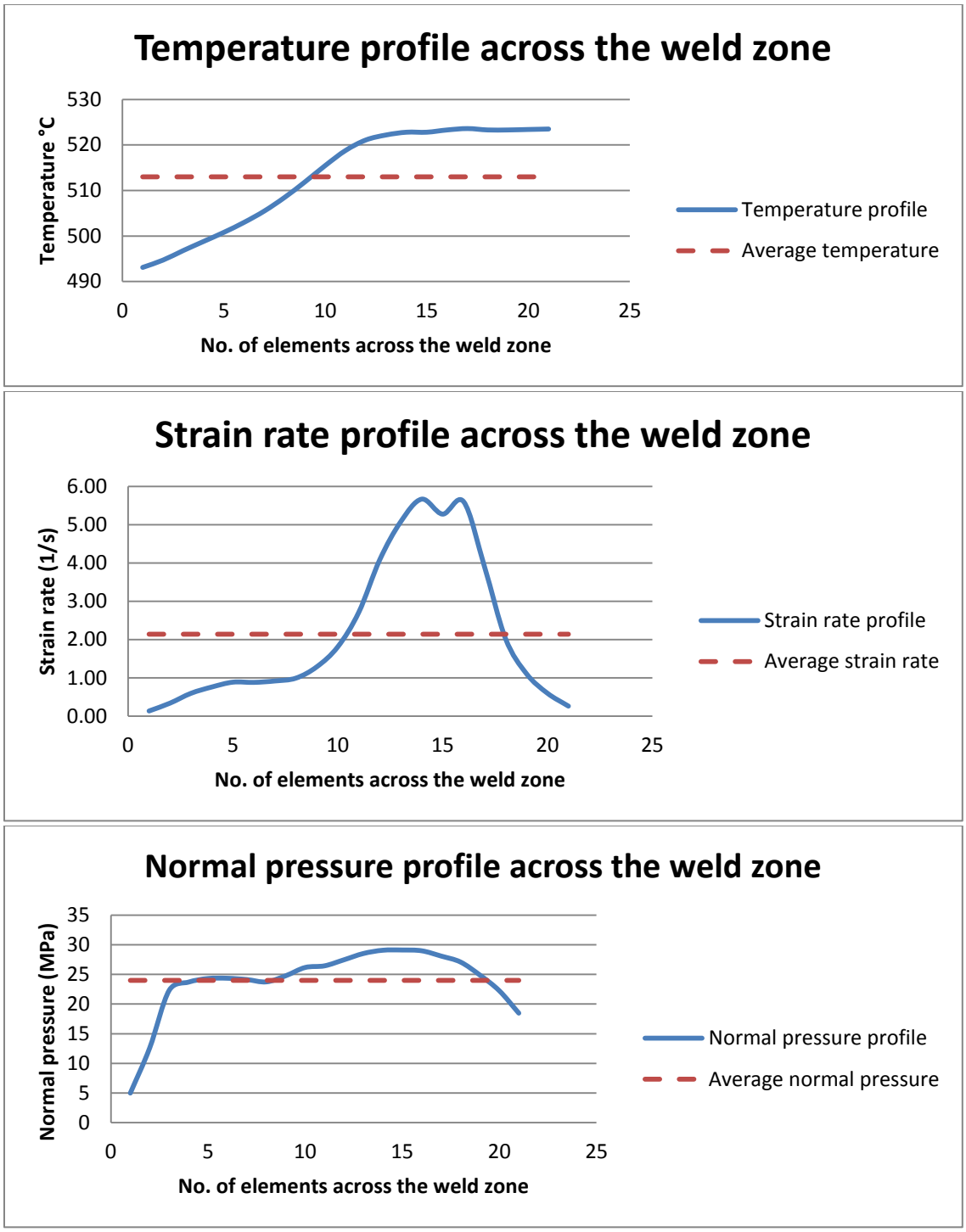

Figure 5-5. Predicted FEM values - temperature, strain rate and normal pressure profiles across the weld zone and their average values for ram speed 1.3mm/sec and billet temperature of 450°C

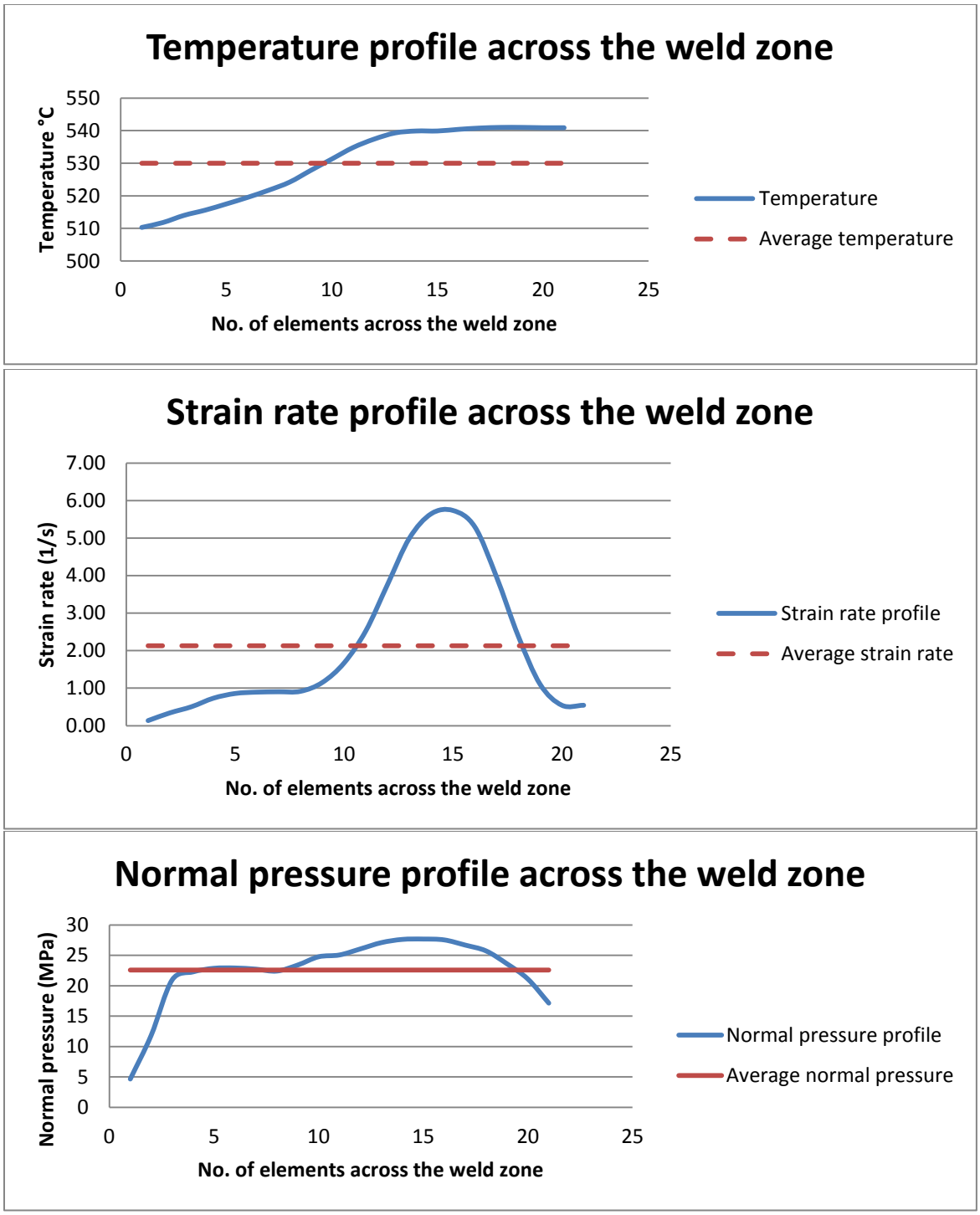

Figure 5-6. Predicted FEM values - temperature, strain rate and normal pressure profiles across the weld zone and their average values for ram speed 1.3mm/sec and billet temperature of 470°C

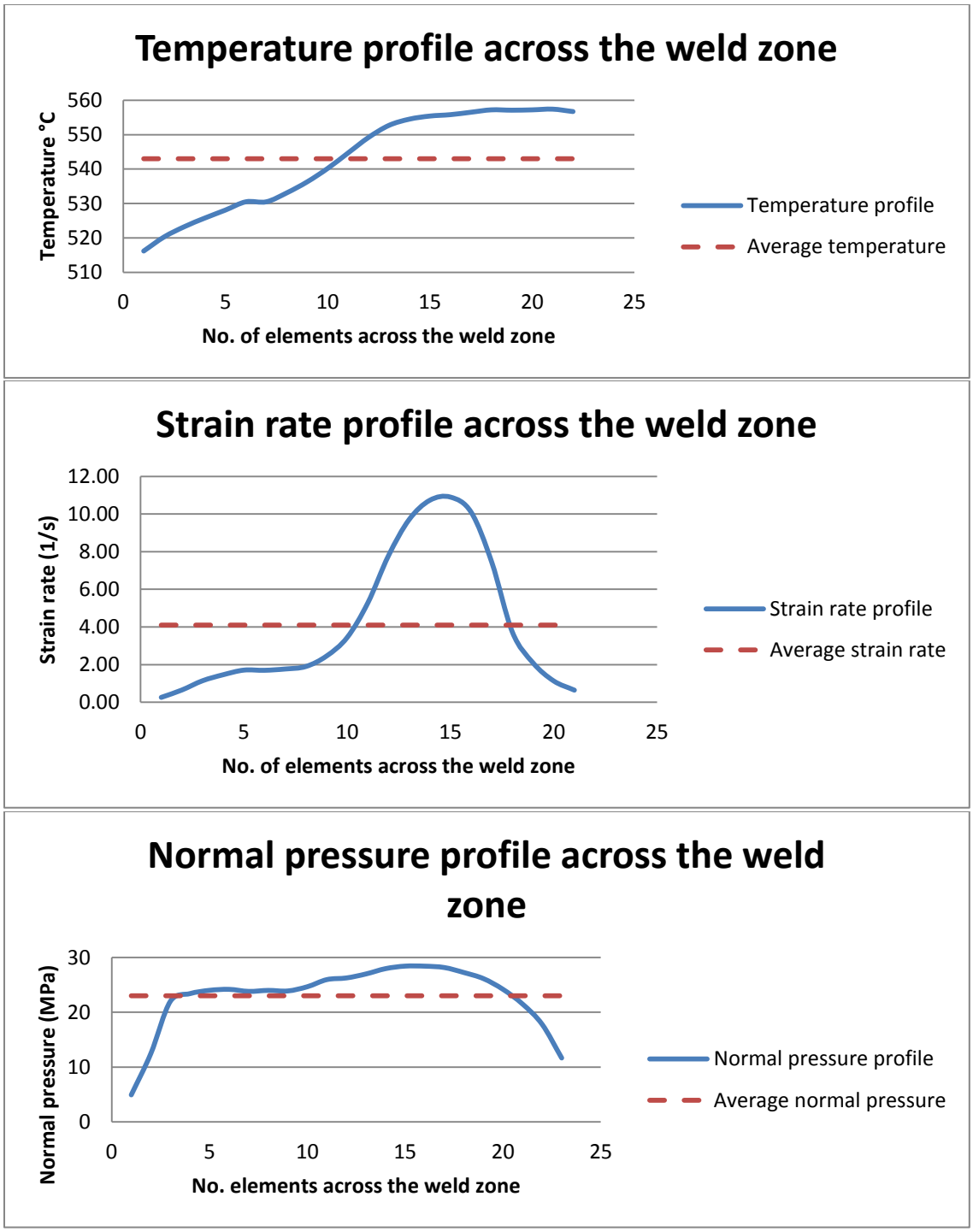

Figure 5-7. Predicted FEM values - temperature, strain rate and normal pressure profiles across the weld zone and their average values for ram speed 2.5mm/sec and billet temperature of 450°C

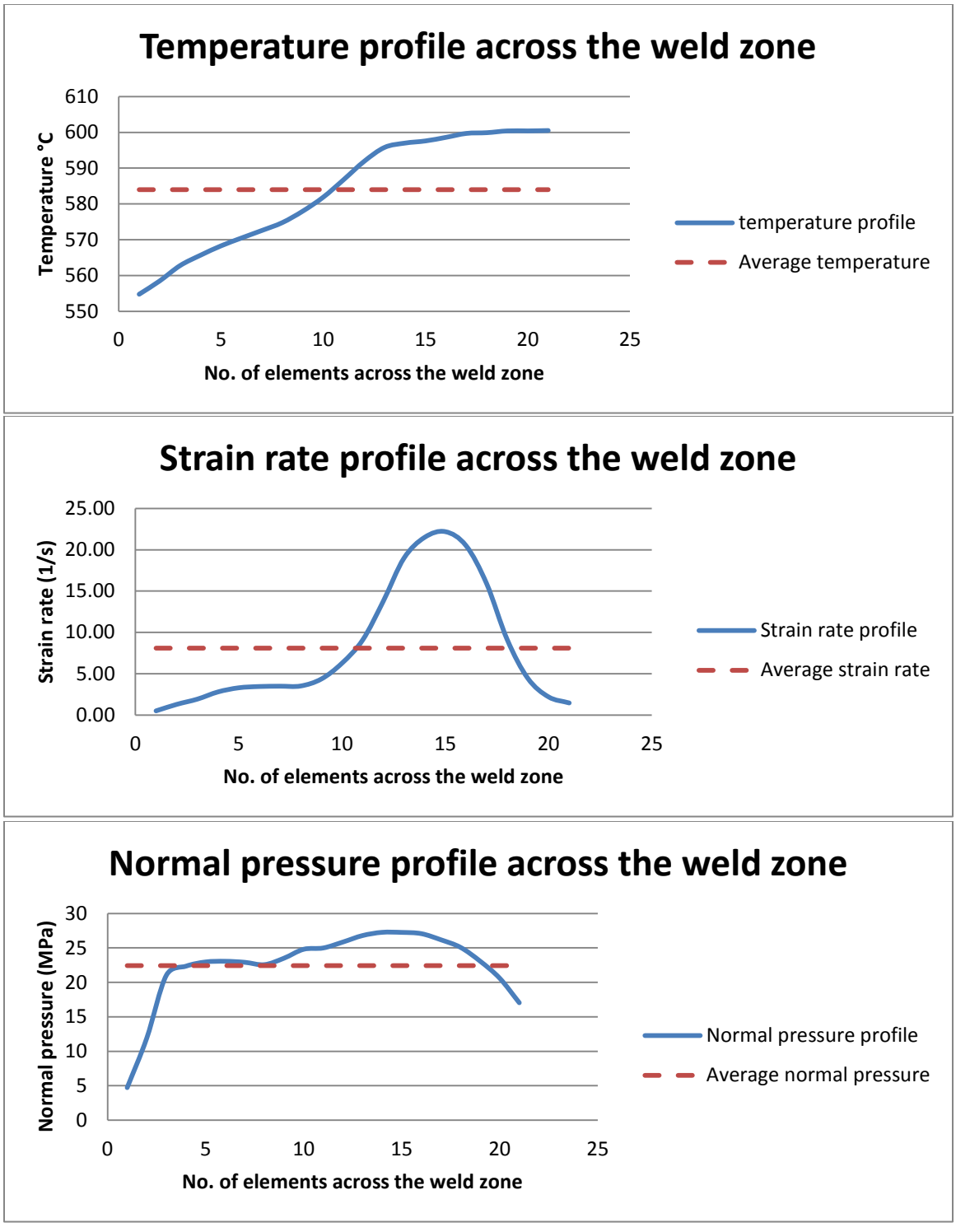

Figure 5-8. Predicted FEM values - temperature, strain rate and normal pressure profiles across the weld zone and their average values for ram speed 5mm/sec and billet temperature of 450°C

The averaged results of temperature and strain rate for all obtained values from the numerical simulation were projected in Figure 4-21 in the previous chapter. The flow stress model showed a linear relationship with a different strain rate values for different temperatures (See Figure 3-3). In this criterion, an assumption was made to consider the relation between the normal pressure and strain rate for a specific temperature as linear. Based on the numerical simulation results of selected path, the average values of normal pressure, strain rate and temperature have been obtained. The same average values of strain rate and temperature from the numerical simulation were used as input to obtain the normal pressure in the physical simulation experiments. Since the physical simulation (See Figure 4-21) was not able to provide all data points for all state variables due to lack of the experimental material, the normal pressure value was interpolated. Consequently, if the average value of the normal pressure from the numerical simulation was greater than the interpolated value from the physical simulation or within the margin of ($\pm$1 MPa) that meant formation of good extrusion weld. It is worth mentioning that the physical simulation values were based on maximum normal pressure value. Therefore, this margin of error was assumed at 5% in the numerical simulation or in physical simulations. The results of the proposed criterion for five cases with different process conditions are summarized and compared to ensure good weld integrity Table 5-2 and Figure 5-9.

Table 5-2. The results of the proposed new extrusion welding criterion

Case No	Process conditions	Average Temp. (C)	Average Strain Rate (1/s)	Average Normal Pressure (MPa)	Interpolated Normal Pressure (MPa)	Weld Integr-ity?
1	430°C 1.3 mm/sec	496	1.97	25.05	25.76	Yes
2	450°C 1.3 mm/sec	513	2.14	24	22.42	Yes
3	470°C 1.3 mm/sec	530	2.13	22.58	19.38	Yes
4	450°C 2.5 mm/sec	543	4.10	23	19.28	Yes
5	450°C 5 mm/sec	584	8.10	22.43	22.07@550	Yes

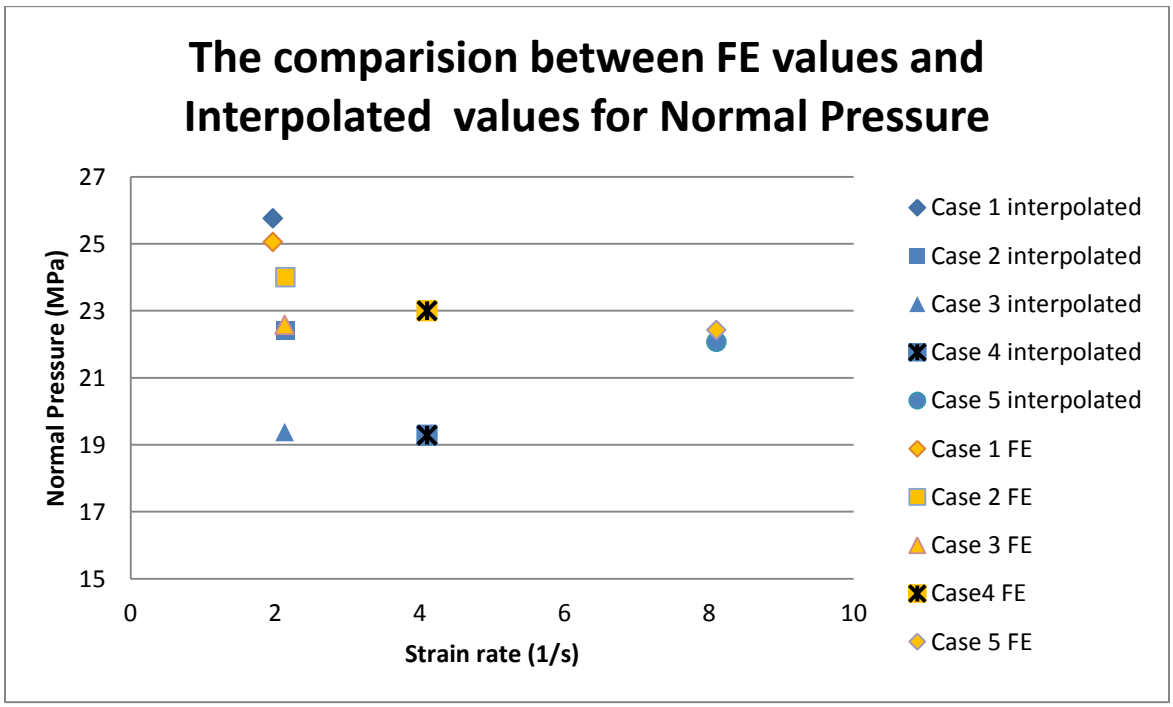

Figure 5-9. Comparison between FEM simulation and the interpolated values of normal pressure

As it can be seen from the data presented in Table 5-1 that all cases which have been simulated by HyperXtrude^{TM} software had formed a good weld. In all these cases, the experimental results have exhibited positive results proving that the process conditions were sufficient enough to guarantee weld integrity. However, this criterion cannot predict the exact normal pressure that ensures the good weld. However, based on physical simulation results and the obtained values from the FEM simulation we can foresee qualitatively that formation of good weld will occur. Due to the limited amount of Magnesium alloy AM30 since it is not a commercial alloy yet, a set of experiments using 40 samples was performed. For more precise comparison values, more physical simulations tests are needed. Also, this criterion can be applied to any metal alloys using the same approach. A subroutine can be written and run in conjunction with HyperXtrude for weld integrity tracking during a transient simulation. Finally, the proposed work is less expensive than industrial trails and less time consuming than other criteria [19] [37] [38] [58] [59].

6 Summary, Conclusion and Future work

A comprehensive analysis of the extrusion welding of Magnesium alloy AM30 was performed using multiple approaches. The objective was to achieve a better understanding of the extrusion welding phenomenon and to evaluate the quality of extrusion welding specifically in Magnesium alloys. Microstructure characterization and mechanical testing for an industrial "double hat" extrudate of Magnesium alloy AM30 were conducted and are described in Chapter 2. This was done using different techniques such as Light Optical Microscopy (LOM), Electron Backscattered Diffraction (EBSD) and micro hardness testing. Furthermore, in Chapter 3, numerical simulation of hot extrusion for a "double hat" of Magnesium AM30 for various process conditions was performed using a commercial finite element based software HyperXtrude™. Accordingly, in Chapter 4, physical modeling of extrusion welding for different process conditions based on the numerical simulation predictions for Magnesium alloy AM30 was performed using the thermo-mechanical simulator Gleeble® 3500. The microstructure characterization and mechanical testing were conducted for the physically modeled samples. Finally, a new criterion for evaluating the extrusion welding quality based on the numerical simulation and the physical modeling outcomes was proposed and applied to Magnesium alloy AM30.

The following sections will summarize the results in a form of conclusions from the performed studies.

6.1 *Microstructure Characterization of AM30 and Mechanical Testing*

The objective of this part of the performed studies was to focus on the integrity of the welding area of the industrial hollow profile of Magnesium alloy AM30 in terms of microstructure and mechanical testing.

During the investigation, a microstructure characterization was conducted for the regions in the vicinity of the extrusion weld by using a light optical microscope - Olympus® Nikon. Furthermore, additional analysis was performed using electron backscatter diffraction (EBSD) technique on Hitachi 4300SE/N scanning electron microscope to study the orientation map of the grains and the average grain sizes in the extrusion welding regions in comparison to the microstructure of the pre-extruded billet.

In terms of mechanical testing, micro hardness tests were performed in different regions around the weld. The focus was on the hardness profiles for three samples: A - sample from the pre-extruded billet, B - sample from location (A), which contains a weld with good integrity, C - sample from location (C), which contains a characteristic weld line.

Based on the performed studies, the following conclusions were made:

- Two types of extrusion welding were observed: one without a visible weld line, which indicates the preferred extrusion welding, and the other with a weld line.
- The formation of straight and tortuous weld lines in the extrusion weld zone depends on the velocities of the two neighboring strands entering the weld zone, their surface roughness, and the level of applied stresses.
- During the hot extrusion of the double hat profile, dynamic recrystallization occurs especially inside the welding chamber and around the weld line causing ‘‘necklacing’’ of a small grains around the weld line.
- Due to the noticeable temperature gradient within the portholes and welding chamber, the grain growth differs from location (A) to location (C) in the analyzed profile.
- There is a significant microstructural response to extrusion conditions measured by the average grain size. The pre-extruded billet, which was homogenized by extrusion, has small grains of 5.3 μm in diameter. However, the average grain size at the weld zones is 32 μm while the weld line is present. The small grains formed at the vicinity of weld line on average are 12 μm in diameter but there is very high percentage of very fine grains

between 2 and 6 µm. A good weld without a characteristic weld line has much bigger grains of 93 µm in diameter. These values lead to different hardness levels and consequently different mechanical properties in different locations in weld vicinity. However, in every tested sample the hardness profile shows consistent values across the weld zone.

- Different grain orientation maps are observed for all evaluated samples. The pre-extruded material shows $\langle 1000 \rangle$ orientation, while the sample with good weld integrity shows strong $\langle 2\bar{1}\bar{1}0 \rangle$ orientation also, the sample with a pronounced weld line shows $\langle 10\bar{1}0 \rangle$ orientation.
- The difference in crystallographic orientations in various types of welds could be explained by the dynamic recrystallization taking place during the extrusion. However, this very complex metallurgical phenomenon needs further in-depth investigations.

6.2 *Numerical Simulation of "Double Hat" Magnesium Alloy AM30 Extrudate*

Numerical simulation of the hot extrusion of Magnesium alloy AM30 using HyperXtrude^{TM} software was performed. The objective of this study was to determine the influence of different ram speeds and billet temperatures on the state variables such as temperature, strain rate and normal pressure within the welding chamber. The results of numerical

simulations were used to design the physical modeling experiments of the extrusion welding, which have been presented in Chapter 4. In addition, the state variables of the performed simulations have been used in the new criterion for evaluating the quality of extrusion welding for Magnesium alloy AM 30 (Chapter 5). The simulations of the extrusion process of "double hat" Magnesium alloy AM30 were successfully performed for different billet temperatures (430°C, 450°C, 470°C) and ram speeds (1.3 mm/sec, 2.5 mm/sec, 5 mm/sec)

From this effort, the following conclusions were made:

- The increase of billet temperature as well as heat generated due to friction and deformation have a significant effect on the temperature distribution within the weld zone.
- The temperature increases rapidly within the portholes and welding chamber because of the high localized strain and strain rate values during metal splitting at bridges and re-joining within the welding chamber.
- The temperature is not uniformly distributed within the weld zone and reaches its highest value at the bearing land near the core mandrel because of the high strain and lower heat loss in comparison to the material near the outer side walls of the welding chamber.

- Strain rate has non uniform distribution especially in the weld zone and increases in weld zone towards the bearing land due to the high strain and high velocity near the exit of the die.
- The highest value of strain rate is located at the beginning of the bearing land. On the other hand, the lowest strain rate was located at the corner of the welding chamber side wall and die face which could represent a dead metal zone.
- There is non-uniform distribution of normal stress at weld zone because of the curvature of the geometry of the welding chamber.
- The normal stress is gradually decreased from its highest value at the beginning of the bearing land.
- The lowest normal pressure can be observed near the side wall of the welding chamber where the shear stress is dominant due to the high friction between the flowing metal and stationary chamber's side wall and a mandrel.

6.3 *Physical Simulation of Extrusion Welding of Magnesium Alloy AM30*

In this dissertation, a new criterion for the weld integrity during the extrusion of hollow profiles has been introduced based on the combination of inputs from both the numerical and the physical simulations. The physical simulation for different state variables has been conducted on

Gleeble 3500 thermo-mechanical simulator to establish the optimal welding conditions and to help the verification of the obtained results from the numerical simulation step.

The objective of the experiments was to measure the required normal pressure that ensures weld integrity. Therefore, the experiments were divided into two parts. The first set of samples was used to evaluate six strain values (2.5%, 5%, 10%, 20%, 25%, and 30%) of the compressed samples at lowest temperature of 480°C and higher strain rate 20/s. From the first set, one strain value was chosen for the next set of tests to measure the normal pressure that ensures a good integrity weld. It was expected that if the lowest temperature and the highest strain rate resulted in good weld integrity, the same should happen for less beneficial conditions of higher temperature and lower strain rate. The second set was used to measure the normal pressure at different temperatures and different strain values at 20% strain. A physical simulation experiments for the extrusion welding based on compression of two faced cylinders for three temperatures 480°C, 500°C, 550°C and three strain rates 1/s, 10/s, 20/s were performed.

From this effort, the following conclusions were made:

- Many voids are present along the weld line in the compressed samples at strain values of 2.5% and 5%. These voids are an indication of a weak weld and consequently poor weld integrity at

these strain conditions. The hardness profiles of the samples show drop in the measured hardness values at the weld line.

- Good weld integrity is predicted for the compressed sample at 10% and 20%. This expectation is supported by microstructure observation and hardness measurement. There are no void along the weld line and the hardness values are consistent across the weld zone.
- The compressed samples at higher strains of 25% and 30% look also very promising. There are no voids along the weld line and the hardness profiles are uniform, however both samples started to buckle during compression. The deformation conditions exceeded permissible strain for these tests.
- The higher the strain rate the higher the flow stress needed to deform the material. Accordingly, there is a need for die design optimization to ensure a uniform strain rate distribution within the weld zone.

6.4 *A new criterion for extrusion welding quality*

A new criterion for evaluating extrusion welding quality based on physical and numerical simulation is proposed for the hot extrusion of Magnesium Alloy AM30. The proposed application can be extended to other metals and alloys and requires following of the same test algorithm.

The new extrusion welding criterion is different from the previous criteria in a few ways. It is applicable and practical once the peak of normal pressure at the weld interface has been established in the laboratory physical compression test. The previous criteria required an experimental work for each set of process parameters for the actual industrial extrusion process. This approach is very expensive and labor intensive. The new proposed criterion is based on the numerical simulations of the hot extrusion and the experimental physical test of the deformation welding phenomenon such as compression test. From the results of numerical simulation performed using HyperXtrude^{TM} software, the state variables such as temperature, strain rate and normal pressure for the selected path in the welding zone (including welding chamber and bearing land) were averaged and compared with the physical simulation results.

From this effort, the following conclusions were made:

- All cases covered by this study were simulated by HyperXtrude^{TM} software and confirmed good weld integrity while following requirements of the new extrusion welding criterion.
- The proposed criterion cannot predict directly the exact normal pressure that ensures a good weld. However, based on physical simulation results and the obtained values from the

FEM simulation we can foresee qualitatively if the formation of good weld will occur.

- This criterion can be applied to all metals and alloys.

6.5 *Future work*

As an extension to this research effort, there are areas where an additional work should be performed to allow better understanding of the engineering science applied to extrusion welding of various materials:

- For more precise assessment of mechanical properties, tensile tests are recommended for different extrusion welding types.

- Fatigue tests should be performed to understand the influence of the cyclic loading on life of the extrudate containing extrusion welding.
- Additional microstructure characterization using Transmission Electron Microscopy to better analyze the differences between the crystallographic orientations within the weld zones should be performed. Transmission Electron Microscopy is used to assist in defining whether the recrystallized grain is still free of dislocations or it has been exposed to further deformation that could change the crystallographic orientation.

- The numerical simulation of hot extrusion should be performed for different process conditions in transient analysis to study the influence of changing of the state variables during extrusion.
- With sufficient data from the physical test, subroutine code including the new criterion can be applied in conjunction with a transient FEM simulation. This could help to evaluate the extrusion welding for every FE element in the weld zone at different time step during the extrusion.

References

[1] R. Moz, "Global and China Automotive Magnesium Alloy Industry Report, 2012 - 2015 | Researchmoz.us." [Online]. Available: http://www.academia.edu/3612001/Global_and_China_Automotive_Magnesium_Alloy_Industry_Report_2012_-_2015_Researchmoz.us. [Accessed: 20-Nov-2013].

[2] USCAR, "USAMP MAGNESIUM FRONT-END PROJECT RESULTS IN SIGNIFICANT WEIGHT SAVINGS AND PARTS REDUCTION." Nov-2006.

[3] B. Mordike and T. Ebert, "Magnesium: Properties — applications — potential," *Mater. Sci. Eng. A*, vol. 302, no. 1, pp. 37–45, Apr. 2001.

[4] M. H. Yoo, "Slip, twinning, and fracture in hexagonal close-packed metals," *Metall. Trans. A*, vol. 12, no. 3, pp. 409–418, Mar. 1981.

[5] B. C. Wonsiewicz, "Plasticity of magnesium crystals.," Thesis, Massachusetts Institute of Technology, 1966.

[6] I. J. Polmear, *Light alloys: metallurgy of the light metals*. E. Arnold, 1982.

[7] Levesque, J.; Inal, K.; Neale, K. W.; Luo, A.; Mishra, R. K.; Jiang, L, "Numerical Modelling of Large Strain Deformation in Magnesium Alloy AM30," presented at the MAGNESIUM TECHNOLOGY SYMPOSIUM, Orlando, FL, United states, 2007, pp. 11–16.

[8] Levesque J, Inal K, Neale KW, Mishra RK, Luo AA, "Numerical modelling of large strain deformation in magnesium," presented at the MAGNESIUM TECHNOLOGY SYMPOSIUM, San Antonio, TX, United states, 2006, pp.239.

[9] ASM INTERNATIONAL, "Selection and Applications of Magnesium and Magnesium Alloys," in *Metals Handbook Desk Edition*, 1998, pp. 559–570.

[10] A. A. Luo and A. K. Sachdev, "Development of a new wrought magnesium-aluminum-manganese alloy AM30," *Metall. Mater. Trans. Phys. Metall. Mater. Sci.*, vol. 38, no. 6, pp. 1184–1192, 2007.

[11] C. Bettles and M. Barnett, *Advances in Wrought Magnesium Alloys: Fundamentals of Processing, Properties and Applications*. Elsevier, 2012.

[12] C. Bettles and M. Gibson, "Current wrought magnesium alloys: Strengths and weaknesses," *JOM*, vol. 57, no. 5, pp. 46–49, May 2005.

[13] R. S. Busk and International Magnesium Association, *Magnesium products design*. New York: M. Dekker, 1987.

[14] L. L. Rokhlin, *Magnesium Alloys Containing Rare Earth Metals: Structure and Properties*. CRC Press, 2003.

[15] F.F. Kraft and J.S. Gunasekera, "Conventional Hot Extrusion, Metalworking: Bulk Forming," in *ASM Handbook*, vol. 14A, 2005, pp. 421–439.

[16] T. Altan, S.-I. Oh, and H. L. Gegel, *Metal forming: fundamentals and applications*. American Society for Metals, 1983.
[17] K. B. Muller, "Indirect extrusion with active friction (ISA)," in *Proceedings of the 6th Asia-Pacific Symposium on Engineering Plasticity and Its Applications (AEPA2002), December 2, 2002 - December 6, 2002*, 2002, vol. 233–236, pp. 323–328.
[18] P. Saha, *Aluminum extrusion technology*. ASM International, 2000.
[19] Akeret R., "Extrusion welds-quality aspects are now center stage," 1992, vol. Chicago, ET, pp. 319−336.
[20] M. Bauser, G.Sauer, K. Siegert, *Extrusion*, Second. ASM International, 2006.
[21] M. Engelhardt, N. Grittner, D. Bormann, and F.-W. Bach, "Microstructural weld seam characterisation in the as extruded condition for Al-Mg-Si-alloys; Mikrostrukturelle Pressschweinahtcharakterisierung im strangpressten Zustand fur Al-Mg-Si-Legierungen," *Mater. Werkst.*, vol. 42, no. 6, pp. 531–541, 2011.
[22] H. Matsuoka, L. Neumann, H. Hamano, and M. Sakaguchi, "Effect of microstructures on tensile properties of a 6061 extruded alloy containing weld parts," *KeikinzokuJournal Jpn. Inst. Light Met.*, vol. 52, no. 4, pp. 155–160, 2002.
[23] A. Loukus, G. Subhash, and M. Imaninejad, "Mechanical properties and microstructural characterization of extrusion welds in AA6082-T4," *J. Mater. Sci.*, vol. 39, no. 21, pp. 6561–6569, Nov. 2004.
[24] N. Nanninga, C. White, T. Furu, O. Anderson, and R. Dickson, "Effect of orientation and extrusion welds on the fatigue life of an Al–Mg–Si–Mn alloy," *Int. J. Fatigue*, vol. 30, no. 9, pp. 1569–1578, Sep. 2008.
[25] W. H. van Geertruyden, S. R. Claves, and W. Z. Misiolek, "Electron backscatter diffraction analysis of microstructural evolution in hot-deformed 6xxx series aluminum alloys," *Metall. Mater. Trans. A*, vol. 33, no. 3, pp. 693–700, Mar. 2002.
[26] R. Sikand, A. M. Kumar, A. K. Sachdev, A. A. Luo, V. Jain, and A. K. Gupta, "AM30 porthole die extrusions-A comparison with circular seamless extruded tubes," *J. Mater. Process. Technol.*, vol. 209, no. 18–19, pp. 6010–6020, 2009.
[27] B. F. Gerard, "Investigating microstructural gradients and high strain rate deformation mechanisms in industrial magnesium alloy components," M.S., Lehigh University, United States -- Pennsylvania, 2009.
[28] N. H. Alharthi and W. Z. Misiolek, "Microstructure Characterization of Extrusion Welding in a Magnesium Alloy Extrudate," *Metallogr. Microstruct. Anal.*, vol. 2, no. 6, pp. 395–398, 2013.

[29] CIHA K, "CHEMICAL POLISHING IN METALLOGRAPHY," *Prakt. Metallogr. Metallogr.*, vol. 8, no. 1, pp. 26–39, 1971.
[30] J. A. Del Valle, M. T. Perez-Prado, and O. A. Ruano, "Deformation mechanisms responsible for the high ductility in a Mg AZ31 alloy analyzed by electron backscattered diffraction," *Metall. Mater. Trans. Phys. Metall. Mater. Sci.*, vol. 36, no. 6, pp. 1427–1438, 2005.
[31] M. R. Barnett, "Twinning and the ductility of magnesium alloys: Part I: 'Tension' twins," *Mater. Sci. Eng. A*, vol. 464, no. 1–2, pp. 1–7, Aug. 2007.
[32] R. D. Cook, D. S. Malkus, M. E. Plesha, and R. J. Witt, *Concepts and Applications of Finite Element Analysis, 4th Edition*, 4 edition. New York, NY: Wiley, 2001.
[33] Matthias Goelke, "Practical Aspects of Finite Element Simulation – A Study Guide," *Altair University*, 2012. .
[34] Hyperworks- Altair Engineering, "Manufacturing Solutions 12.0-HyperXtrude User Guide." 2013.
[35] C. Zhang, G. Zhao, Z. Chen, H. Chen, and F. Kou, "Effect of extrusion stem speed on extrusion process for a hollow aluminum profile," *Mater. Sci. Eng. B*, vol. 177, no. 19, pp. 1691–1697, Nov. 2012.
[36] H. . Jo, C. . Jeong, S. . Lee, and B. . Kim, "Determination of welding pressure in the non-steady-state porthole die extrusion of improved Al7003 hollow section tubes," *J. Mater. Process. Technol.*, vol. 139, no. 1–3, pp. 428–433, Aug. 2003.
[37] Plata, M. and J. Piwnik., "Theoretical and experimental analysis of seam weld formation in hot extrusion of aluminum alloys," 2000, vol. Chicago, ET, pp. 205−211.
[38] L. Donati and L. Tomesani, "The prediction of seam welds quality in aluminum extrusion," *Proc. Int. Conf. Adv.*, vol. 153–154, no. 1–3, pp. 366–373, 2004.
[39] Y. A. Khan and H. S. Valberg, "Metal flow in idealised a-symmetric 2D extrusion welding," *Int. J. Mater. Form.*, vol. 3, pp. 383–386, 2010.
[40] J. Liu, G.-Y. Lin, D. Feng, Y.-M. Zou, and L.-P. Sun, "Effects of process parameters and die geometry on longitudinal welds quality in aluminum porthole die extrusion process," *J. Cent. South Univ. Technol. Engl. Ed.*, vol. 17, no. 4, pp. 688–696, 2010.
[41] G. Liu, J. Zhou, and J. Duszczyk, "Prediction and verification of temperature evolution as a function of ram speed during the extrusion of AZ31 alloy into a rectangular section," *J. Mater. Process. Technol.*, vol. 186, no. 1–3, pp. 191–199, May 2007.
[42] G. Liu, J. Zhou, and J. Duszczyk, "FE analysis of metal flow and weld seam formation in a porthole die during the extrusion of a magnesium alloy into a square tube and the effect of ram speed on

weld strength," *J. Mater. Process. Technol.*, vol. 200, no. 1–3, pp. 185–198, May 2008.
[43] L. Li, H. Zhang, J. Zhou, J. Duszczyk, G. Y. Li, and Z. H. Zhong, "Numerical and experimental study on the extrusion through a porthole die to produce a hollow magnesium profile with longitudinal weld seams," *Mater. Des.*, vol. 29, no. 6, pp. 1190–1198, 2008.
[44] A. A. Luo and A. K. Sachdev, "Development of a New Wrought Magnesium-Aluminum-Manganese Alloy AM30," *Metall. Mater. Trans. A*, vol. 38, no. 6, pp. 1184–1192, Jun. 2007.
[45] H. J. McQueen and N. D. Ryan, "Constitutive analysis in hot working," *Rate Process. Plast. Deform. II Unified Const. Theory Deform. TMS Fall Meet. 2000*, vol. 322, no. 1–2, pp. 43–63, 2002.
[46] A. A. Parkar, "On modeling and experimental validation of extrusion process of lightweight alloys," M.S., Mississippi State University, United States - Mississippi, 2011.
[47] Y. X. Wang, X. Q. Zeng, W. J. Ding, A. A. Luo, and A. K. Sachdev, "Development and Validation of Extrusion Limit Diagram for AZ31 and AM30 Magnesium Alloys," *Mater. Sci. Forum*, vol. 546–549, pp. 327–332, 2007.
[48] "Dynamic Systems for Materials Research - 3500." [Online]. Available: http://www.gleeble.com/index.php/products/gleeble-3500.html.
[49] J. Zasadzinski, J. Richert, and W. Z. Misiolek, "Weld quality in extruded aluminium hollow sections," *Light Met. Age*, vol. 51, no. 3–4, pp. 8–13, 1993.
[50] U. Chakkingal and W. Z. Misiolek, "Welding phenomena in extruded aluminum hollow profiles," in *Proceedings of the 1998 TMS Annual Meeting*, , pp. 195–205, 1998.
[51] S.-P. Edwards, A. J. den Bakker, J. Zhou, and L. Katgerman, "Physical Simulation of Longitudinal Weld Seam Formation During Extrusion to Produce Hollow Aluminum Profiles," *Mater. Manuf. Process.*, vol. 24, no. 4, pp. 409–421, 2009.
[52] S.-P. Edwards, A. J. Den Bakker, J. L. Neijenhuis, W. H. Kool, and L. Katgerman, "The influence of the solid-state bonding process on the mechanical integrity of longitudinal weld seams," *JSME Int. J. Ser. Solid Mech. Mater. Eng.*, vol. 49, no. 1, pp. 63–68, 2006.
[53] E. Ceretti, L. Fratini, F. Gagliardi, and C. Giardini, "A new approach to study material bonding in extrusion porthole dies," *CIRP Ann. - Manuf. Technol.*, vol. 58, no. 1, pp. 259–262, 2009.
[54] S. M. Fatemi-Varzaneh, A. Zarei-Hanzaki, and M. Haghshenas, "A study on the effect of thermo-mechanical parameters on the deformation behavior of Mg–3Al–1Zn," *Mater. Sci. Eng. A*, vol. 497, no. 1–2, pp. 438–444, Dec. 2008.

[55] M. R. Barnett, Z. Keshavarz, and X. Ma, "A semianalytical sachs model for the flow stress of a magnesium alloy," *Metall. Mater. Trans. A*, vol. 37, no. 7, pp. 2283–2293, Jul. 2006.
[56] M. A. Mostafaei and M. Kazeminezhad, "Hot deformation behavior of hot extruded Al–6Mg alloy," *Mater. Sci. Eng. A*, vol. 535, pp. 216–221, Feb. 2012.
[57] Z. Zachariah, S. S. V. Tatiparti, S. K. Mishra, N. Ramakrishnan, and U. Ramamurty, "Tension–compression asymmetry in an extruded Mg alloy AM30: Temperature and strain rate effects," *Mater. Sci. Eng. A*, vol. 572, pp. 8–18, Jun. 2013.
[58] Udaya K. Sajja1, a, Mahender P. Reddy 1,b*, Ravisankar S. Mayavaram1, "Prediction of Longitudinal Seam Weld and Weld Strength in Extrusion," in *Advances in Hot Extrusion and Simulation and 5th Extrusion Benchmark*, Dortmund – Germany, pp. 31–39, 2013.
[59] L. Donati and L. Tomesani, "The effect of die design on the production and seam weld quality of extruded aluminum profiles," *AMPTANMEOS Part 2*, vol. 164–165, pp. 1025–1031, 2005.
[60] B. Bourqui, A. Huber, C. Moulin, A. Bunetti, "Improved weld seam quality using 3D FEM simulations in correlation with practice," in *First EAA (European Aluminum Association – Extruders Division*, Montichiari, Brescia, Italy, 2002.
[61] Y. Xu and W. Z. Misiolek, "Numerical Modeling of Extrusion Welding in Magnesium Alloys," *Key Eng. Mater.*, vol. 491, pp. 159–171, Sep. 2011.
[62] E Ceretti, C Giardini, "Development and implementation of an algorithm for the simulation of material welding in extrusion process," *The First International Conference on Sustainable Manufacturing*, 2007.
[63] Nabeel H. Alharthi, Sedat Bingöl, Anthony P. Ventura, Wojciech Z. Misiolek, "Analysis of Extrusion Welding in Magnesium Alloys – Numerical Predictions and Metallurgical Verification," in *October 19-24, 2014*, Nagoya Congress Center, Nagoya, Japan.(Accepted)

Appendix (A) -Publications and Awards

Journal and conference proceedings papers:

1. Microstructure Evolution of Asymmetrically Rolled AA-5182
   Nabeel Alharthi and W.Z.Misiolek
   ASME District A 2011 Student Professional Development Conference, Temple University, Philadelphia, PA

2. Surface Grain Structure Evolution in AA6082 Hot Direct Extrusion
   Nabeel. H. Alharthi, L. De Pari Jr., A. Jäger, A. Güzel, W.Z. Misiolek, A.E. Tekkaya
   The 12th International Aluminium Conference, 2013, Montréal, Québec,Canada

3. Microstructure Characterization of Extrusion Welding in a Magnesium Alloy Extrudate
   Nabeel. H. Alharthi and W. Z. Misiolek, ,
   Metallogr. Microstruct. Anal.v2, p 395-398

4. Extrusion welding in a magnesium alloy (AM30) hollow section extrudate
   Nabeel. H. Alharthi and W. Z. Misiolek
   Advanced Materials and Processes, v 172, n 2, p 16-17, February 2014

5. Analysis of Extrusion Welding – Numerical Predictions and Metallurgical verifications.
   Nabeel H. Alharthi, Sedat Bingöl, Anthony P. Ventura, Wojciech Z. Misiolek
   11th International Conference on Technology of Plasticity, ICTP 2014, October 19-24, 2014, Nagoya , Japan (sumitted)

6. Physical Simulation for Extrusion Welding of Magnesium Alloy AM30
   Nabeel H. Alharthi, Anthony P. Ventura, Wojciech Z. Misiolek
   (will be submitted for publication)

7. New Criterion for Extrusion Welding Quality- Magnesium Alloy AM30
   Nabeel. H. Alharthi and W. Z. Misiolek
   (will be submitted for publication)

Awards:

1. “Jacquet-Lucas Award” for excellence in metallography from ASM International in 2013

2. “2014 Outstanding Scholar in USA” from the Ministry of Higher Education –Saudi Arabia

VITA

Nabeel Alharthi was born in Taif, Saudi Arabia. He is the son of Hussain Alharthi and Norah Alharthi. In 1996, he graduated from the high school and he moved to Jeddah to study mechanical engineering in King Abdulaziz University (KAU). In 2001, he graduated from KAU and started his job in Saudi Arabian Monetary Agency in Riyadh as a researcher for one year. Then, he joined Saline Water Conversion Corporation in Jubail as a mechanical engineer for one year. In 2003, he moved back to Jeddah to work for Saudi Arabian Airlines for four years as a material specialist. In 2005, he went back to academic life to pursue an Executive Master of Business Administration degree from King Abdulaziz University on a part time basis. While he was studying there he got a job in King Saud University at Riyadh and a scholarship to purse the Master of Science degree and Doctor of Philosophy degrees. In 2008, he joined Mechanical Engineering and Mechanics Department at Lehigh University, Bethlehem, PA, US. He published five papers in different journals and conferences. He received two awards for his researchs during his graduate studies, “Jacquet-Lucas Award” for excellence in metallography from ASM International in 2013 and “2014 Outstanding Scholar in USA” from the Ministry of Higher Education –Saudi Arabia. After pursuing Doctor of Philosophy degree, he will go back to Saudi Arabia -Riyadh to work as assistant professor at Mechanical Engineering Department in King Saud University. Among his many hobbies are soccer and various outdoor activities.